Iron Modification of Rhodium Nano-crystallites for CO Hydrogenation

Dumani Nozonke

BSc (Chemical Engineering), UCT

Thesis submitted to the University of Cape Town in partial fulfilment of the academic requirements for the degree of **Master of Science** in Chemical Engineering

Centre for Catalysis Research

Department of Chemical Engineering

October 2013

Declaration

I, Nozonke Dumani certify that this submission is my own, unaided work, except for the information obtained from literature sources and my prescribed supervisor. All sources of information have been adequately acknowledged and referenced. I have not received assistance from any other source in completing this submission.

Signature:…….. Date:…….

Nozonke Dumani

Acknowledgements

First and foremost, I would like to thank my supervisor, Prof Michael Claeys, for giving me the opportunity to do the project, for his guidance, support and advice throughout the project.

Many thanks to Francious, Mohammed and Miranda from the Electron Microscope Unit for their help with TEM and SEM-EDX analysis. Thanks to Theresa for XRD, STEM-EDX and her guidance and contribution to my project, Christian for helping with GC x GC analysis.

I would like to thank my colleagues, Zandile, Nothando, Doreen, Lizzy, Kubefu, Conrad, just to mention a few for providing an interesting, fun environment in which I could learn and your desire to help is greatly appreciated.

Most of all, a special thank you to Rukaya, Aliya and Grace for their support, encouragement when times were hard and putting smile on my face when I needed it and going out with me to distress. Best buddies ever. I love you guys.

I would also gratefully thank the financial support from DST-NRF Centre of Excellence in Catalysis, c*change, and NRF Scarce Skills scholarship program throughout my project.

Lastly, my family deserves a very special thanks for their support, encouragement and love throughout the project. Endless thanks to my dad, my brothers (Bongile and Saider) and my sisters (Topsy, Nandie, Lindie, ‘twin’ Zandie, Bongs and Mphiwe). This thesis is dedicated to my mommy who passed away in Feb 2011.

Synopsis

The catalytic conversion of syngas over rhodium-based catalysts has been found to selectively produce C_{2+} oxygenates (Burch and Petch, 1992a). Amongst the Fischer-Tropsch active catalysts (Co, Fe, Ni, Ru, Rh), rhodium is the most selective to oxygenate formation. The catalytic activity and selectivity towards the formation of C_{2+} oxygenates on rhodium-based catalysts have been found to depend on the choice of promoter (Mo et al., 2009a). The effect of promoters on rhodium-based catalysts has been categorised into two types namely those which increase the catalytic activity and those which change the product distribution such as Fe (Burch and Petch, 1992a).

The aim of this study was to investigate the effect of iron on alumina-supported well defined nano-sized rhodium crystallites on the activity and selectivity for CO hydrogenation. The objective was to prepare model catalysts with similar average crystallite size and narrow size distribution.

Model catalysts with dispersed nano-sized crystallites no larger than 5 nm, with narrow size distributions supported on alumina were successfully prepared using the reverse micelle technique. This technique unlike other techniques (e.g. impregnation) has the ability to produce nano-crystallites with tunable size and narrow distribution. The sizes of the crystallites can be tuned by the reverse micelle composition, particularly varying the water to surfactant ratios. Therefore in order to prepare model catalysts with similar crystallite sizes the weight water to surfactant ratio was kept constant at 0.2 (g/g). These catalysts were suited to investigate the effect of iron on alumina-supported rhodium catalysts as the crystallite sizes were kept constant and therefore eliminating the effects of crystallite sizes. The catalysts contained 10 wt % rhodium with varying iron loadings, three Rh:Fe molar ratios were chosen in the study. The catalyst of a low Rh:Fe ratio (Rh:Fe = 1:0.1), intermediate Rh:Fe ratio (Rh:Fe = 1:0.5) as well as higher Rh:Fe ratio (Rh:Fe = 1:1). A reference catalyst containing 10 wt % iron, but no rhodium, was also included in the study. The pure iron sample resulted in an average crystallite size of 8.5 nm.

Catalysts were characterised at different stages (calcined, reduced, and spent). Characterisation of the model catalysts in the reduced state using HRTEM and STEM revealed that the rhodium-containing nano-sized crystallites in the range of 4-5 nm were well dispersed on the support with narrow crystallite size distributions. Also the pure iron in the

reduced state had the crystallite size of 8.5 nm and was well dispersed on the support. EDX analysis confirmed the formation of bimetallic crystallites with the samples with high loading of iron (Rh:Fe = 1:0.5 and Rh:Fe = 1:1 molar ratios). Furthermore, XRD analysis for the reduced bimetallic samples with high loadings of iron (Rh:Fe = 1:0.5 and Rh:Fe = 1:1 molar ratios) showed characteristic peaks for RhFe alloys. However, EDX and XRD analyses for the sample with low loading of iron (Rh:Fe = 1:0.1) showed that the catalyst contains no alloys and has a behaviour more like the pure rhodium catalyst. TPR analysis on alumina-supported Rh/Fe catalysts provided clear evidence of a close interaction between rhodium and iron. It was observed that the hydrogen consumption increased with increasing iron loading and was more than the required amount to achieve complete reduction of Rh_2O_3 to metallic rhodium.

Fischer-Tropsch testing of the model catalysts was carried out at low conversion and mild conditions (180°C and 10 bar) to minimize potential effects of sintering in this model study. The conversion of CO as well as surface specific activity (TOF) normalised with respect to Rh and Fe were observed to increase upon addition of iron to the rhodium catalysts. This was attributed to the close interaction between rhodium and iron as well as due to the formation of alloys.

Methane selectivity was observed to increase with increasing iron loading while the chain growth probability decreased on the alumina-supported rhodium catalysts. The olefin content in linear hydrocarbons as well as the α-olefin content in the linear olefins was found to decrease with increasing iron content for the Rh/Fe catalysts. The pure iron sample resulted in less methane, high chain growth probability as well as high α-olefins in the linear olefins compared to rhodium and Rh/Fe catalysts.

Finally, it was observed that the total oxygenates selectivity increased with increasing iron loading. Furthermore, with iron promoted rhodium catalysts, a high selectivity to methanol and ethanol coupled with a low selectivity to acetaldehyde was observed compared to the pure rhodium catalyst. Addition of iron to the rhodium based catalysts led to the more hydrogenated product. Pure iron catalyst was very different from rhodium and Rh/Fe catalysts and resulted in a high selectivity towards C_{2+} hydrocarbons and was selective mainly to the formation of methanol.

It was observed that the Rh/Fe catalyst (Rh:Fe = 1:0.5) with iron loading of 2.7 wt % was the limiting value of iron loading and a further increase in iron loading resulted in substantially high methanol selectivity, even compared with the increase in ethanol selectivity. It was shown that C_{2+} oxygenates selectivity of up to 40 C% with ethanol the dominant C_2 oxygenates could be achieved with an alumina-supported rhodium catalyst containing 10 wt % rhodium and 2.7 wt% iron. The Rh/Fe catalyst with iron loading of 2.7 wt% was optimum because iron specific FT behaviour starts to dominate with the catalyst with high iron loading (Rh:Fe = 1:1). These results have not been previously reported in literature under the conditions of the study and employing reverse micelle approach to prepare model catalysts.

The main novelty of the study is the method (reverse micelle) used to prepare the model catalysts in order to investigate the Rh/Fe system. This method eliminates the size effects and result to the preparation of catalysts with close interaction between Rh and Fe for the Rh/Fe system.

Table of Contents

List of Figures

List of Tables

Nomenclature

Abbreviations

3WV	Three Way Valve
ASF	Anderson-Schulz Flory
CV	Flow Control Valve
EDX	Energy Dispersive X-ray Spectroscopy
FID	Flame Ionisation Detector
FT	Fischer-Tropsch
FTS	Fischer-Tropsch Synthesis
GC	Gas Chromatography
HC	Hydrocarbon
HRTEM	High Resolution Transmission Electron Microscopy
HTFT	High Temperature Fischer-Tropsch Process
ICP	Inductively Coupled Plasma
LTFT	High Temperature Fischer-Tropsch Process
MFC	Mass Flow Controller
NTP	Normal Temperature and Pressure
PI	Pressure Indicator
SASOL	Suid Afrikaanse Steenkool en Olie
SEM	Scanning Electron Microscopy
SMSI	Strong Metal Support Interactions
STEM	Scanning Transmission Electron Microscopy

TCD	Thermal Conductivity Detector
TEM	Transmission Electron Microscopy
TPR	Temperature Programmed Reduction
VOC	Volatile Organic Compound
WGS	Water Gas Shift
w/o	Water in Oil
XRD	X-Ray Diffraction

1. Introduction

Catalytic synthesis of C_{2+} oxygenates from syngas derived from coal, natural gas or biomass has been of great research interest. C_{2+} oxygenated compounds include very important compounds such as ethanol, acetic acid and acetaldehyde, which can be used as additives (e.g. ethanol) for improving gasoline octane value and burning efficiency (Yin, 2003), or as precursors in the chemical and pharmaceutical industry. The widely accepted mechanism for the formation of C_{2+} oxygenates requires CO dissociation followed by alkyl chain growth through the addition of a CH_2 species, and CO insertion (Trevino et al., 1995). It is vital to develop catalysts for producing C_{2+} oxygenates. When the commercial Fischer-Tropsch catalysts (cobalt and iron) are employed, only minor quantities of oxygenates are produced, i.e. below 10 wt % (Dry, 1999). Rhodium has been found to be very active for the synthesis of C_2 and higher oxygenates from syngas (Ojeda, 2004a). This was attributed to the unique characteristic of rhodium metal, allowing both dissociation of CO and insertion of non-dissociated CO.

Catalytic activity and selectivity of rhodium-based catalysts for CO hydrogenation depends mainly on the catalyst support and promoters. The effect of promoters on the activity and selectivity towards C_{2+} oxygenates on rhodium-based catalysts is of interest. Catalyst promoters for CO hydrogenation on rhodium-based catalysts can be classified into two categories: those which increase the catalytic activity (containing elements such as Mn, La, Mo, Fe etc.) and those which affect the product distribution (comprising elements such as Fe, Li, K, Ir, Ti etc.) (Burch and Petch, 1992a). Furthermore, the promoters that alter the product distribution can be further split into those that enhance ethanol selectivity, such as Fe, Ti and those that improve acetic acid selectivity such as Li or K (Burch and Petch, 1992a). This study will focus on iron as a promoter for rhodium-based catalysts in CO hydrogenation.

Iron was one of the first elements to be studied as a promoter for rhodium (Bhasin et al., 1978). The bimetallic supported rhodium-iron catalyst system is of interest since alloy formation could occur. The alloying of two metals generally improves catalytic properties such as selectivity, activity and stability compared to the constituent monometallic catalysts (van't Blik and Niemantsverdriet, 1984) as well as to reduce the cost of precious metal by

combining with a cheaper metal therefore minimizing the amount of the precious metal used (Kim et al., 2007). It has been reported that addition of iron to rhodium-based catalysts in CO hydrogenation results in an increase in catalytic activity and selectivity towards oxygenates and furthermore changes the product distribution toward ethanol (Fukushima et al., 1985; Burch and Petch et al., 1992b; Haider et al., 2009a). It has been suggested that the effect of iron on rhodium may be related to the oxidation state of iron (Mo et al., 2009a). The promotional role of iron on rhodium-based catalysts is still unclear and a number of explanations have been proposed such as boosting the hydrogenation of acetaldehyde to form ethanol, stabilizing an acyl species and impeding CO dissociation (Mo et al., 2009a; Chen et al., 2011).

The effect of iron on rhodium-based catalysts on the activity and selectivity towards formation of C_{2+} oxygenates has been studied by many researchers for CO hydrogenation (Bhasin et al., 1978; Fukushima et al., 1985; Burch and Petch, 1992a; Guglielminotti et al., 1995; Schunemann et al., 1995; Burch and Hayes, 1997; Haider et al., 2009; Mo et al., 2009a). However silica has been the most frequently used support and only Burch and Hayes, (1997) reported an ethanol selectivity of 50 C% over an alumina supported 2 wt% Rh-10 wt% Fe catalyst. Furthermore, all the studies reported in literature investigating iron as promoter for Rh-based catalysts for CO hydrogenation used either an impregnation or precipitation method to prepare the model catalysts. These methods led to the synthesis of catalysts with very broad crystallite size distributions and provided less control of the final crystallite size. Therefore these methods could not be used to prepare the model catalysts required for the study. Model catalysts with controllable crystallite size and narrow size distribution were required for this study. The model catalysts were synthesized using the reverse micelle microemulsion technique. This method has the ability to produce nano-crystallites with tunable size and narrow size distribution (Erikson et al., 2004). This eliminated the effects of crystallite sizes as the method allowed for preparation of model catalysts with constant crystallite sizes and therefore the effect of iron addition was the only parameter investigated in this study.

It was important to eliminate the effects of crystallite sizes as it is reported that very small crystallites of rhodium, iron, cobalt and ruthenium below a specific minimum crystallite size display lower specific catalyst activity for Fischer-Tropsch synthesis than larger crystallites and also resulted with increased methane selectivity as well as increased paraffin to olefin ratio (Ojeda et al., 2004a; Mabaso, 2005; Barkhuizen et al., 2006; Bezemer et al., 2006;

Welker, 2007; Fischer, 2011; Yuan et al., 2012). Yuan et al. (2012) observed that for rhodium, the most significant crystallite size effects were observed below 6 nm, whereas rhodium crystallites larger than 6 nm showed no chemical or geometrical effect in structure sensitive reactions. The crystallite size effects have been attributed to a combination of structural and electronic effects as well as oxidation effects.

In order to obtain high oxygenates selectivity model catalysts with small crystallites were required for the study. This is because it has been reported that smaller crystallites prefer formation of oxygenates due to reactions of CO-insertion preferably occur on metal sites with low coordination and these are preferably formed on small crystallites (Schulz et al., 2002). Previous studies on the effect of iron as promoter for rhodium little has been reported about the crystallite size effects and if the parameter was controlled.

The aim of the study is, therefore, to investigate the effect of iron on alumina-supported rhodium crystallites on the activity and selectivity for CO hydrogenation. The objective is to prepare model catalysts with a narrow size distribution using the reverse micelles method.

2. Literature Review

2.1. Fischer-Tropsch Synthesis

The Fischer- Tropsch synthesis is the conversion of synthesis gas ($CO+H_2$) derived from coal and natural gas to a wide range of hydrocarbons. The Fischer-Tropsch synthesis has been well studied with over 90 years of research and application. In 1902, Sabatier and Senderens first reported the synthesis of methane over a nickel catalyst. Later in the 1920s, Franz Fischer and Hans Tropsch headed research on the FTS and during their studies obtained an oxygenate rich mixture from a synthesis gas mixture over an alkalised iron catalyst at high pressure called synthol. Fischer-Tropsch derived fuels became increasingly of interest because it was viewed as an alternative to crude derived fuel with the added advantage of being sulphur and nitrogen free. Today there are Fischer-Tropsch plants that are currently being commissioned and constructed in Nigeria (SASOL) and China adding to the existing plants in Malaysia (Shell), Qatar (SASOL and Shell) and South Africa (SASOL and PetroSA).

2.2. The Fischer-Tropsch Reactions

The Fischer-Tropsch synthesis is the reaction converting synthesis gas to long chain hydrocarbons over a metallic catalyst. The highly exothermic reaction can be represented stoichiometrically as follows:

$$CO + 2H_2 \rightarrow -(CH_2)- + H_2O \quad \Delta H_{rxn}\,(240\ ^\circ C) = -153.7\ kJ/mol \qquad (2.1)$$

Water is the main co-product of the FT synthesis. The Fischer-Tropsch reaction is a surface polymerisation reaction with a broad product distribution. The product spectrum consists primarily of linear α-olefins and n-paraffins with minor quantities of branched hydrocarbons and oxygenates such as alcohols and aldehydes.

The extent of the chain growth of the produced hydrocarbons is influenced by the temperature, pressure, catalyst used, promoters and feed gas composition (Dry, 2002). The operating pressure for the Fischer-Tropsch synthesis is typically between 15 and 40 bar (Dry, 1981). There are two modes of operation of Fischer-Tropsch synthesis applied industrially; the High Temperature Fischer-Tropsch process, 320-350˚C (HTFT), which is used for the production of mainly gasoline and olefins (Dry, 2002) and the Low Temperature Fischer-

Tropsch process, 220-250˚C (LTFT), which is used for the production of long chain hydrocarbons, mainly wax (Dry, 2002). Both cobalt and iron are used for LTFT process whereas only iron catalysts are used for the HTFT process. Although all transition metals have the ability to catalyse the FT synthesis, the most active metals are iron, cobalt, nickel and ruthenium (Dry, 2002). Depending on the catalyst used and reaction conditions different side reactions can occur under Fischer-Tropsch conditions. The Water Gas Shift (WGS) (equation 2.2) reaction is catalysed by iron catalyst while little if any WGS activity occurs when cobalt, nickel and ruthenium are used.

$$CO + H_2O \Leftrightarrow CO_2 + H_2 \qquad \Delta H_{rxn}(240\ ^\circ C) = -39.7\ kJ/mol \tag{2.2}$$

This reaction is unwanted because it results in the formation of carbon dioxide which is an undesirable product (Dry, 2004b). The other side reaction is the Boudouard reaction (equation 2.3).

$$CO \rightarrow C + CO_2 \qquad \Delta H_{rxn}(240\ ^\circ C) = -172.9\ kJ/mol \tag{2.3}$$

The Boudouard reaction leads to the formation of carbon dioxide and carbon on the catalyst surface which can cause deactivation (Dry, 2004b). However, carbon deposition irrespective of whether Ni, Co, Ru or Fe based catalysts are used depends on the Fischer-Tropsch temperatures (Dry, 2004b). Below about 240˚C, no elemental carbon is deposited on the catalysts, however, at about 280-350˚C with iron based catalysts, elemental carbon is deposited throughout the run at a fairly constant rate (Dry, 2004b).

2.3. Mechanisms in Fischer-Tropsch Synthesis

The Fischer-Tropsch synthesis is a polymerisation reaction involving the following; reactant adsorption onto the catalyst surface, formation of a chain initiator, chain growth, chain termination, desorption of the products, re-adsorption of reactive products and further reaction. The general assumption is that not a single pathway exists, but rather a number of parallel operating reaction pathways occur during the FT synthesis. Over the years numerous reaction pathways have been proposed to account for the various products observed in the Fischer-Tropsch synthesis. The four most popular and accepted mechanisms in the FTS are alkyl, alkenyl, enol and the CO-insertion mechanisms (Claeys and van Steen, 2004). The following mechanisms will be discussed further.

2.3.1. Alkyl Mechanism

The alkyl mechanism (see figure 2.1) is the most accepted mechanism for chain growth in the FT synthesis (Claeys and van Steen, 2004). Chain initiation occurs via dissociative CO-chemisorption resulting in generation of carbon and oxygen atoms on the metal surface. The surface oxygen is removed from the surface by reacting with adsorbed hydrogen to form water or with adsorbed carbon monoxide to form carbon dioxide. The surface carbon in a sequential reaction is hydrogenated to CH, CH_2 and CH_3 surface species. The CH_3 surface species is considered the chain initiator and CH_2 surface species the monomer for chain propagation. The chain growth is thought to occur via incorporation of the monomer surface species into a surface alkyl species. Finally, the chain termination step of this species occurs via β-H-elimination to form α-olefins or H-addition to form n-paraffins.

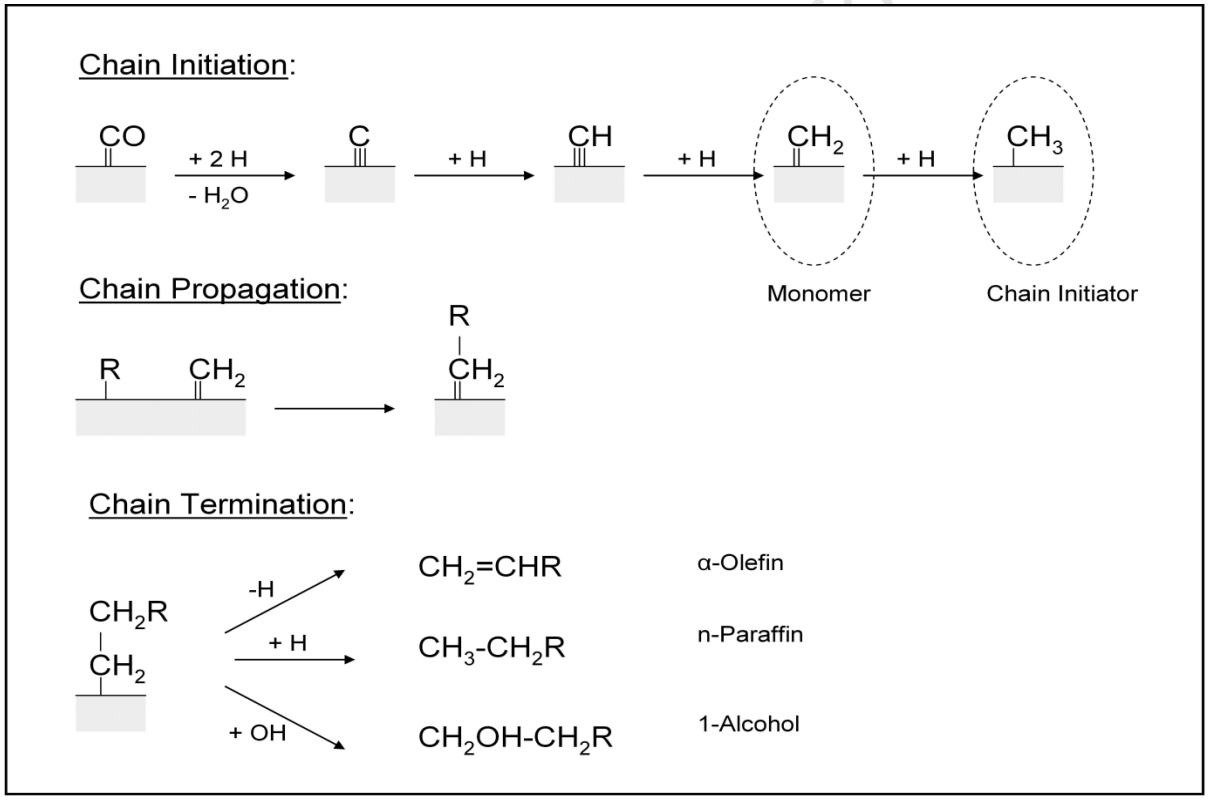

Figure 2.1: Reaction pathway for alkyl mechanism in Fischer-Tropsch synthesis (Adapted from Claeys and van Steen, 2004)

However, the alkyl mechanism does not explain the formation of oxygenates. It has been suggested that the addition of surface hydroxyl groups into the alkyl groups may lead to the formation of oxygenates (Johnston and Joyner, 1993). No experimental evidence of this reaction pathway has been reported in literature.

2.3.2. Alkenyl Mechanism

Alkenyl mechanism (see figure 2.2) was proposed by Maitlis et al. (1999) as an alternative reaction pathway for the formation of olefins in the FT synthesis. The formation of the monomer (CH_2) surface species in this mechanism is the same as for the alkyl mechanism. The chain initiator, a vinyl surface species is formed through coupling methylidyne (CH) and methylene (CH_2). The chain propagation occurs through the addition of a methylene (monomer) species to a surface vinyl (chain initiator) species forming allyl species, followed by isomerisation to form an alkenyl species. Product desorption in the alkenyl mechanism involves the addition of hydrogen to an alkenyl species to form α-olefins.

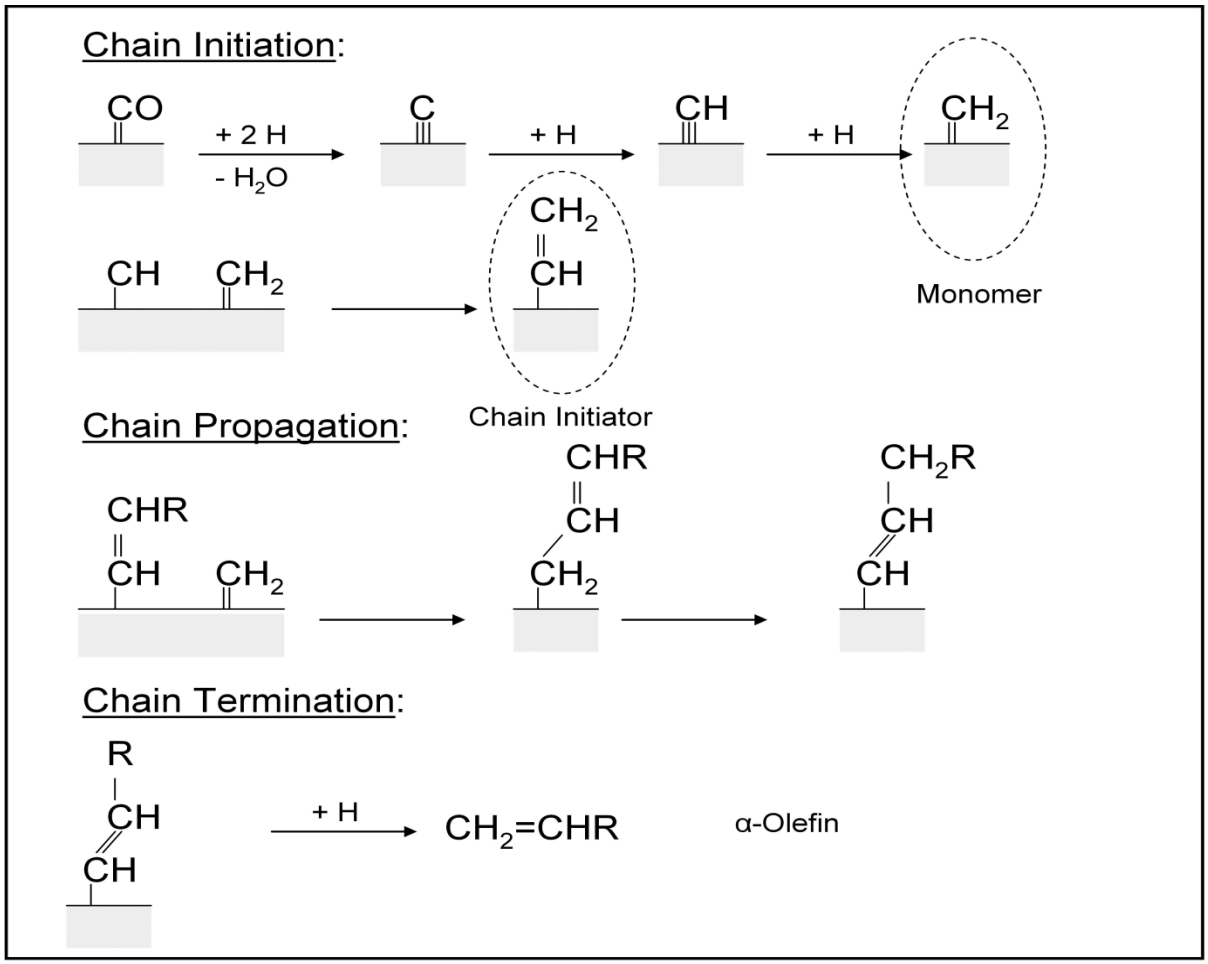

Figure 2.2: Reaction pathway for alkenyl mechanism in Fischer-Tropsch synthesis (Adapted from Claeys and van Steen, 2004)

This mechanism cannot explain the primary formation of n-paraffins (Claeys and van Steen, 2004) and formation of oxygenates, therefore an alternative co-existing reaction pathway is required to account for these products.

2.3.3. Enol Mechanism

The enol mechanism (see figure 2.3) was proposed by workers at the Bureau of Mines (Storch et al., 1951) and involves the oxygen containing surface species. This mechanism provides a possible pathway for the formation of oxygenates in the FT synthesis. In this mechanism chemisorbed CO is hydrogenated to form enol surface species. The enol surface species is both the monomer and chain initiator. Chain growth occurs through condensation between two neighbouring enol species with the elimination of water. Termination of the chain growth yields oxygenates and α-olefins (Claeys and van Steen, 2004).

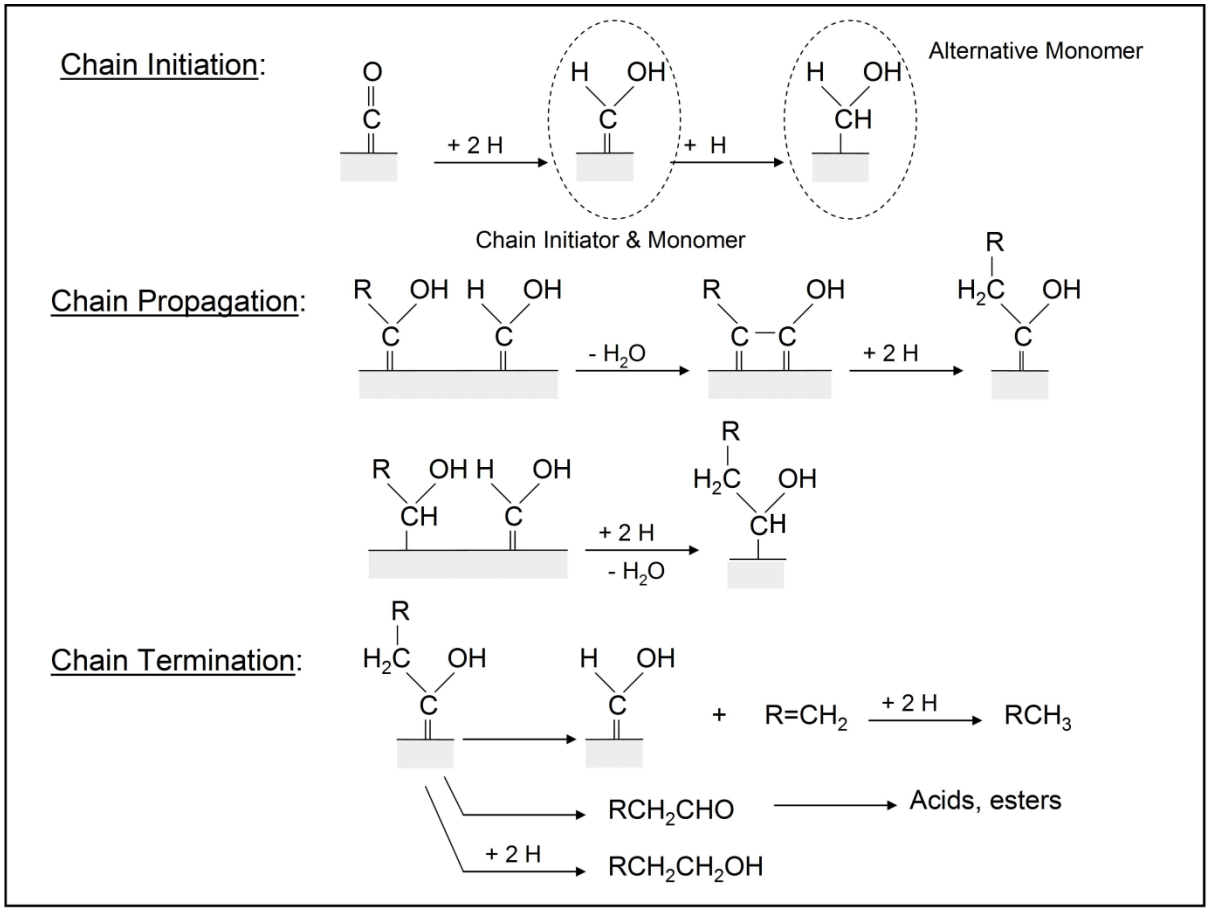

Figure 2.3: Reaction pathway for enol mechanism in Fischer-Tropsch synthesis (Adapted from Claeys and van Steen, 2004)

However, as with the alkenyl mechanism the enol mechanism does not explain the primary formation of n-paraffins and therefore an alternative reaction pathway would be required for the primary formation of n-paraffins. This mechanism explains that the n-paraffins can be formed in secondary reactions by hydrogenation of primarily formed olefins.

2.3.4. CO-Insertion Mechanism

The CO-insertion mechanism (see figure 2.4) is believed to be the main reaction pathway which accounts for the formation of oxygenates in FTS (Hindermann et al., 1993). It was first proposed by Sternberg and Wender (1959) and Roginski (1965) and further refined by Pichler and Schulz (1970). In this mechanism chemisorbed CO is the monomer while the surface methyl species is the chain initiator. Chain propagation involves the reaction between a surface metal-alkyl species and a chemisorbed CO leading to a surface acyl species. Chain termination of these species can either lead to the formation of olefins or n-paraffins or to the formation of aldehydes and alcohols from oxygen containing surface species (Claeys and van Steen, 2004).

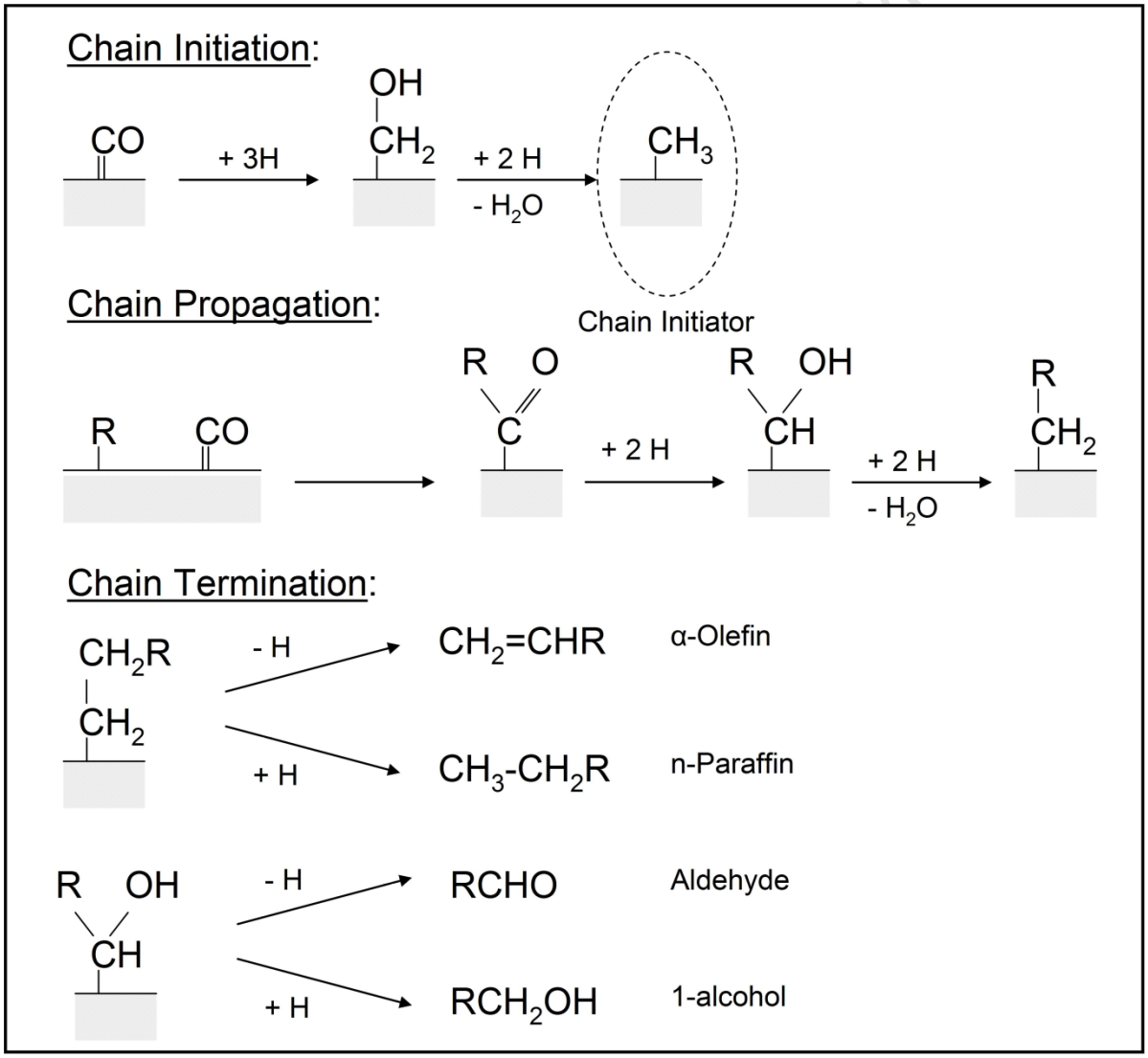

Figure 2.4: Reaction pathway for CO insertion mechanism in Fischer-Tropsch (Adapted from Claeys and van Steen, 2004)

2.4. Fischer-Tropsch Products

Different products are obtained from the FT reaction as it is considered a surface polymerisation reaction and therefore implies it is not selective. The main products of FTS are n-olefins (primarily α-olefins, some olefins with internal double bond) and n-paraffins. A typical FT product spectrum also contains side-products in small amounts, such as oxygenates (1-alchohols, aldehydes, ketones and carboxylic acids) as well as branched compounds (mainly mono-methyl branched). The product spectrum is often affected by secondary reactions as olefins and oxygenates can re-adsorb on the catalyst surface and undergo secondary reactions such as hydrogenation or double bond shift (Schulz and Claeys, 1999). The factors that affect the FT product selectivity are synthesis gas ratio, temperature, pressure, residence time as well as the catalyst choice (Claeys and van Steen, 2004).

The product distribution of the FTS can be described mathematically with the Anderson-Schulz-Flory equation:

$$\log\left(\frac{W_N}{N_C}\right) = N_C.\log(p_g) + \log\left(\frac{(1-p_g)}{p_g}\right) \tag{2.4}$$

where W_N is the weight or mole fraction of a product with a certain number, N_C is the respective carbon number and p_g is the chain growth probability.

The chain growth probability, p_g is defined as:

$$p_g = \frac{r_g}{r_g + r_d} \tag{2.5}$$

where r_g is the rate of chain growth and r_d is the rate of product desorption. The chain growth probability can be obtained from the slope of the straight line plot of the semi-logarithmic molar product distribution.

However, the actual Fischer-Tropsch product distribution often deviates from the ideal behaviour based on Anderson-Schulz-Flory kinetics. The molar methane content is often relatively high due to additional sites responsible for solely methane production (Schulz et al. 1995). A lower than expected molar C_2-content is observed due to ethene being very reactive in secondary FT reaction steps (Schulz and Claeys, 1999). A chain length depends on the chain growth probability, leading to a curved ASF distribution and higher formation of heavy products. Further chain growth is attributed to re-insertion of olefins which is due to carbon

number dependent solubility (Schulz and Claeys, 1999) or carbon number dependent diffusion rates (Iglesia et al, 1993) which lead to higher residence times of the longer chained olefins and therefore an increased chance for readsorption.

Factors influencing the FTS have opposing effects on methane selectivity and chain growth. Methane selectivity increases with increasing temperature and with an increase of the hydrogen to carbon monoxide ratio. The influence of total pressure is due to the combination of effects of individual partial pressures of feed and product gases.

2.4.1. Oxygenates Products

The FT reaction yields different products including oxygenates. Oxygenated compounds in the FT synthesis are produced as side products; typical up to 10 wt % of oxygenates can be formed in industrial processes (Dry, 1999). The synthesis of oxygenates in larger quantities has been of interest since they are of high value. Oxygenates are important chemicals especially C_2-oxygenates. C_{2+}-oxygenates can be used as additives (e.g ethanol) for improving gasoline octane value and burning efficiency (Yin, 2003), or as precursors in the chemical and pharmaceutical industry. Typically, in order to increase the selectivity of oxygenates, olefins are converted to oxygenated compounds by hydroformylation (Dry, 2002). The linear oxygenates have a selling price about six times higher than that of fuel (Dry, 2002). The oxygenates formed during FTS, alcohols, aldehydes, acids and ketones, have been shown to interact and interconvert rapidly with each other (Cairns, 2008).

2.5. Typical Fischer-Tropsch Synthesis Catalysts

All transition metals have the ability to catalyse the FT synthesis but only the four transition metals, nickel (Ni), ruthenium (Ru), iron (Fe), and cobalt (Co) have the required FT activity for industrial application (Dry, 2002). Nickel based catalysts are capable of producing high molecular hydrocarbons (Schulz, 1999). However, under FT conditions nickel is highly selective to methane, making it unsuitable (Dry, 1996). In addition, at lower temperatures and under high pressures used in FT, volatile nickel carbonyls are formed resulting in continuous loss of the catalyst from the reactors (Dry, 2001 and Dry, 2004a). Ruthenium is the most active FT catalyst as it produces the highest molecular weight hydrocarbons without the requirement of promoters and works at the lowest reaction temperature (Schulz, 1999). However, the availability of Ru is very limited and consequently is far too expensive for large scale industrial FT application (Dry, 2004a).

This leaves Co and Fe as the only practical catalysts available for commercial FT application. Cobalt-based catalysts are only employed in the LTFT process because hydrogenation activity of Co is higher than that of Fe and at higher temperatures excess methane and less olefins are produced (Dry, 2002). Cobalt catalysts are more active than their Fe counterparts and have longer lifetime (Dry, 2001). However, Co is very expensive so it is desirable to minimize the amount used in the catalyst while maintaining high activity and long effective catalyst life (Dry, 2004a). To achieve this, the Co is dispersed on a suitable high stable area support such as Al_2O_3 or SiO_2 (Dry, 2002). Syngas derived from natural gas is used when the Co-based catalysts are in employed in the FT process because Co catalysts are inactive for WGS and a hydrogen synthesis with H_2:CO ratio of about 2 is required for the FT process (Dry, 1981).

Iron catalysts are used for both HTFT and LTFT processes. The use of iron based catalyst is primarily due to the high availability of iron (Dry, 2004a). In addition, the Fe-based catalysts are usually prepared in the 'bulk' form because it is by far the cheapest (Dry, 2001). The lifetime of the Fe catalysts is very short compared to Co (Dry, 2001). Potassium promotion is required in iron based FT to attain high activity, stability and improve selectivity (Schulz, 1999). Syngas derived from coal gasification with lower H_2:CO is used when Fe catalysts are employed in the FT process because Fe is active for the WGS reaction in contrast to Co catalysts. Hydrogen is the main product in the WGS so it compensates for the insufficient hydrogen of the coal derived syngas (Dry, 1981).

Another metal that has been of interest for the FT synthesis is rhodium. This is because rhodium was discovered to display unique high selectivity towards oxygenates mainly C_2 oxygenates in the FT process which are valuable chemicals (Ojeda, 2004a). These valuable oxygenates include alcohols, acids, aldehydes, acetates. The catalytic conversion of syngas over a rhodium catalyst to selectively produce C_{2+} oxygenates was discovered in 1975 (Bhasin and O'Connor, 1975; Bhasin, 1975; Burch and Perch, 1992a). It is the only metal able to produce high selectivity of oxygenates amongst the typical FT catalysts. Usually FT catalysts (Co, Fe, Ru) favour the formation of hydrocarbon and only minor quantities of oxygenates are produced, up to 10 wt% in commercial processes (Dry, 1999). The difference in product selectivity has been attributed to differences in their capabilities to catalyse CO dissociation, hydrogenation and CO insertion (Chuang et al., 2005). Fe, Co, Ni and Ru exhibit excellent CO dissociation and hydrogenation activities producing hydrocarbons whereas Cu and Pd adsorb CO insertion forming methanol (Burch and Petch, 1992a; Chuang

et al., 2005). Rhodium, on the other hand, has the ability to catalyse CO dissociation and CO insertion and it is this unique characteristic which accounts for the selectivity of C_{2+}-oxygenates (Burch and Petch, 1992a). When Rh-based catalysts are used for the FT process, up to 60 wt % oxygenates are obtained (Xu et al., 2000; Tago et al., 2000; Hayashi et al., 2002a; Chen et al, 2006).

Vannice (1975) has attempted to compare the various metals (supported on γ-alumina) with respect to activity and selectivity in the FT CO hydrogenation. For methane formation the following activity sequence was reported Ru > Fe > Ni > Co > Rh. This does not take into account effects of crystallite size. More recently, Bligaard et al., (2004) reported the following activity sequence for methanation: Ru ≈ Co > Ni ≈ Fe ≈ Rh.

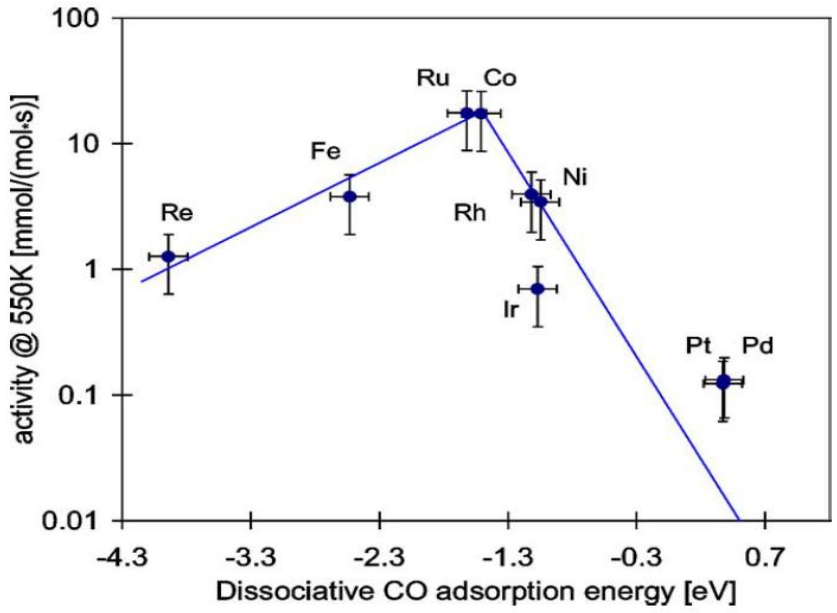

Figure 2.5: Activities of different supported transition metals as a function of the reaction energy for dissociative CO chemisorption (adapted from Bligaard et al., 2004)

On a metal basis the approximate relative costs of Fe:Co:Ni:Ru:Rh are 1:1000:250:50 000:700 000 (Dry, 2001). Therefore, due to the high cost of rhodium, it is very important to minimize the amount of the metal used. This can be achieved by maximizing the metal surface area through the use of very small rhodium nano crystallites, which are dispersed on highly porous support materials such as Al_2O_3 and SiO_2. Moreover promoters have been shown to affect the CO hydrogenation over Rh-based catalysts.

2.6. Promoters for Fischer-Tropsch Synthesis Catalysts

2.6.1. Structural Promoters

Structural promoters are also referred to as supports. Supports are typically micro porous metal oxides which have a high surface area and high thermal, chemical and mechanical stability. The primary functions of the catalyst support are to disperse the catalytically active phase and reduce sintering, enhance mechanical stability of the catalyst particle and minimize mass transport limitations (Dry, 1981). The most common materials used as supports are alumina, silica, titania, zirconia, magnesia and zeolites for FT processes.

The choice of support is very important as it has an effect on the activity and selectivity due to strong metal-support interactions (SMSI) (Dry, 1981). Supported catalysts with very strong support interaction tend to be reduced at higher temperatures than expected.

2.6.2. Chemical Promoters

The function of chemical promoters is to enhance the activity by chemical interaction with the metal and to improve catalyst selectivity. Chemical promoters facilitate the adsorption of and dissociation of CO by modifying the electronic properties of the catalyst active sites (Dry, 1981). Potassium is used as a chemical promoter for iron catalysts to improve the selectivity of the catalyst toward longer hydrocarbon chains and enhance the catalyst activity (de Smit, 2009).

2.6.3. Reduction Promoters

Reduction promoters improve the reducibility of the catalyst. After catalyst calcination, the oxides formed are exposed to hydrogen at elevated temperature in order to reduce them to their active metallic form. This is because generally, FT catalysts with high degrees of reduction are more active. However, such degrees of reduction can often only be achieved at higher temperatures where sintering becomes dominant, which leads to a loss of active metal surface area. The addition of a reduction promoter decreases the temperature required to reduce the metal oxide. This effect is explained by hydrogen spill-over from the easily reducing reduction promoter to the metal oxide (de Smit et al., 2010). Copper is generally used as a reduction promoter for iron FT catalysts (de Smit et al., 2010) whilst noble metals such as Pt, Pd or Ru are often used for cobalt based catalysts.

2.7. Promotional Effect of Iron on Rhodium-Based Catalysts for Fischer-Tropsch Synthesis

Fischer-Tropsch products highly depend on the nature of the catalyst. The activity and selectivity of the catalyst can be influenced by the size and shape of the metal crystallites, and by the choice of support and promoter. Generally smaller metal crystallites have a high metal surface area and ideally would expect to give high overall activity (on a mass basis) due to the large number of atoms available on the metal crystallite surface. However this is not the case, crystallites smaller than a certain size cause a decrease in activity. Ojeda et al. (2004a) showed that the smaller crystallites of rhodium displayed lower specific activity (lower turn-over frequency) and preferred formation of oxygenates. It is thought that enhanced oxygenate selectivity on small crystallites is due to reactions of CO-insertion which might preferably occur on metal sites with low coordination. These sites are found on corners and edges of small crystallites leading to oxygen containing products (Schulz et al., 2002).

Research on the high oxygenate selectivity of supported Rh catalysts has been of importance for some time. A considerable amount of research on rhodium catalyst has been undertaken. Ojeda et al. (2004a) studied the effect of rhodium nano-crystallites on CO hydrogenation using a reverse micelle method to synthesis the model catalysts. The catalysts were prepared with different particle sizes ranging from <5 to 30 nm and equal metal content of 2 wt%. CO conversion decreased as the rhodium particle size increased, however the catalytic activity per active site and time unit (turn-over frequency) increased with increased rhodium particle size. Product selectivity was also affected by the rhodium crystallite size. Methane selectivity increased on the smaller particles compared to larger particles (61.3 C% for particle of <5 nm compared to 42.7 C% for particle of 30 nm) as well as oxygenates selectivity (26.4 C% for particle of <5 nm compared to 17 C% for particle of 30 nm). Increased oxygenates formation was explained by the metal-support interaction which increases as the particle size decreases, leading to partially oxidised rhodium atoms.

Considerable efforts have been devoted to study the effect of crystallite size on Fischer-Tropsch synthesis. Mabaso (2005) and Barkhuizen et al. (2006) reported on iron, Bezemer et al. (2006) and Fischer (2011) on cobalt, Barkhuizen et al. (2006) and Welker (2007) on ruthenium catalysts. They all reported that crystallites below a certain metal crystallite size were less active for FTS than larger crystallites and display lower specific catalyst activity (TOF). Furthermore, they observed an increase in methane selectivity as well as the paraffin

to olefin ratio with smaller crystallites. The crystallite size effects have been attributed to a combination of structural and electronic effects as well as oxidation effects. Some complex reactions like FTS which comprises a large number of reaction steps require a minimum number of adjacent surface atoms, defined as "ensembles" in order for the reaction to take place (Bezemer et al., 2006; Welker, 2007). This is known as the Ensemble Theory. Small crystallites (below a minimum size) results in a decrease of the required ensembles, consequently displaying both lower selectivity and activity. Small crystallites are observed with high methane selectivity because methane formation is a simpler product and requires few sites or less number of atoms to take place. Schulz et al. (2002) proposed that FT reactions take place on different sites and that CO dissociation would preferentially occur on hole and valley sites of high coordination, chain growth would occur on peak sites and mountain sites of low coordination with several free valences for binding surface species and "ligands" and CO-insertion would take place on top sites of low coordination. Low coordination are preferably formed on small crystallites which explain high oxygenate selectivity on small crystallites. On smaller crystallites hydrogen dissociation is enhance but not the carbon monoxide dissociation which lead to enhanced availability of atomic hydrogen on the catalytic surface thereby increasing methane selectivity and lowering chain growth probability (Bezemer et al., 2006; Welker, 2007). Furthermore, smaller crystallites seem to be easier to oxidize than larger crystallites under Fischer-Tropsch conditions. van Steen et al. (2005) performed thermodynamic calculations on cobalt crystallites at a certain water to hydrogen ratio and observed that smaller crystallites are more likely to re-oxidize than larger crystallites. This has been shown on a theoretical level and this was recently confirmed experimentally by Fischer (2011) and Clapham (2012) using in-situ characterisation. In contrast to cobalt, in iron-based Fischer-Tropsch catalysts iron oxides are typically observed.

Various research studies on rhodium catalysts looked at different catalyst synthesis methods (impregnation and microemulsion) (Chen et al., 2006 and Hayashi et al., 2002a). Both papers investigated the effect of the catalyst preparation technique (impregnation and microemulsion) in CO hydrogenation. Catalysts were supported on silica in both papers. It was observed that the catalysts prepared using a microemulsion method selectively produced oxygenates while the catalyst prepared using impregnation was highly selective towards hydrocarbons formation. Chen et al. (2006) observed that catalyst prepared from a microemulsion gave high selectivity towards C_{2+} oxygenates (50.1 C%) while when using impregnation the catalyst displayed the lowest selectivity towards C_{2+} oxygenates (25.8 C%).

Hayashi et al. (2002a) showed that microemulsion prepared catalysts exhibit high selectivity towards C_{2+} oxygenates (33.3 C%) while catalysts prepared by impregnation gave high selectivity towards hydrocarbons (94.3 C%). The catalyst prepared using impregnation also displayed high selectivity towards methane. This was attributed to the different electronic state of rhodium metals existing in microemulsion and impregnation catalysts which was due to the difference in the interaction between rhodium metals and support. The electronic state of rhodium metals in the impregnation catalyst was compared to that of rhodium metals in the microemulsion catalyst by means of X-ray photoelectron spectroscopy (Hayashi et al., 2002a). It was found that the rhodium metals existed as Rh^0 in the impregnation catalyst whereas in the microemulsion catalyst existed as Rh^+. Furthermore, IR spectra of chemisorbed CO on the microemulsion and impregnation catalysts were reported. Rhodium ability to chemisorb CO was reported to be dependent on the electronic state of rhodium and thus becomes weak as the electron density on rhodium particles decreases (Loannides and Verykios, 1993). Impregnation catalyst was reported to strongly chemisorb CO, in which metal exist as Rh^o resulting to small quantity of H_2 adsorption whereas rhodium particles chemisorb H_2 enough to promote the surface reaction with CO on the microemulsion catalyst which exists as Rh^+ (Hayashi et al., 2002a). The insertion of CO into alkyl group on Rh metals is known to be promoted as the electron density on Rh metals decreases (Hayashi et al., 2002a; Ojeda et al., 2004b). The density of Rh^+ species was higher for the microemulsion catalyst, as a result promoted the insertion of CO into alkyl group leading to a high selectivity of oxygenates. Therefore the technique used to prepare the catalyst is of importance in CO hydrogenation.

CO hydrogenation over rhodium catalysts can result in a wide range of different products; methane, C_{2+} hydrocarbons as well as oxygenates such as methanol, ethanol, acetaldehyde and acetic acid. The activity and selectivity of rhodium catalysts can be significantly altered by many parameters including choice of support and promoters used. Addition of promoters such as oxides of Fe, Mn, Ce, Li and La on supported rhodium catalysts favour the formation of mainly C_2 oxygenates (Burch and Petch, 1992b). Depending on the choice of promoter it is possible to adjust the selectivity to a specific oxygenate (acetic acid, acetaldehyde or ethanol) (Burch and Petch, 1992b).

Iron was one of the first elements to be investigated as a promoter for rhodium (Bhasin et al., 1978). Addition of iron to the rhodium catalysts has been observed to drastically increase the selectivity of oxygenates especially ethanol (Bhasin et al., 1978; Fukushima et al., 1985;

Burch and Petch, 1992a; Guglielminotti et al., 1995; Schunemann et al., 1995; Burch and Hayes, 1997; Haider et al., 2009; Mo et al., 2009a).

Bhasin et al. (1978) published a study on the effect of iron over supported rhodium catalysts on the FT activity and selectivity. The catalysts were prepared by incipient wetness impregnation with constant rhodium loading of 2.5 wt % and iron loadings which varied from 0.05 to 0.5 wt %. The reaction was carried out at temperatures ranging from 200 to 350°C and at pressure ranging from 25 to 200 bar using H_2:CO ratios ranging from 1:10 to 10:1. The authors observed that the addition of even a small amount of iron affected the selectivity, resulting in an increase in the production of ethanol and virtually no acetic acid and acetaldehyde production (see Table 2.1). The methane selectivity also dropped slightly and methanol became a major product. The results showed no change in catalytic activity when iron was added.

Table 2.1: Effects of iron addition on the activity and selectivity of rhodium-based catalysts for CO hydrogenation

Catalyst	**CO (%)**	**CH_4**	**MeOH**	**AcH**	**EtOH**	**AcOH**	**C_{2+} Oxy (C%)**
[a] 2.5% Rh/SiO_2	2.0	55.6	1.70	16.0	11.5	11.2	38.7
2.5%Rh-0.1%Fe/SiO_2	4.2	49.6	5.60	2.60	33.6	6.50	42.7
[b] 2% Rh/SiO_2	0.84	40.0	0	19.0	0.50	7.40	29.8
2%Rh-1%Fe/SiO_2	1.76	35.0	18.0	0.60	37.0	0	39.0

[a] Bhasin et al. 1978: Temperature = 300°C, Pressure =10 bar, H_2:CO = 1

[b] Burch and Petch, 1992a: Temperature = 250°C, Pressure = 20 bar, H_2:CO = 1

MeOH = methanol, AcH = acetaldehyde, EtOH = ethanol, AcOH = acetic acid, C_{2+} oxy = total C_{2+} oxygenates.

In 1992a Burch and Petch investigated the synthesis of oxygenates from syngas on supported rhodium catalysts. The objective of the research was to investigate the role of promoters in the synthesis of oxygenates over rhodium based catalysts. The promoters studied contained elements such as Fe, Mn, Ce, Li and Ir. All catalysts were prepared by wet co-impregnation. The reaction was carried out at temperatures ranging from 210 to 300°C and at a pressure of 20 bar using H_2/CO of 1. It was observed that the promoters affected the product distribution

of oxygenates. Reducible oxide promoters (Fe, Mn, Ce) were observed to improve the ethanol selectivity with the complete elimination of acetic acid and reduced selectivity of acetaldehyde (see Table 2.1). It was further reported that the addition of Fe resulted in an increase in activity while Mn hardly affected the activity of the catalyst and Ce caused catalyst deactivation. Iridium was found to have only a small effect on either the activity or selectivity of the catalyst.

Furthermore it was reported that the addition of alkali promoter (Li) to rhodium catalysts resulted in high selectivity of acetaldehyde and acetic acid, however, it inhibited the activity of rhodium and gave a low selectivity to methane. Reducible oxide promoters (Fe, Mn, Ce) function by enhancing availability of hydrogen on the catalyst surface and increase the stability of the acetyl species (proposed intermediate for the formation C_2 oxygenates), thus allowing time for their hydrogenation to ethanol instead of desorption to acetaldehyde. Alkali promoter (Li) decreased the hydrogenation ability of rhodium thereby suppressing the methane formation and resulting in high selectivity of acetaldehyde and acetic acid. Furthermore, lithium partial blocked rhodium surface, thereby inhibiting reaction steps like CO dissociation that requires large ensembles of atoms (Egbebi et al., 2010) leading to high selectivity of oxygenates. In this paper, it is clear that promoters on supported rhodium catalysts can be added to produce a high selectivity of a specific oxygenate especially C_2 oxygenates.

In a study by Schunemann et al. (1995) iron promoted rhodium clusters in zeolite NaY were characterised and tested in CO hydrogenation. All catalysts were synthesised by ion-exchange. The catalysts were tested at 10 bar, 250°C and H_2/CO of 2. It was reported that rhodium was reduced to metallic form and iron existed in two electronic states i.e. Fe^0 and Fe^{2+}. Metallic iron (Fe^0) formed an alloy with metallic rhodium and was thought to be the reason for the increase in activity. Again, as reported in other studies, addition of iron increased the selectivity towards oxygenates, in particular ethanol. Enhanced oxygenates were suggested to be due to the formation of Fe^{2+} species in close contact with Rh particles.

A study by Burch and Hayes (1997) investigated the effect of iron loading on catalytic activity and selectivity on an alumina-supported Rh catalyst in CO hydrogenation. Again, the catalysts were prepared by impregnation. The impregnation step of iron promoter and rhodium active phase on the support was of importance in order to optimise a close interaction between promoter and active rhodium resulting to the development of a catalyst

selective to produce high selectivity of oxygenates. The iron oxide promoter was firstly deposited onto the γ-alumina. Alumina-supported iron oxide promoter systems were then dried at 120°C overnight and finally calcined in a muffle furnace in air at 400°C for 4 hours. Lastly rhodium precursor was deposited onto the promoter oxide-support phase catalysts. The catalysts prepared with both the promoter and active phase were dried in a 120°C oven overnight and finally air calcined at 500°C for 4 hours. γ-Alumina support was used because it possesses a high density of reactive surface hydroxyl groups and could produce a close packed monolayer of the supported iron oxide phase which would be beneficial to enhance the close interaction between iron oxide and rhodium (active phase). Wachs et al. (1993) showed that monolayer of the alumina support would occur at a level equivalent to 0.58 mmol of deposited metal oxide per 100 m^2 of support. This is then equivalent to 17 wt % of Fe_2O_3 or 11.7 wt % Fe and therefore high loading of promoter were essential in order to result with the desired interaction between active phase and promoter. Catalysts containing a constant nominal rhodium surface loading of 2 wt % and nominal surface iron loadings which varied from 0 to 14 wt % were prepared. The catalysts were tested at 10 bar, 270°C and H_2/CO of 1. It was shown that the activity of the catalysts increased with promoter loading up to a maximum value which is suggested to occur when the promoter coverage approaches a monolayer. Increasing the promoter loading further was reported to result in decrease in the overall catalytic activity. Increased ethanol selectivity at the expense of methane selectivity was observed with increase in iron loading. This was suggested to be due to the increase in the number of active sites for oxygenate formation on the catalyst surface. Again up to a maximum iron loading was beneficial for oxygenate synthesis. The authors concluded that the increase in activity and oxygenate selectivity with increase in iron loading could be due to the intimate contact between rhodium and iron. They achieved 50 C % ethanol selectivity with an alumina-supported rhodium catalyst containing 2 wt % rhodium and promoted by 10 wt % iron.

It is widely accepted that the mechanism for the formation of C_{2+} oxygenates requires dissociative adsorption of CO and H_2 to produce CH_x species followed by alkyl chain growth through the addition of a CH_2 species and CO insertion into the CH_x species (Trevino et al., 1995). A considerable amount of research has been undertaken in order to study the mechanism of ethanol formation (Burch and Petch, 1992b; Burch and Petch, 1992c and Chuang et al., 2005). It is still not clear whether ethanol is formed as a primary product from syngas or as a secondary product by hydrogenation of acetaldehyde. Understanding the

mechanism for the ethanol formation will help explain the role of the iron promoter on supported rhodium catalysts. Burch and Petch, 1992b reported that formation of acetaldehyde with low ethanol production is favoured over unpromoted catalysts while the addition of iron favoured the formation of ethanol with low production of acetaldehyde. C_2 oxygenates (acetaldehyde and ethanol) have been suggested from literature to form from an adsorbed acetyl intermediate (Fukushima et al., 1985; Burch and Petch, 1992b; and Haider et al., 2009, Mo et al., 2009a). The presence of iron as promoter was proposed to increase the stability of the acetyl intermediate, thus enhancing hydrogenation to ethanol instead of desorption to acetaldehyde (Fukushima et al., 1985; Burch and Petch, 1992b; Burch an Hayes, 1997; Haider et al., 2009, Mo et al., 2009a). An alternative explanation for the increase in ethanol selectivity when iron was added to supported rhodium catalysts was that iron served as a H_2 reservoir to increase hydrogen availability (Burch and Petch, 1992a and b; Mo et al., 2009a).

In most of the research that has been conducted on the effect of iron promoter over supported rhodium catalysts little has been reported about the crystallite sizes and distribution of the model catalysts. It is crucial for the investigation of iron promoter effects on the supported rhodium that all catalysts prepared have similar crystallite sizes with narrow distributions.

2.7.1. Formation of Bimetallic Nanoparticles

Bimetallic nanoparticles in the form of alloy, core-shell or monometallic mixtures structures have received much attentions because combination of two different metallic elements, have been reported to enhance catalytic activity, selectivity and stability as well as reduce cost by mixing precious metal with inexpensive metals (Kim et al., 2007). Depending on the preparation route, miscibility and reduction kinetics of metal ions the bimetallic nanoparticles will either be in a core-shell or alloy form (Tojo et al., 2009).

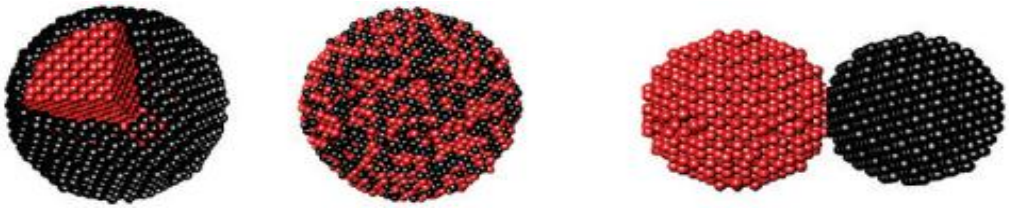

Core/Shell	Alloys	Aggregate mixtures
Ru@Pt	RuPt (1:1) alloy	Ru + Pt monometallic nanoparticles

Figure 2.6: Schematic diagram of bimetallic nanoparticles in different structures such as alloys, core/shell or monometallic nanoparticles (adapted from Alayoglu, et al., 2009)

Alloys contain two or more metals and can form a homogeneous alloy or surface segregation (Ponec, 2001). Furthermore the alloy system is also affected by the size and sign of the mixing enthalpy change (Ponec, 2001). When alloying two metals, one metal is usually active while the other metal is virtually inactive under the experimental conditions. Alloys improve catalytic activity and selectivity of the catalyst because of the electronic interaction between the metals (Burch, 1982).

The Rh-Fe bimetallic system has been of interest because it was reported that it can produce a mixture of methanol and ethanol with a high selectivity in FTS, while rhodium catalyst give a mixture of acetaldehyde and acetic acid (Ichikawa et al., 1986). It is very important to understand the modifying role of the iron in the supported Rh catalyst. Techniques such as EXAFS, in-situ Mössbauer etc. have been applied in order to obtain information about chemical state of iron which would help to explain the enhanced selectivity of methanol and ethanol (van't Blik et al., 1984; Minai et al., 1984; Ichikawa et al., 1986). Minai et al. (1984) reported that iron on the silica support existed either as Fe^0 in the Rh-Fe alloy or as Fe^{3+} in the Rh-Fe metal cluster compounds. It was found that Fe^{3+}/Fe^0 ratio depended on the Fe/Rh atomic ratio in the catalysts. It was reported that the Fe^{3+}/Fe^0 ratio decreased with increase in the Fe/Rh ratio. This was then related to the increase in methanol formation which implies that Fe^0 fraction as Rh-Fe alloy in the Rh-Fe catalyst may be responsible for the formation of active sizes which favour the formation of methanol. Ichikawa et al. (1986) also reported the same findings that catalyst of a low Fe/Rh, Fe atoms are mostly present in the state of Fe^{3+} while the fraction of Fe^0 increases with increase of the Fe/Rh ratio.

Swartzendruber, (1984) reported the Rh-Fe alloy system. The equilibrium phase of the Fe-Rh system is shown in Figure 2.7. It can been seen from the diagram that depending on the composition of rhodium in the Fe-Rh alloy system as well as the temperature that the crystal structure of the alloy can be determined.

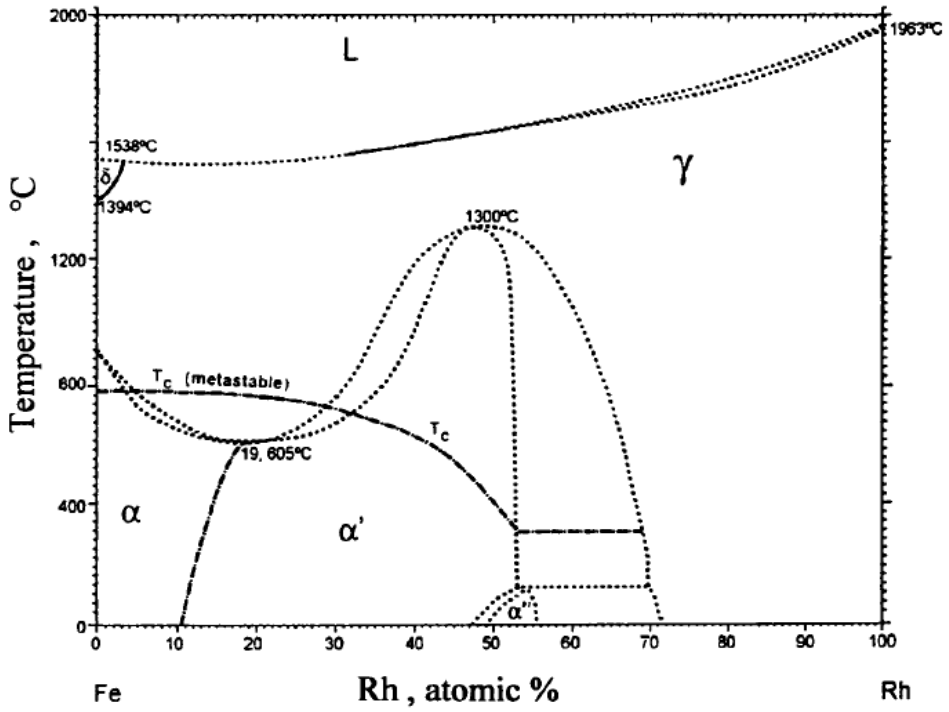

α – low temperature bcc phase, α' – ordered phase with CsCl structure, γ – fcc phase, δ – high temperature bcc phase, L – liquid

Figure 2.7: The Fe-Rh equilibrium phase diagram (adapted from Swartzendruber, 1984)

2.8. Conventional Catalyst Preparation Methods

There are two methods used on a commercial scale to prepare FT catalysts namely impregnation and precipitation.

2.8.1. Impregnation

Impregnation is the most commonly used method to prepare catalysts due to its simplicity and ease (Huang and Schwarz, 1987). In this technique a support is first selected based on its desired specification, size and shape (Mabaso, 2005). The most important desired specification of a support is high surface area to create small metal particles with a large surface area. The porous support is contacted with a solution containing the catalyst precursor. The amount of water used to dissolve the metal salt as the catalyst precursor equals the amount of water needed to fill the pores of the support completely ("incipient wetness"). Therefore, the amount of water to be used depends on the pore volume of the support material. During impregnation, the catalytically active species is transported onto the support.

The solvent (water) is then removed by evaporation or calcination leaving the oxidic metal precursor in the pores of the support.

It is not easy to prepare catalysts with high metal loadings and to obtain good dispersion of the metal on the surface of the support (Dry, 1981) using impregnation. Therefore, this method is not suitable for the preparation of catalysts required for this work because the crystallite size is not easily tunable and it is quite difficult to obtain a narrow crystallite size distribution.

2.8.2. Precipitation

In the precipitation method, the precursors of the active metals are dissolved in a solvent such as water to form a homogeneous solution (Dry, 1981). The pH of the solution is then adjusted to force the metal ions to precipitate. The pH adjustment can either be done in the presence of a support material or the support material can be formed via co-precipitation (Dry, 1981). In the co-precipitation method, the support material is formed via a simultaneous precipitation with the corresponding precursor or metal salt (Dry, 1981). This method generally yields much smaller metal crystallites on the support compared to catalysts prepared using the impregnation method (Reuel and Bartholomew, 1984). When using the precipitation method it is also possible to prepare catalysts with a high metal loading and obtain better dispersion of the metal on the surface of the support (Reuel and Bartholomew, 1984). However, it is not easy to control the crystallite size which is very important when preparing the catalysts required in this work.

2.9. Microemulsion

Schulman and Friend first defined the term microemulsion in 1949 (Eriksson et al., 2004). Gault, in collaboration with Friberg, came up with the idea of using microemulsion systems for catalyst preparation (Eriksson et al., 2004). Boutonnet et al. in 1982 were the first to report the preparation of metal nanoparticles using the microemulsion technique (Eriksson et al., 2004). The microemulsion technique is expected to produce small nanoparticles of narrow size distribution and allows for better control of particles size as well as bimetallic particles of controlled composition by varying the composition of the microemulsion due to the specific structure of a microemulsion (Eriksson et al., 2004).

2.9.1. The Microemulsion System

A microemulsion is a thermodynamically stable, optically isotropic system consisting of two immiscible liquids such as water and oil stabilised by the presence of a surfactant (amphiphile) and, in some cases, a co-surfactant. The surfactants are molecules that possess polar heads and non-polar tails (Figure 2.8). The polar head of the surfactant is hydrophilic and interacts strongly with the hydrophilic phase (water), and the non-polar tail is hydrophobic and interacts with the hydrophobic phase (oil) (Capek, 2004). There are three types of surfactants, namely ionic, non-ionic and amphoteric. The most commonly used surfactants to prepare microemulsion systems are sodium bis(2-ethylhexyl) sulfosuccinate (AOT), sodium dodecyl sulphate (SDS) and cetyltrimethyl ammonium bromide (CTAB). However, these ionic surfactants contain sodium and sulphur which can have negative effects on the resulting catalyst. These components may affect the catalyst performance or even poison the catalyst if not removed effectively. As an alternative, non-ionic surfactants are often used instead. Sometimes co-surfactants are added to modify the rigidity of the micelle core, thus allowing for modification of transport processes through the core (Stenius et al., 1984; Boutonnet et al., 1987).

A microemulsion looks like a homogeneous solution at macroscopic scale while at molecular scale it appears to be heterogeneous. Different types of microemulsion are known such as water-in-oil (w/o) and oil-in-water (o/w). The type of microemulsion at a given temperature is determined by the ratio of its constituents. At high water concentration, the internal structure of the microemulsion consists of small oil droplets in a continuous water phase (Figure 2.8). This system called oil-in-water is also referred to as normal micelles. The oil droplets are stabilized with the non-polar tail of the surfactant. As the concentration of oil increases, a bicontinuous phase without any clearly defined shape is formed. At high oil concentration, the bicontinuous phase is transformed into a structure of small droplets in a continuous oil phase (Figure 2.8). This system is called water-in-oil also referred to as reverse micelles. The water droplets are stabilized by the polar head of the surfactant.

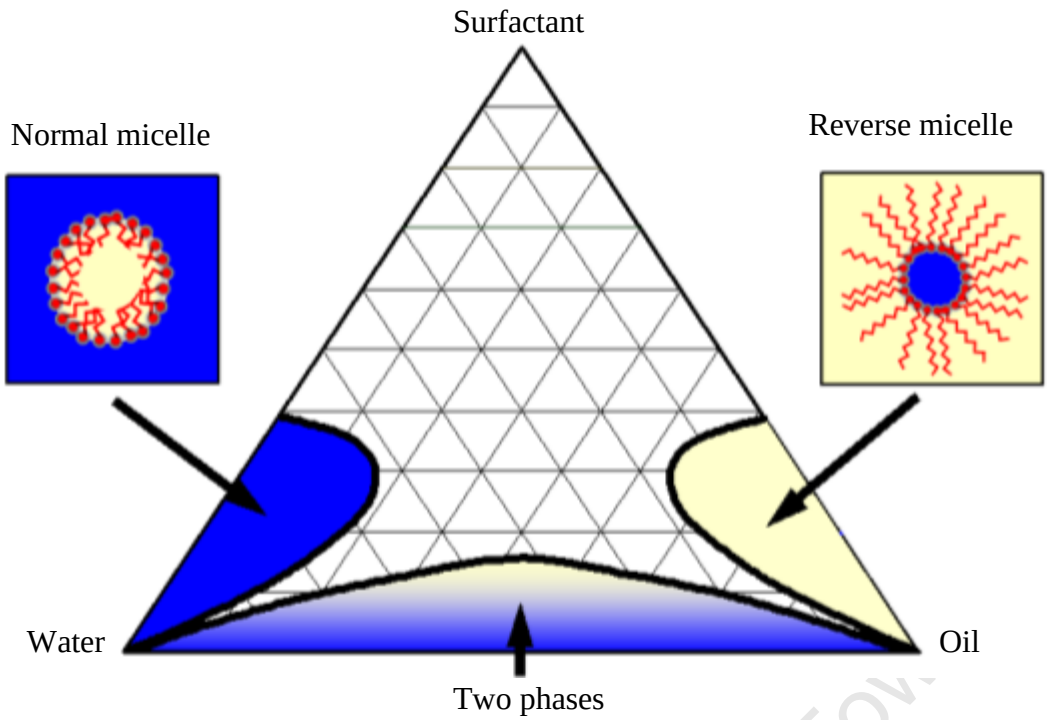

Figure 2.8: Schematic phase diagram of surfactant-oil-water system (adapted from Mabaso, 2005)

The systems are very sensitive with respect to temperature, particularly in the case of non-ionic surfactants. Increasing the temperature will destroy the oil droplets while the water droplets will be destroyed by a temperature decrease (Eriksson et al., 2004).

2.9.2. Preparation of Nanoparticles

Reverse micelles have an internal structure consisting of small water droplets. Therefore, this makes them well suited for the preparation of nano-sized particles. The water soluble metal salt can be dissolved in water and added onto the oil phase containing surfactant forming reverse micelles.

There are two common ways of preparation in order to obtain nano-particles from reverse micelle solutions. The first preparation of nano-particles occurs by mixing two reverse micelle solutions, one containing the metal salt (precursor) in the aqueous phase and the other the precipitating or reducing agent (Eriksson et al., 2004). After mixing the reverse micelle solutions containing metal salt and precipitating or reducing agent, the reactants collide with each other due to the collision and coalescence of the water droplets and a precipitate forms (Eriksson et al., 2004; Capek, 2004). A schematic picture of this process is shown in Figure 2.9.

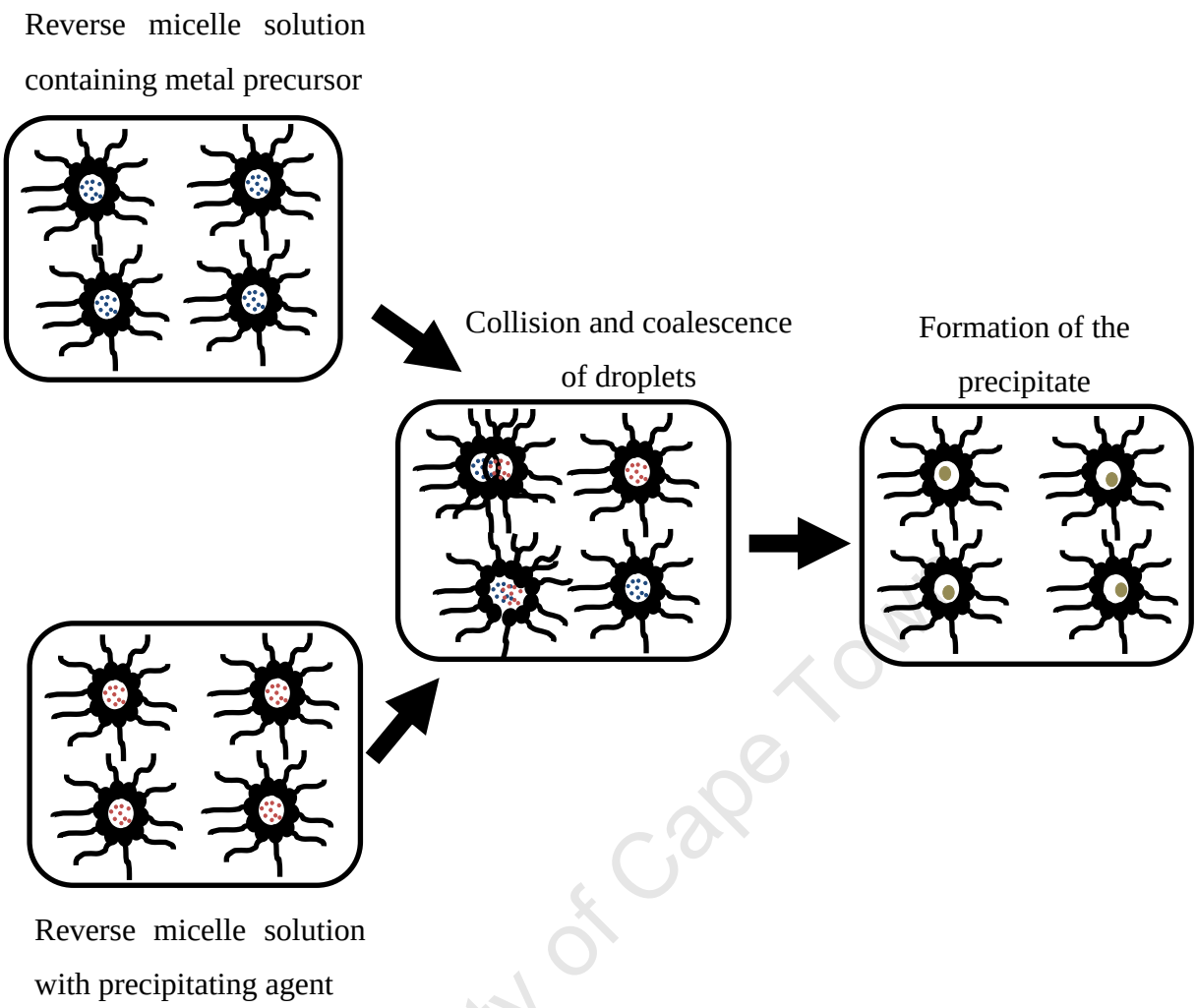

Figure 2.9: Schematic representation of the preparation of nano-particles using two reverse micelle solutions; one containing the metal precursor in the aqueous phase, the other the precipitating or reducing agent (adapted from Eriksson et al., 2004)

Another method used to obtain nano particles from the reverse micelle solution is the direct addition of the precipitating or reducing agent to the reverse micelle solution containing the dissolved metal precursor (Eriksson et al., 2004). A schematic picture of this process is shown in Figure 2.10.

In both nano-particle preparation methods, the water droplets containing the metal salt are surrounded by surfactant molecules (Ojeda et al., 2004a). These surfactant stabilised water droplets can be pictured as nano-reactors preventing the excess aggregation of the particles. The size of the final precipitated nano-particles will depend on the size of the water droplets in the reverse micelles (Eriksson et al., 2004). Mabaso (2005) found a linear relationship of crystallite size with water to surfactant ratio. Ojeda et al. (2004a) found that the water to

surfactant ratio is not the only factor governing the particle size. They considered the surfactant to oil ratio and found that the particle size decreased with decreasing water to surfactant ratio for a fixed surfactant to oil ratio.

The reverse micelle system is dynamic, meaning that during the formation of particles a constant collision of aggregates takes place. The formation of particles proceeds in two steps; nucleation followed by growth. The growth rate is controlled by the presence of the surfactant which sterically prevents the nuclei from growing rapidly and, consequently, favours the formation of particles of homogeneous size distribution (Eriksson et al., 2004).

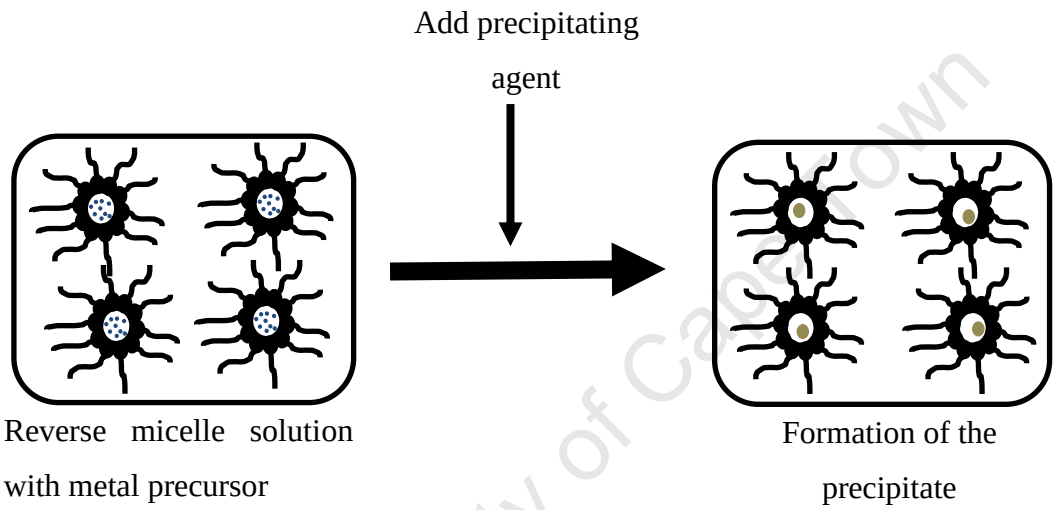

Figure 2.10: Schematic representation of the preparation of nano-particles by direct addition of precipitating or reducing agent to a reverse micelle solution containing the dissolved metal precursor (adapted from Eriksson et al., 2004)

Parameters influencing the crystallite size and crystallite size distribution are the reaction time, the chemical nature of the precursor, the constituents of the micelle system and their composition as well as the subsequent drying or calcination conditions (Boutonnet et al., 1982).

The use of reverse micelle to prepare supported nano-particles is of importance. This technique is suitable for the preparation of catalysts with controllable crystallite size, a narrow size distribution and good dispersion of the metal crystallites onto the support material. The reverse micelle containing nano-particles is a very stable solution and, therefore, it is a challenge to separate the particles from the constituents of the reverse micelle, especially from the surfactant as its molecules are strongly adsorbed onto the

particles **(**Eriksson et al., 2004). In order to obtain the homogenous supported catalyst when transferring the particles onto support it is necessary to maintain the homogeneous distribution. Several approaches to deposit the precipitate on the support have been reported. One approach to prepare supported nano-particles is to form the support in situ through co-precipitation with a support precursor material (Kishida et al., 1996; Hayishi et al., 2002b). However, this can lead to an encapsulation of the active metal crystallites by the support material and therefore a loss in catalyst activity. A second approach is the pre-synthesized support can be mixed with reverse micelle solution after nano-particle precipitate formation while the reverse micelle system is still intact. This is then followed by the breakage of the reverse micelles causing the nano-particles to settle onto the support (Mabaso, 2005). In the final approach the support is added directly in the reverse micelle solution containing metal precursor without precipitating the metal salt at all. The active metal precursor is deposited onto the support via interionic interaction followed by the reverse micelle break up **(**Eriksson et al., 2004; Welker, 2007). The problem with the last two approaches is that some of the particles may not be deposited onto the support and the desired metal loading is not achieved.

Studies to investigate the effect of crystallite size in FTS have been done using reverse micelles. Ojeda et al. (2004a) worked on rhodium, Mabaso (2005) on iron, Welker (2007) on ruthenium and Fischer (2011); Fischer et al. (2013) on cobalt catalysts. Although reverse micelles have been substantially researched to prepare nanoparticles, there are few studies on the preparation of bimetallic nanoparticles. Bimetallic nanoparticles in the form of either alloys or core-shell nanostructures have received significant attention because combination of two kinds of metals can results to improve catalytic activity, selectivity and stability as well as to reduce the cost of precious metals such as platinum (Kim et al., 2007). Various preparation methods of bimetallic nanoparticles have been employed because preparation route is very crucial. It is of great difficulty to synthesize bimetallic nanoparticles with controlled nanoparticle size, composition and structure (Tojo et al., 2009). Impregnation/deposition methods are usually employed for the synthesis of bimetallic nanoparticles catalysts and often results to well-dispersed, highly active systems, but it is very difficult to control structure, composition as well as obtain nanoparticles of narrow size distribution (Alayoglu et al., 2009). The preparation of Pt-Ru (Liu, Z et al., 2002; Kim et al., 2007), Pt-Cu (Weihua et al., 2006), Au-Ag (Chen and Chen, 2002) have been researched using reverse micelles. The reverse micelle method was suitable to prepare bimetallic nanoparticles with a narrow distribution, controlled size, composition and morphology of

nanoparticle due to the specific structure of reverse micelles (Kim et al., 2007). However, no studies have been undertaken to research the preparation of iron-rhodium bimetallic nanoparticles using reverse micelles. This method is suitable for the preparation of model catalysts required for this study.

3. Experimental Methodology

3.1. Materials used for Model Catalyst Preparation

List of all the chemicals used in the study for model catalyst preparation (see Table 3.1).

Table 3.1: Chemicals used to prepare model catalysts

Chemical	Information
Acetone	Kimix (99.5 % purity)
γ-Alumina	Puralox (Batch 9574), SCCa 5-150
	Sasol Germany, SBET = 162 m^2/g
	Average pore diameter = 115 Å
Ammonium hydroxide	Kimix (25 % purity)
n-Hexane	Kimix (96 % purity)
Iron (III) nitrate. $9H_2O$	Sigma-Aldrich Inc. (99 % purity)
Penta-ethyleneglycol-dodecylether, Berol 050	Akzo Nobel
Rhodium (III) nitrate. $6H_2O$	Strem Chemicals (10 wt % Rh)

3.2. Catalyst Preparation

The reverse micelle technique was used to prepare supported model catalysts with similar crystallite sizes.

3.2.1. Synthesis of Supported Model Catalysts Using Reverse Micelles

This study investigates the effect of iron loading on porous alumina-supported rhodium catalysts on the activity and selectivity in the FT synthesis. The catalysts were prepared using the reverse micelle technique and contained rhodium (10 wt %) with varying iron loadings (see Table 3.2). A reference catalyst containing 10 wt % iron, but no rhodium, prepared using the same procedure was also included in the study. Model catalysts were required to have similar crystallite sizes with narrow crystallite size distribution.

The reverse micelle system is made up of three phases; an aqueous phase, organic phase and a surfactant. Berol 050 (Penta-ethylneglycol-dodecylether) was used as the surfactant, the organic phase was n-hexane and the aqueous phase was a solution of the nitrate salt. The

reverse micelle solution was formed at room temperature by mixing n-hexane and Berol 050 in an Erlenmeyer flask and leaving the solution for 24 hours to stabilise. The aqueous metal salt solution was then added into the mixture under stirring for 2 hours at room temperature. The metal salt used when preparing rhodium crystallites was rhodium nitrate ($Rh(NO_3)_3.6H_2O$, 0.5M), when preparing the iron crystallites was iron nitrate ($Fe(NO_3)_3.9H_2O$, 0.5M) and both nitrates when preparing rhodium crystallites modified with iron. Three iron promoted on the alumina-supported rhodium catalysts, having an Rh:Fe atomic ratio of 0.1-1 were prepared. The catalyst of a low Rh:Fe ratio (Rh:Fe = 1:0.1), intermediate Rh:Fe ratio (Rh:Fe = 1:0.5) as well as higher Rh:Fe ratio (Rh:Fe = 1:1). These ratios were chosen because Ichikawa et al. (1986) reported that depending on the Rh:Fe ratio, Fe atoms are present in different chemical states. Depending on the content of iron on the catalysts, different results on the activity and selectivity were observed. The mixture was then left for another 24 hours in order to allow for the formation of stable reverse micelles. The ternary diagram (Figure 2.5) established by Targos, (1987) and Mabaso, (2005) was used to determine the amounts of Berol 050, n-hexane and water required to remain within the stability region of reverse micelle. In order to obtain a similar final size of crystallites of the catalysts the water to surfactant ratio and oil to surfactant ratio were kept constant. A precipitating agent (sodium hydroxide 25%) was then added drop wise to the reverse micelle solution and stirred for an hour. At this point in the preparation the rhodium containing solution changed colour from yellow to a yellow-orange; the iron containing solution from orange to a yellow-orange and the rhodium with iron containing solution from yellowish to brown-blackish depending on the loading of iron in the catalyst. The γ alumina support was added into the mixture and stirred for 2 hours resulting in the deposition of the precipitate onto the support. The reverse micelle solution slightly discoloured after the addition of support which is a result of the uptake of the metal salt. Acetone was then added drop wise to the solution while stirring in order to break the micelles. After decanting, the resulting precipitate on alumina was washed several times with acetone to remove residual surfactant.

The rhodium loading was kept constant at 10 wt % for all the model catalysts. The iron loading depended on the molar ratio of rhodium to iron. Table 3.2 lists compositions of the reverse micelles created, anticipated loadings and molar ratios of rhodium: iron of the model catalysts. The catalysts were numbered/labelled according to the rhodium: iron molar ratio i.e. the rhodium catalyst without iron was the first and the last was the iron catalyst without rhodium.

Table 3.2: Composition of the reverse micelles created, anticipated loadings and molar ratio of Rh:Fe of the model catalysts

Sample Code	Rh (wt %)	Fe (wt %)	Rh:Fe (molar)	H_2O (g)	Berol 050 (g)	Hexane (g)	Al_2O_3 (g)	w/s
Rh/Al_2O_3	10	-	1:0	5.83	29.2	156	2.7	0.2
Rh1Fe0.1	10	0.54	1:0.1	6.40	32.0	172	2.68	0.2
Rh1Fe0.5	10	2.7	1:0.5	8.75	43.8	235	2.62	0.2
Rh1Fe1	10	5.4	1:1	11.7	58.3	312	2.54	0.2
Fe/Al_2O_3	-	10	0:1	10.7	53.7	288	2.7	0.2

After decanting the residual acetone, the solid was dried at room temperature overnight and then in the oven at 120°C for 24 hours. Finally all catalysts were calcined in a fluidized bed reactor in 30 ml(NTP)/min air at 300°C with a temperature ramp of 2°C/min for 16 hours and further reduced in 50 ml(NTP)/min H_2 at 500°C with a temperature ramp of 1°C/min for 2 hours to form the activated metallic phase and passivated with CO_2 for minimum of 2 hrs at room temperature. The high reduction temperature was selected from TPR experiments (data shown later), where reduction of iron oxide to metallic iron was around 500°C.

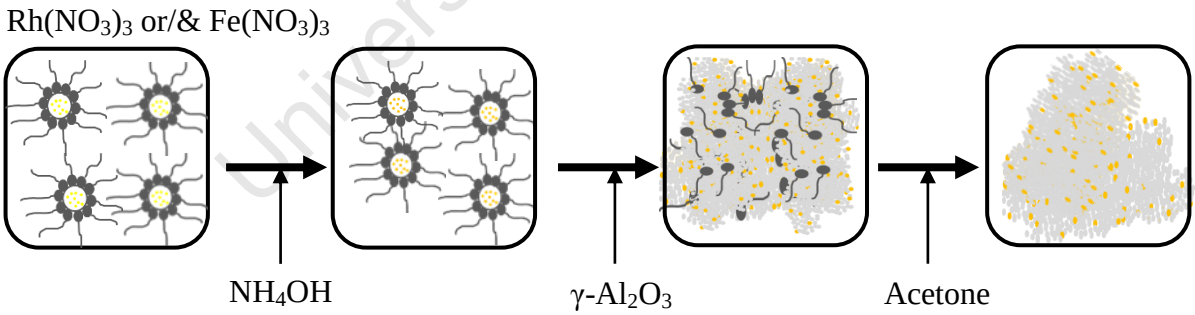

Figure 3.1: Schematic representation of catalyst preparation by direct addition of precipitating agent to a reverse micelle solution containing the dissolved metal salt, followed by support addition

3.3. Catalyst Characterization of Supported Model Catalysts

3.3.1. Transmission Electron Microscopy (TEM)

The average crystallite sizes and crystallite size distributions of the calcined and reduced supported catalysts were determined using Transmission Electron Microscopy (TEM). Two different instruments were used. A FEI Technai G20 operating at 200kV was used to determine the size distributions and crystallite sizes of the model catalysts. A high resolution TEM (HRTEM) equipped with a field emission gun as electron source (FEI Technai F20) operated at 200kV was also used as it allowed for studies using scanning transmission electron microscopy (STEM) and energy dispersive X-ray spectroscopy (EDX) which was used to identify rhodium and iron species on the alumina support and to determine the extent of the interaction of the metals. The sample preparation for TEM analysis begins by ultrasonically suspending sample powders in methanol. A drop of each sample was applied to a carbon film supported by a copper grid and then dried under a Xenon lamp before viewing in the microscope. Digital photos of the model catalysts were taken and later studied using software Image J for crystallite size analysis. A minimum of 150 crystallites was measured per sample in order to obtain the crystallite size distribution and the average crystallite size.

The mean volume diameter of a crystallite distribution was determined using equation 3.1 in order to compare with the XRD data which is sensitive to the volume of crystallites (Bergeret and Gallezot, 1997).

$$d_{C,V-TEM} = \frac{\sum n_i d_{c,1-TEM}^4}{\sum n_i d_{c,1-TEM}^3} \quad (3.1)$$

with $d_{c,l-TEM}$ the crystallite diameter as obtained from TEM micrographs.

3.3.2. X-ray Diffraction Spectroscopy (XRD)

X-ray Diffraction Spectroscopy measurements were carried out in a Bruker D8 Advance laboratory X-ray diffractometer equipped with a cobalt source (λ = 1.78897Å) and a position sensitive detector (Bruker Vantec). The diffractograms of the samples were recorded from 10˚ to 90˚ 2θ with step size of 0.0122°/s. X-ray analysis was used to analyse the crystalline phases and the average crystallite sizes of the calcined, reduced and spent samples. Diffraction peaks of crystalline phases were compared with those of standard compounds reported in the JCPDS data files. The average crystallite sizes were calculated from peak broadening using the Debye-Scherrer equation:

$$d_{average} = \frac{k\lambda}{\beta\cos\theta} \tag{3.2}$$

where k is the shape factor (k=0.9), λ is the X-ray wavelength, β is the line broadening in radians and θ is the diffraction angle in degrees. Rietveld refinement could not be used to determine the crystallite sizes as the alumina (mixture of γ-Al_2O_3 and δ-Al_2O_3 phases) support used in this study has an unknown crystal structure.

3.3.3. Inductively Coupled Plasma Spectrometry (ICP)

The rhodium and iron metal loadings of the model catalysts were determined using Inductively Coupled Plasma Spectrometry. The loadings of the samples obtained by ICP were then compared with the anticipated values. The samples were analysed by ICP optical emission spectroscopy using a Varian Vista-Pro instrument (Varian, USA) with radial torch configuration and scandium as internal standard. This spectrometry is highly sensitive and can be used for quantitative detection of trace amounts of metals.

3.3.4. Scanning Electron Microscopy (SEM) and Energy Dispersive X-Ray Analysis (EDX)

A scanning electron microscope (LEO S444 SEM, La:Ka, UK) equipped with a Four Quadrant Back Scatter Detector and an energy dispersive Fissons Kevex X-ray spectrometer (EDXA) with a sigma analysis software was used to also determine the actual rhodium and iron loadings on the calcined catalyst. Samples were prepared by sprinkling the dry powder of the sample on an aluminium stub coated with glue containing graphite. Graphite is used to conduct electrons and thus prevent charge build up. The samples were then coated with carbon which does not interfere with the elemental analysis.

3.3.5. Temperature-Programmed Reduction (TPR)

Temperature programmed reduction (TPR) experiments were conducted to determine the reduction behaviour of the catalyst samples. TPR characterisation also provided information on the effect of promoter loading on the ease of reducibility of both the noble metal oxide and the promoter oxide. TPR was carried out in a U-type quartz reactor on a Micromeritics AutoChem 2950 (Micromeritics Instrument Corp., USA). The sample (m = 40 mg) was placed in the reactor and reduced under a 5% H_2/Ar gas mixture at a flow rate of 50 ml(NTP)/min, from 60˚C to 900˚C with a constant heating rate of 10˚C/min. Prior to the reduction, the catalyst was dried in argon at 120°C for 2 hours. The hydrogen consumption was measured with a thermal conductivity detector (TCD). The instrument was regularly calibrated using Ag_2O. The hydrogen consumption is therefore quantified for each catalyst prepared.

3.4. Fischer-Tropsch Synthesis Experiments

3.4.1. Test Unit Set-up

The schematic experimental set-up used for Fischer-Tropsch testing is shown in Figure 3.2. During the reaction, carbon monoxide and hydrogen were fed to the reactor via mass flow controllers MC 2 and 3 (Brooks instruments). The mass flow controllers were calibrated before use. Argon was used to control and maintain the pressure of the system via the back pressure regulator, I-4.

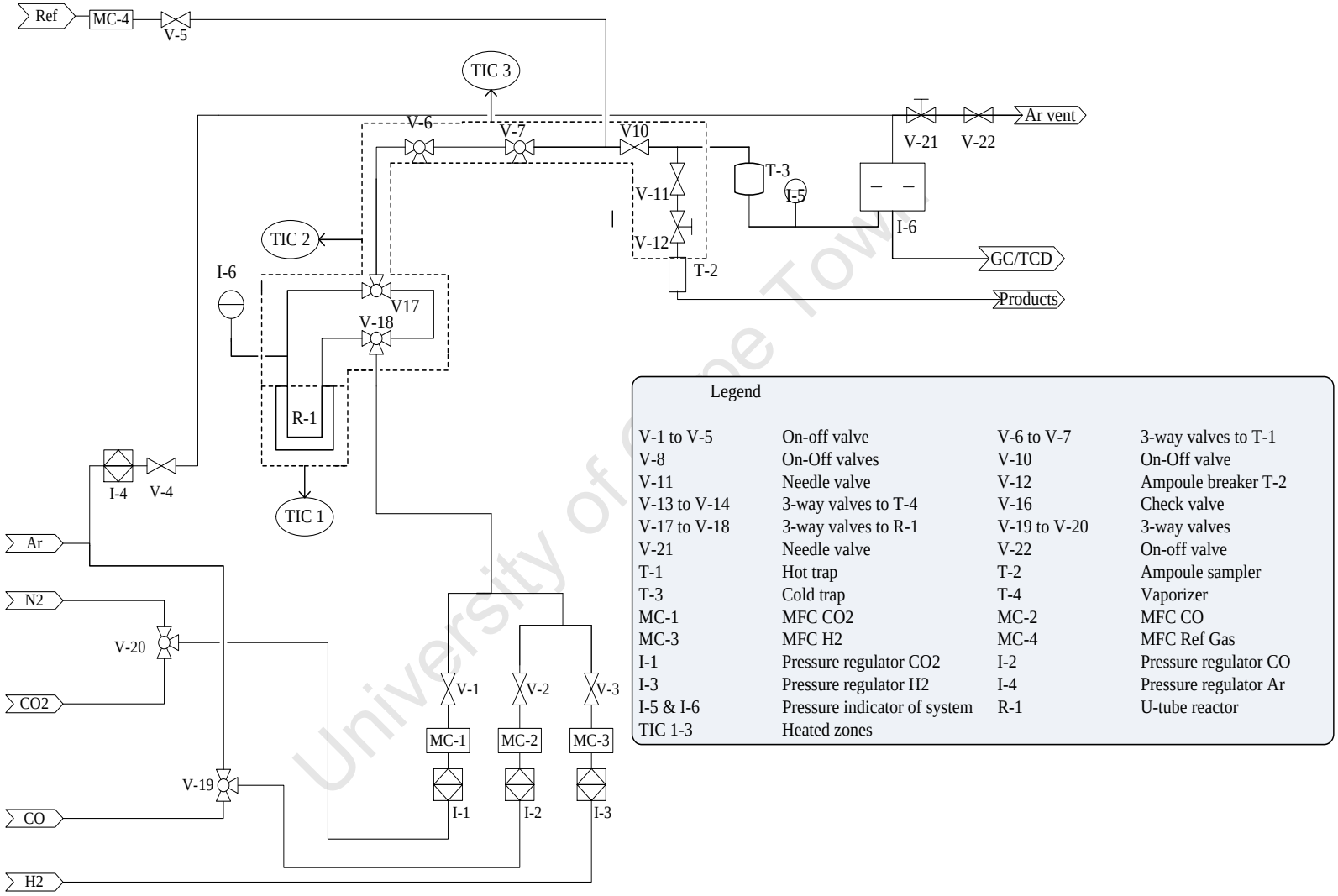

Figure 3.2: Experimental set up for Fischer-Tropsch synthesis

Nitrogen via mass flow controller MC-1 was used as an internal standard for online gas analysis using the Gas Chromatograph Thermal Conductivity Detector (GC-TCD). A N_2/cyclohexane mixture containing 0.1 vol % cyclohexane was fed via mass flow controller MC-4 into the product line before the product ampoule breaker. Cyclohexane was used as an internal standard for offline gas analysis using the Gas Chromatograph with Flame Ionisation Detector (GC-FID). Carbon dioxide via mass flow controller MC-1 was used for passivation of the catalyst at the end of the experimental run to protect catalyst from re-oxidation.

Two 3-way valves (V-17 and V-18) were used to change the flow of the gases from bypass to the reactor. All gases were fitted with control valves. All the lines after the reactor were heated using heating wires and kept at 160°C while the reaction temperature was 180°C.

3.4.2. Experimental Procedure

The reactor used for the Fischer-Tropsch synthesis was a U-tube fixed bed reactor made from stainless steel (O.D. 1/4", I.D. 4.4mm) (see Figure 3.3). The reactor was loaded by plugging the outlet with glass wool and adding 1 g of catalyst. More glass wool was used to separate the catalyst from the silicon carbide which was subsequently added to provide a preheating zone for the reaction gases before reaching the catalyst bed. The reactor was packed tightly to prevent the catalyst bed from moving during the reaction. The reactor was then placed inside an insulating aluminium block containing two heating cartridges and a thermocouple which was placed centrally in order to control the temperature.

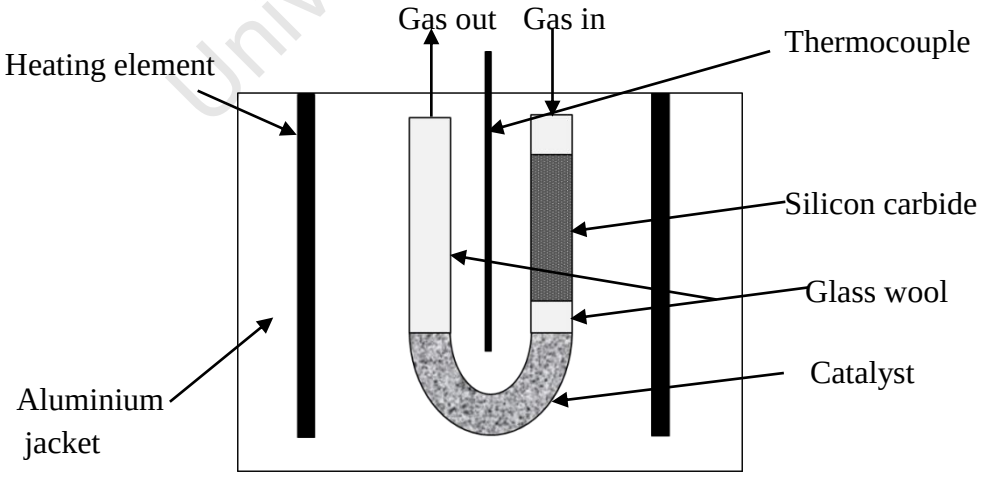

Figure 3.3: Schematic set-up of fixed bed U-tube reactor used for testing model catalysts in CO hydrogenation

Prior to the FT experiment, the catalyst was reduced at atmospheric pressure in-situ in 50 ml/min (NTP) H_2 at 500°C with a temperature ramp of 1°C/min for 2 hours. After reduction, the temperature of the reactor was decreased to the reaction temperature of 180°C. The inlet and outlet 3-way valves were positioned such that the gasses were run through the bypass and the reactor pressure was set at 10 bar and maintained with a back pressure regulator. The flow rates of CO and H_2 were set at 10 ml/min (NTP), (H_2/CO = 1) by mass flow controllers. The H_2:CO ratio of 1:1 was used to make C_2-oxygenates stoichiometrically. The reference gas was also set at 10 ml/min (NTP). The gas hourly space velocity was 20 $ml/g_{catalyst}$.min (NTP). Flow rates of CO, H_2 and feed ratio relative to the reference gas (N_2) were confirmed using the TCD over several bypass analyses. After this, the 3-way valves were switched from bypass to the reactor and this marked the start of the experiment. Immediately, regular ampoule sampling was done for offline analyses. Ampoules were taken in the first 15 minutes, then every 15 minutes for the first hour, every 30 minutes until 3 hours had elapsed and then every hour until the 10^{th} hour and the last 4 hours of the reaction. Ampoules were analysed using a GC equipped with an FID for detection of organic products. Online gas sampling was also performed regularly using micro GC with TCD detectors in order to analyse the inorganic products and methane. The reaction was run for 25 hours. At the end of the experimental run, the flows of H_2 and CO were switched off and the system was flushed with N_2 for 2 hours after which the catalyst was passivated with carbon dioxide for 5 hours at atmospheric pressure and room temperature. The catalyst was then removed from the reactor for characterization.

3.4.3. Analytical Procedures

3.4.3.1. Offline Sampling Procedure

Offline sampling of the gaseous FT products and the reaction gases was performed using the ampoule sampling procedure developed by Schulz et al. (1984). Commercially available Pasteur pipettes were used to prepare the glass ampoules. These ampoules were made with one side of the pipette formed to a capillary and sealed off, evacuated with a vacuum pump and sealed using a butane/oxygen flame.

When sampling to collect the gases, the capillary end of the evacuated ampoule was inserted through an airtight septum heated ampoule sampler into the product stream. The breaking fork was turned breaking the tip of the capillary and products were sucked into the evacuated

ampoule which was immediately sealed off with a butane flame. This is illustrated in Figure 3.4.

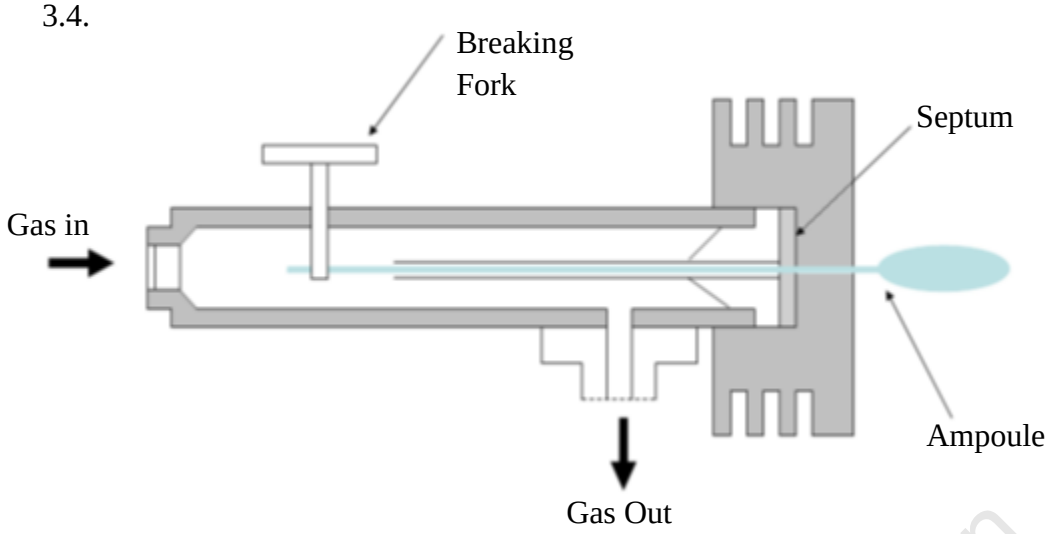

Figure 3.4: Ampoule Sampling Procedure

The ampoules were stored and later analysed by either using a special ampoule breaker connected to a GC with a FID (Claeys, 1997) or manually breaking the ampoule and injecting the organic products with a gas tight syringe. This procedure enabled investigation of the fast initial changes of catalyst activity and selectivity which occur mainly at the start of the FT reaction.

3.4.3.2. Analysis of Inorganic Products and Methane

A 3-channel micro Gas Chromatograph (Varian CP-4900) equipped with Thermal Conductivity Detectors (TCD) was used to analyse reactants H_2, CO, the reference gas N_2 as well as product CH_4 (see example of chromatograph Appendix B, Figure B.1). The GC was connected to the outlet line of the reactor providing online analysis and gasses were injected into the chromatograph at the sampling times automatically. This technique provides information of reactant conversion as well as product formation. GC conditions at which the analyses took place are given in Table 3.3. Relative error (repeatability) of this analysis technique is typically ±3%.

Table 3.3: Conditions for online GC analysis using TCD detection (Varian CP-4900)

Gas Chromatograph	**Channel 1**	**Channel 2**	**Channel 3**
Detector	TCD	TCD	TCD
Compounds analysed	CO, N_2, CH_4	CO_2, CH_4	H_2
Column	Molecular Sieve 5A (20 m)	Porapac Q (10 m)	Molecular Sieve 5A (10 m)
Column temperature (°C)	80	60	80
Carrier Gas	H_2	H_2	Ar
Inlet Pressure (kPa)	150	100	150
Injection time (ms)	120	120	120
Injector temperature (°C)	40	40	40
Backflush time (s)	160	-	160
Sampling time (s)	180	180	180

3.4.3.3. Analysis of Volatile Organic Products (VOC's)

Organic products in the gas phase were analysed using a GC with a Flame Ionisation Detector (FID)-Varian CP-3900. The ampoules taken during the experimental run were injected into the GC manually (see example chromatograph appendix B, Figures B.2-B.4). Analysis of the volatile compounds from the ampoule was done by breaking the tip of the ampoule, drawing the products into a gas tight syringe and injecting the sample into the injector of the GC. Hydrogen gas was used as a carrier in which the separation of the organic products, including organic standard, cyclohexane (CH_x) was conducted on a 60 m OV-1 type capillary column. The gas chromatographic conditions at which the analyses took place are given in Table 3.4. Relative error (repeatability) of this analysis technique is typically ±1%.

The FID response of the organic products is carbon specific, however, the response of all carbons are not equal. A carbon atom bonded to an oxygen atom gives a weaker response. In order to account for this, theoretical mass response factors suggested by Kaiser (1969) were used. All carbon atoms not bonded to an oxygen atom have a response of 1. Carbon atoms bonded to a single oxygen atom have a response of 0.55 and carbon atoms with a double bond to an oxygen atom have no response.

Table 3.4: Conditions for offline GC analysis using FID

Gas Chromatograph	**Varian CP-3900**
Detector	Flame ionisation detector
	$T_{detector}$ = 250 °C
H_2 Flow	30 ml/min (NTP)
N_2 Make up Flow	25 ml/min (NTP)
Air Flow	300 ml/min (NTP)
Column	Column RTx-1 (Restek) fused silica capillary column, 60 m x 0.25 mm stationary phase: 0.5 µm dimethyl siloxane (crosslinked)
Carrier gas	H_2
Oven Coolant	CO_2
Colum head pressure	1.72 bar
Injector	split injector, T = 250 °C
	split ratio: 5
Temperature programme	-55 °C, 1.5 min isothermal
	at 20 °C/min to 0 °C, 0 min isothermal
	at 14 °C/min to 0 °C, 0 min isothermal
	at 16 °C/min to 280 °C, 22.36 min isothermal
Total time	30 minutes

Therefore the response factor for every compound of the FT product can be calculated as follows:

$$f_i = \frac{N_C}{N_{C(no\ O)} + 0.55 N_{C(O)}} \tag{3.3}$$

where f_i is the factor response for compound *i*, $N_{C,i}$ is the total number of carbon atoms in the compound *i*, $N_{C(no\ O)}$ is the number of carbon atoms not bonded to an oxygen atom and $N_{C(O)}$ is the number of carbon atoms with a single bond to an oxygen atom (see Appendix B, Table B.2).

Organic products were also analysed using a GCxGC Leco Pegasus equipped with a Time-of-Flight (TOF) detector. The use of rhodium-based catalysts in CO hydrogenation result in the formation of different oxygenates and it becomes more difficult to identify some compounds when using one-dimensional gas chromatography as some compounds tend to co-elute. The use of two dimensional gas chromatography (GCxGC) solves this issue as it enhances the separation of compounds. The GCxGC contains two columns. The analyte is first separated on the first column (polar) and moves through the secondary column (nonpolar) for further separation. A thermal modulator exists between the two columns which serve as a catch and release system. Liquid nitrogen was used to freeze the effluent sample from the primary column in order to enhance separation of the products before the effluent is injected onto the secondary column to undergo secondary separation.

A mass spectrometer (TOF) was then used to identify the organic analyte. The mass spectrum of the compound was compared with the mass spectra of compounds found in the National Institute of Standards and Technology (NIST) database in order to identify the peaks. GCxGC-TOF analysis in this study was only used for the identification of oxygenates.

Table 3.5: Conditions for the analysis of organic compound on an Agilent 7890/GCxGC-TOF

Mass Spectrometer	Leco Pegasus 4D
Detector	Time-of-Flight (TOF)
	$T_{transfer\ line}$ = 250 °C
Gas Chromatograph	Agilent 7890 (offline)
Modulator	$T_{modulation}$ = 8 s
Injector	Split
	$T_{injector}$ = 225 °C
	Split ratio 80:1
Column 1	CP-Wax 52CB (30 m, 0.25 mm I.D., 0.20 μm film thickness)
Stationary phase	Polyethylene glycol
Carrier gas	Helium
Flow rate	0.6 ml/min
Column head pressure	1.19 bar
Temperature program	40 °C, 1 min isothermal
	At 4.5 °C/min to 215 °C, 5 min isothermal
Column 2	CP-Sil 8 CB (1.8 m, 0.1 mm, 0.10 μm film thickness)
Stationary phase	Polyphenylmethylsiloxane
Carrier gas	Helium
Flow rate	0.6 ml/min
Temperature program	72.5 °C, 1 min isothermal
	at 4.5 °C/min to 250 °C, 5 min isothermal

3.4.4. Data Work-up

Before the Fischer-Tropsch reaction, the reactants, CO and H_2 were bypassed to the reactor and samples were taken using the online TCD chromatograph. The flow rates of reactants were analysed and the calculated flow rates represent the feed into the reactor. During Fischer-Tropsch synthesis, the data was collected both on-line and off-line using TCD and ampoule technique respectively. Internal standards in known quantities were used in order to quantitatively analyse the product and feed on the gas chromatographs. Nitrogen was used as an internal standard for TCD analysis to quantify the molar flow rates of the inorganic compounds.

The molar flow rates for each species were obtained from the TCD chromatogram as follows:

$$\dot{n}_i = f_{TCD,i}\left(\frac{A_i}{A_{N2}}\right)\dot{n}_{N2} \tag{3.4}$$

where $\dot{n}_i$ is the molar flow rate of compound *i*, $f_{TCD,i}$ is the response factor for compound *i* relative to the reference nitrogen (see Appendix B, Table B.1), A_i is the peak area of compound *i* in chromatogram, A_{N2} is the peak area of the reference gas nitrogen in chromatogram and $\dot{n}_{N2}$ is the molar flow rate of the reference gas nitrogen and was determined as:

$$\dot{n}_{N2} = \frac{V_{N2}}{V_m} \tag{3.5}$$

where V_{N2} is volumetric N_2 flow rate at STP and V_m is the Avogadro number ($22.414\ \frac{l}{mol}$)

The response factors relative to nitrogen for the different compounds *i* were determined on a monthly basis using a calibration gas mixture with a known composition of carbon dioxide, hydrogen, carbon dioxide, nitrogen and methane.

Cyclohexane was used as an internal standard in FID analysis for quantification of the molar flow rates of the organic products as it was not part of the FT product spectrum. The molar flow rate of cyclohexane is defined as:

$$\dot{n}_{CHx,ref} = \frac{C_{CHx,ref}.V_{ref}}{V_m} \tag{3.6}$$

where $\dot{n}_{CHx,ref}$ is the molar flow rate of cyclohexane, $C_{CHx,ref}$ is the concentration of cyclohexane in the reference gas, V_{ref} is the volumetric reference gas flow rate and V_m is the Avogadro number (22.414 $\frac{l}{mol}$).

The molar flow rate of organic compound *i* can now be calculated as:

$$\dot{n}_i = \frac{N_{CHx,C}}{N_{i,C}} . \frac{f_i.A_i}{f_{CHx}.A_{CHx}} . \dot{n}_{CHx,ref} \tag{3.7}$$

Or on carbon basis given as: $\dot{n}_{i,C} = N_{CHx,C} . \frac{f_i.A_i}{f_{CHx}.A_{CHx}} . \dot{n}_{CHx,ref}$ (3.8)

where $\dot{n}_i$ is the molar flow rate of compound *i*, $N_{CHx,c}$ is the number of carbon atoms in cyclohexane, $N_{i,C}$ is the number of carbon atoms in compound *i*, f_i is the compound *i* response factor, A_i is the peak area of compound *i* in the GC chromatogram, f_{CHx} is the response factor for cyclohexane, A_{CHx} is the peak area of cyclohexane in the chromatogram and $\dot{n}_{CHx,ref}$ is the molar flow rate of cyclohexane.

3.4.4.1. Conversion, Yield and Selectivity

Further calculations were done once the molar flow rates of the reactants and products were obtained. The conversion of a reactant i which is usually defined as conversion of CO neglecting water gas shift activity (did not occur during experimental runs) is given as:

$$X_{CO} = \frac{\dot{n}_{CO,in} - \dot{n}_{CO,out}}{\dot{n}_{CO,in}} \tag{3.9}$$

where X_{CO} is the conversion of CO, $\dot{n}_{CO,in}$ is the molar feed flow rate of CO, $\dot{n}_{CO,out}$ is the molar outlet flow rate of CO.

However, for this study the conversions were not analysed using the data obtained from the TCD because the changes in gas concentrations were relatively small and would not give accurate results. The conversion was calculated from the rates of FT product formation. Only up to a carbon number of six organic products could be quantitatively measured except for

the pure iron catalyst which was up to seven carbon number. An ASF plot obtained from the measured products with carbon numbers from three to seven was extrapolated to the carbon number of 50.

The conversion was then calculated by summing the molar flows of all FT products on a carbon basis which equalled the difference between the molar feed flow of CO and molar outlet flow of CO assuming no water gas shift activity. Therefore the conversion is defined as:

$$X_{CO} = \frac{\sum_1^{50} \dot{n}_{iC}}{\dot{n}_{CO,in}} \tag{3.10}$$

where X_{CO} is the conversion of CO, $\sum_1^{50} \dot{n}_{iC}$ is the sum of the carbon based flow rates of all FT products from carbon number 1 to 50 and $\dot{n}_{CO,in}$ is the molar feed flow rate of CO.

The yield (Y_i) and the selectivity (S_i) of a product *i* are determined as follow:

$$Y_i = \frac{\dot{n}_i}{\dot{n}_{CO,in}} \tag{3.11}$$

$$S_i = \frac{Y_i}{X_{CO}} \tag{3.12}$$

Or on a carbon basis

$$Y_{i,C} = \frac{\dot{n}_{i,C}}{\dot{n}_{CO,in}} \tag{3.13}$$

$$S_{i,C} = \frac{Y_{i,C}}{X_{CO}} \tag{3.14}$$

3.4.4.2. Turn-over Frequency (TOF)

The surface specific activity (TOF) of the model catalysts was expressed as the number of converted CO molecules per mol exposed rhodium/iron atoms on the catalyst surface.

$$TOF = \frac{X_{CO}.\dot{n}_{CO,in}}{N_{exp,total}}.N_A \tag{3.15}$$

where TOF is the turn-over frequency, X_{CO} is the conversion of CO, $\dot{n}_{CO,in}$ is the molar feed flow rate of CO, $N_{exp,total}$ is the total number of exposed surface atoms.

The total number of exposed surface atoms equals the number of surface atoms per crystallite ($N_{exp,cryst}$) multiplied by number of crystallites per sample, N_{cryst}.

$$N_{exp,total} = N_{exp,cryst}.N_{cryst} \tag{3.16}$$

$N_{exp,cryst}$ was estimated using a method published by van Hardeveld and Hartog (1969) (see appendix A) and N_{cryst} was determined as follows:

$$N_{cryst} = \frac{L_{Rh/and\ Fe}.m_{cat}}{MW_{Rh/and\ Fe}} . \frac{N_A}{N_{total,cryst}} \tag{3.17}$$

where $L_{Rh/Fe}$ is the loading of rhodium or iron (from ICP measurements), m_{cat} is the total mass of the catalyst loaded in the reactor, $MW_{Rh/Fe}$ is the molar mass of rhodium or iron, N_A is the avogadro's number and $N_{total,\ cryst}$ is the total number of atoms in a single crystallite and was obtained using a method published by van Hardeveld and Hartog (1969) (see appendix A). When determining the total number of exposed surface atoms ($N_{exp,total}$) for the iron promoted alumina-supported rhodium catalyst, combined loading of Rh and Fe were used on average molecular weight, depending on actual catalyst composition. In this evaluation it is assumed that Rh and Fe approximately have the same activity as stated by Bligaard et al. (2004).

4. Results and Discussion

4.1. Catalyst Preparation Using Reverse Micelles

The reverse micelle technique was used to prepare alumina-supported rhodium crystallites, iron crystallites and Rh-Fe bimetallic crystallites at various molar ratios of Rh:Fe (1:0.1, 1:0.5 and 1:1). The objective of the study was to investigate the effect of iron on the alumina-supported rhodium catalyst. The initial step was to prepare the model catalysts with similar crystallite sizes because variations in crystallite sizes will cloud the influence of iron on the supported rhodium catalysts during CO hydrogenation as the crystallite sizes can affect the activity and selectivity of the catalyst. The supported nano-sized crystallites were prepared using a method reported by Fischer (2011). This involves direct addition of the precipitating agent to the reverse micelle solution containing the dissolved metal precursor (rhodium (III) nitrate or iron (III) nitrate). Followed by addition of alumina support, then acetone to destabilise the reverse micelles and finally washing with acetone to remove residual surfactant.

It is well-known that the reverse micelle technique is suitable for the preparation of catalysts with controllable crystallite sizes **(**Eriksson et al., 2004; Mabaso, 2005; Welker, 2007; Cheang, 2009; Fischer, 2011). The water to surfactant ratio is the most important factor to vary in order to form different crystallite sizes. Mabaso (2005) reported that variation of the water to surfactant ratio enabled control of iron crystallite, thus leading to the formation of iron crystallites with different crystallite sizes. However, in this study similar crystallite sizes of the model catalysts were required and therefore the water to surfactant ratio was kept constant. The weight water to surfactant ratio used in this work was 0.2 (g/g) within the stable region of reverse micelles. This ratio was selected because it resulted in the formation of small crystallites no larger than 5 nm which were required for the study. Furthermore, Mungwe (2013) found that when using the reverse micelle method to form rhodium crystallites with different crystallite sizes the method only yielded small crystallites < 4 nm under different water to surfactant ratios. This has been ascribed to the noble character of rhodium thus favouring small crystallite formation. Ojeda et al. (2004a) reported that the oil to surfactant ratio was another factor influencing the crystallite size thus it was kept constant in this study. It was observed that the crystallite size decreased with decreasing water to

surfactant ratio for a fixed surfactant to oil ratio. The fixed weight surfactant to oil ratio value used in this study was 0.19 (g/g).

Model catalysts with similar average crystallite sizes and narrow size distributions displaying well dispersed nano-sized crystallites on the alumina support were successfully prepared using the reverse micelle method (to be shown below).

4.2. Results of Characterisation of Model Catalysts

All catalysts were calcined in air at 300°C with a temperature ramp of 2°C/min for 16 hours and subsequently reduced in 50 ml/min (NTP) H_2 at 500°C with a temperature ramp of 1°C/min for 2 hours to form the active metallic phase. Finally, the catalysts for characterisation were passivated with CO_2 under flow for minimum of 2 hours at room temperature. The characterization results are discussed below.

4.2.1. TEM Analysis of Supported Crystallites

TEM analysis was vital to this study and was conducted to determine the crystallite size and distributions of the model catalysts. Furthermore EDX was carried out in order to do elemental analysis. HRTEM micrographs of Rh, Fe and Rh/Fe crystallites at three different molar ratios of Rh to Fe obtained at $\omega_0 = 0.2$ are shown in Figures 4.1 and 4.2.

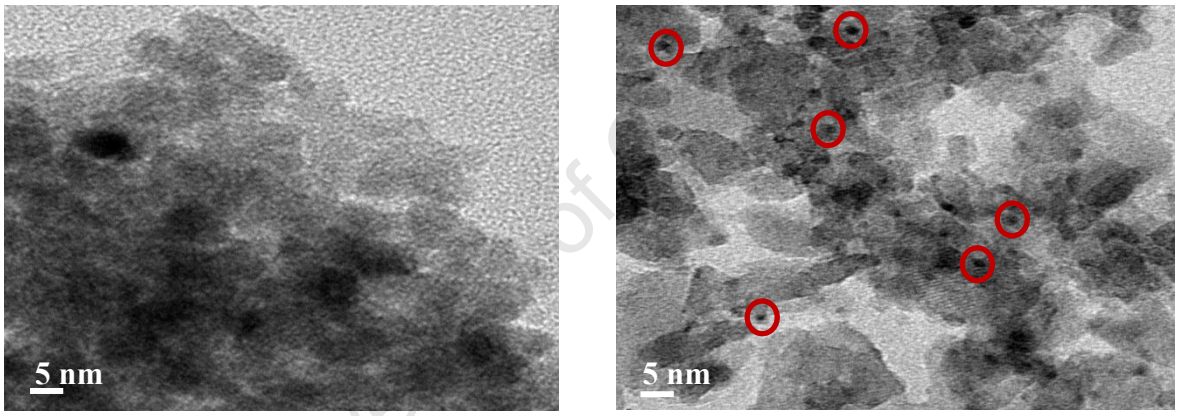

Rh/Al_2O_3

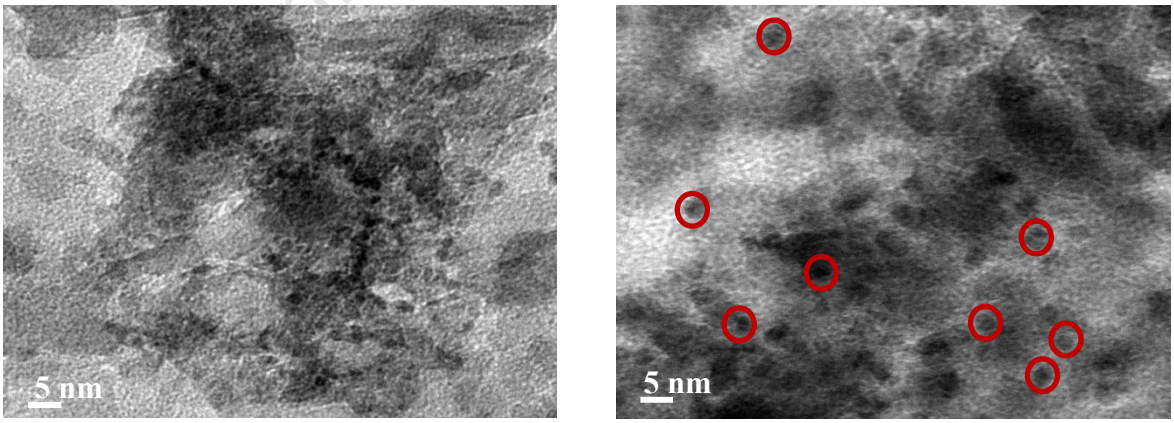

Rh1Fe0.1

Figure 4.1: HRTEM micrographs of alumina supported nano-sized crystallites; left after calcination, right: after reduction and passivation

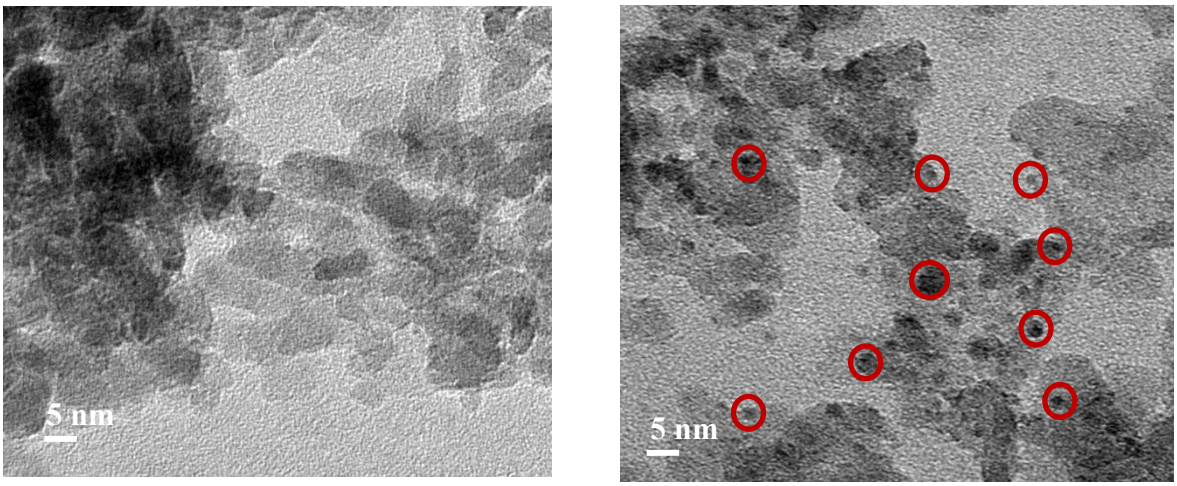

Rh1Fe0.5

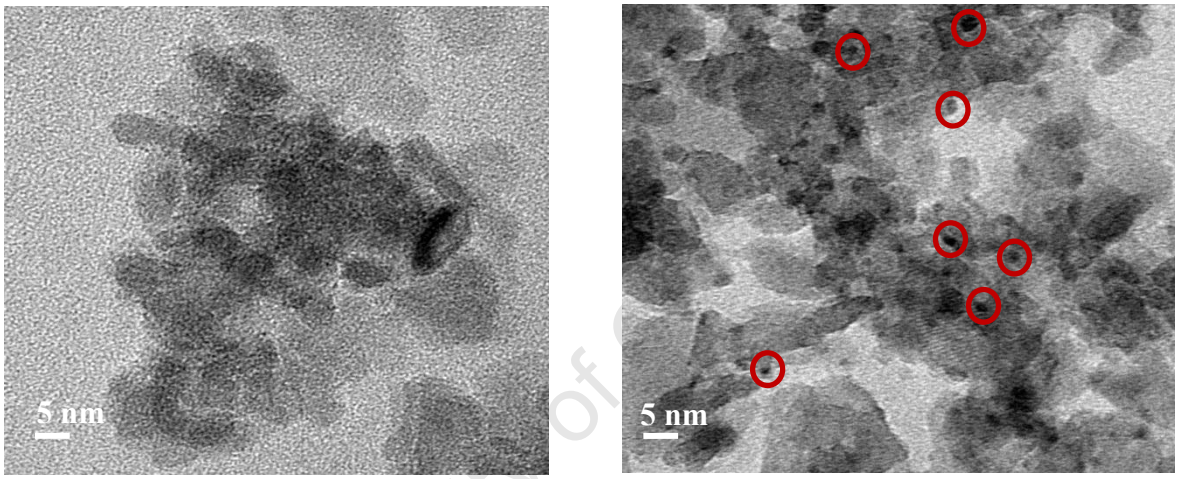

Rh1Fe1

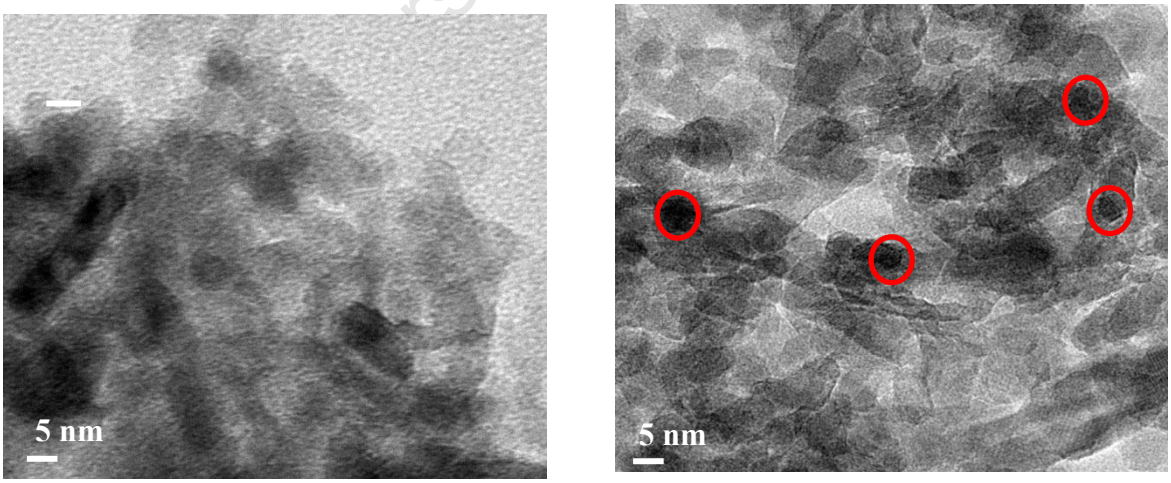

Fe/Al_2O_3

Figure 4.2: HRTEM micrographs of alumina supported nano-sized crystallites; left: after calcination, right: after reduction and passivation

Due to the small crystallite sizes or amorphous phase of the rhodium and iron promoted alumina-supported rhodium catalysts, it was difficult to obtain micrographs of the calcined catalysts with a good resolution (see Figures 4.1 and 4.2 left). Therefore, for these catalysts, reduced samples were used in order to determine the crystallite sizes and distributions. As displayed in Figures 4.1 and 4.2, rhodium, iron and iron promoted alumina-supported rhodium samples with different ratio of Rh:Fe crystallites were well dispersed on the support. HRTEM micrographs of the iron sample in the calcined state and after reduction and passivation had a poor resolution which is due to the similar densities of Fe_2O_3, Fe and the alumina support ($\rho_{Fe_2O_3}$ = 5.24 g/cm^3; ρ_{Fe} = 7.87 g/cm^3; $\rho_{Al_2O_3}$ = 3.95 g/cm^3). The crystallites of iron are larger compared to the rhodium and iron promoted alumina-supported rhodium samples crystallites. This was probably due to sintering during pretreatment ($T_{calcination}$ = 300°C and $T_{reduction}$ = 500°C > $T_{Hüttig}$ = 269°C). It was difficult to distinguish from the HRTEM micrographs of the iron promoted alumina-supported rhodium catalysts whether bimetallic crystallites were formed or whether a physical mixture of the individual metallic carried out in order to determine whether bimetallic crystallites were formed (refer to STEM-EDX work below).

Figure 4.3 shows crystallite size distributions of the prepared model catalysts in the calcined state only for iron and in the reduced and passivated state for all the prepared catalysts. The histograms were obtained by counting a minimum of 150 crystallites from HRTEM micrographs using Image J software. It is important to note that HRTEM analysis on alumina was difficult because of the colour contrast for small crystallites and therefore the distribution of the crystallites shown in Figure 4.3 was the overestimation.

Listed in Table 4.1 are the average crystallite sizes and standard deviations including results obtained by means of STEM characterisation (see below). Figure 4.3 and Table 4.1 show that the model catalysts have generally narrow size distributions. The standard deviations were calculated as follows:

$$\sigma = \sqrt{\frac{1}{N}\sum_{i=1}^{N}(d - \bar{d})^2} \qquad (4.1)$$

where N is the number of crystallites, d is the diameter of a single crystallite *i* and $\bar{d}$ is the average diameter of N crystallites.

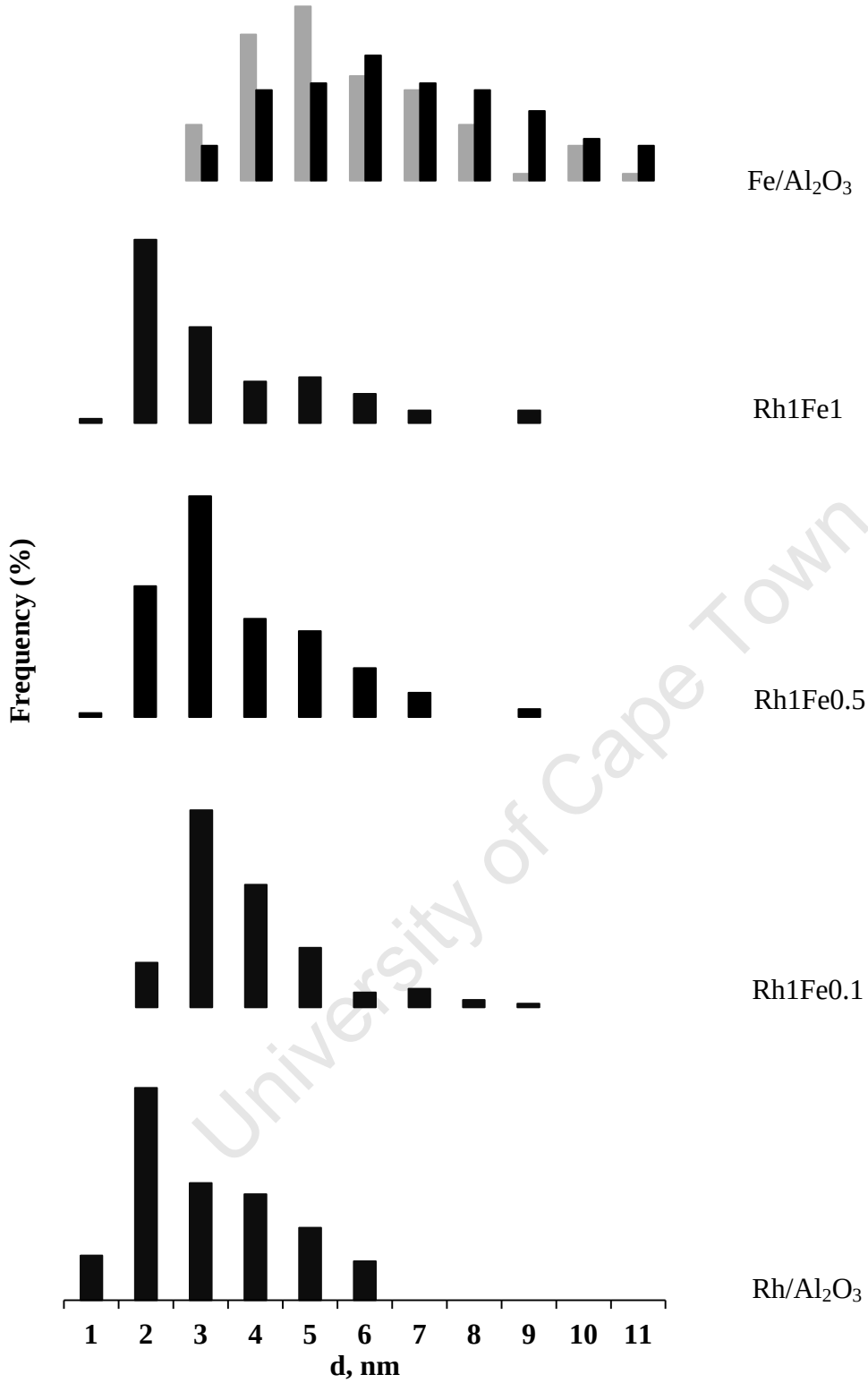

Figure 4.3: Crystallite size distributions of calcined and reduced alumina supported nano-sized crystallites calculated from a minimum of 150 crystallites (■calcined state, ■ reduced state)

Rhodium and iron promoted alumina-supported rhodium catalysts were observed to have similar crystallite sizes which was a desired result because variations in crystallite sizes will cloud the influence of iron on the supported rhodium catalysts during CO hydrogenation. It is interesting to note that the iron promoted alumina-supported rhodium catalysts consisted mostly of larger crystallites as shown on the histograms and TEM pictures as compared to the rhodium catalyst.

It is generally expected that the reduced iron sample would have smaller average crystallite sizes than the calcined sample due to the change in density ($\rho_{Fe_2O_3}$ = 5.24 g/cm^3; ρ_{Fe} = 7.87 g/cm^3). However this was not the case as shown in Figure 4.4 and Table 4.1. This may be a result of sintering of small crystallites during the reduction process as the Hüttig temperature of metallic iron (269°C) (Moulijn et al., 2001) was exceeded. The Hüttig temperature of Rh is 404°C (Moulijn et al., 2001) and sever sintering is therefore not to be expected. It is interesting to note that no large crystallites were observed in the mixed Rh/Fe catalysts, suggesting that mixed phase were formed or no separate crystallites were present and the preparation via reverse micelle system indeed yielded intimately mixed phases. This was confirmed by further characterisation, XRD and EDX (see sections below).

Table 4.1: HRTEM and STEM characterisation of reduced alumina supported nano-sized crystallites

Sample	**Calcined State**	**Reduced and passivated**	**Reduced and passivated**
Code	$d_{c,1} \pm \sigma$, nm (HRTEM)	$d_{c,1} \pm \sigma$, nm (HRTEM)	$d_{c,1} \pm \sigma$, nm (STEM)
Rh/Al_2O_3	-	2.6 ± 1.4	2.0 ± 0.5
Rh1Fe0.1	-	3.4 ± 1.4	2.0 ± 0.6
Rh1Fe0.5	-	3.1 ± 1.5	2.1 ± 0.7
Rh1Fe1	-	2.8 ± 1.7	2.2 ± 0.8
Fe/Al_2O_3	5.2 ± 1.9	6.3 ± 2.3	-

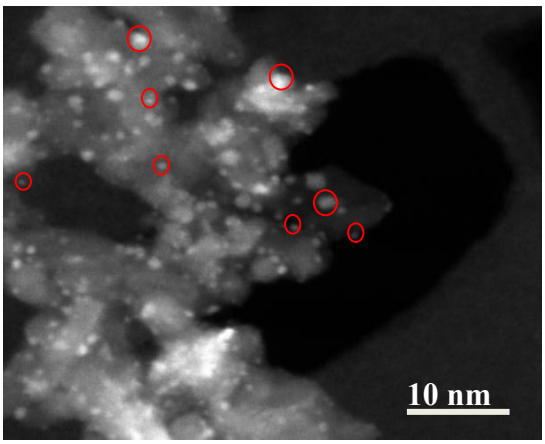

Rh/Al_2O_3

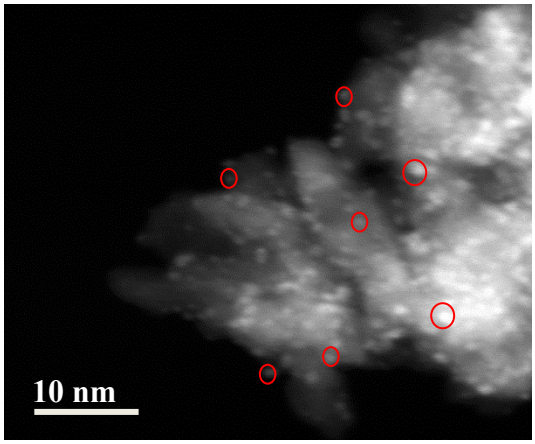

Rh1Fe0.1

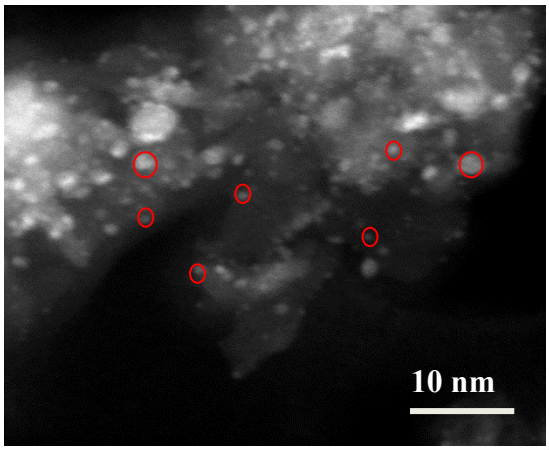

Rh1Fe0.5

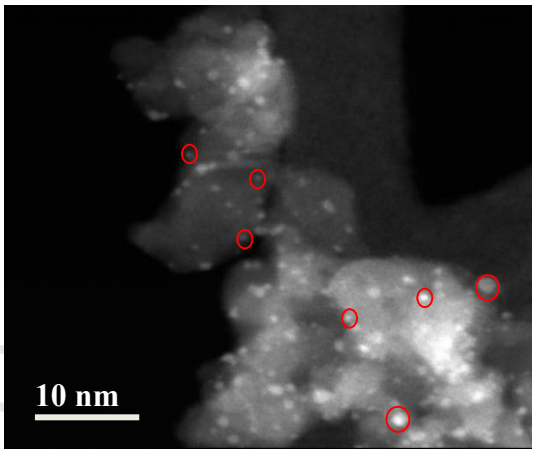

Rh1Fe1

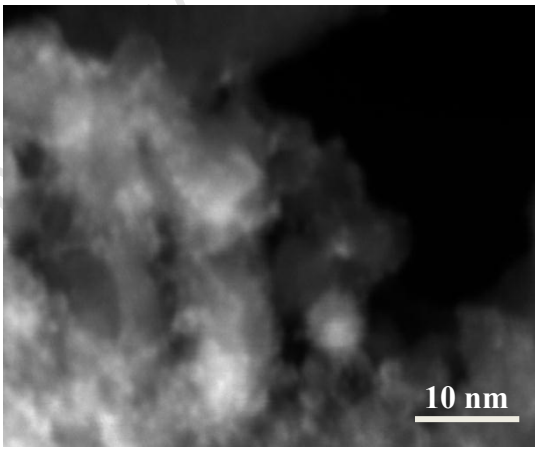

Fe/Al_2O_3

Figure 4.4: STEM micrographs of the reduced alumina supported nano-sized crystallite catalysts

STEM was also used to determine the average crystallites of the model catalysts as listed in Table 4.1. STEM micrographs of the model catalysts in the reduced state are shown in Figure 4.4. The material with higher density appeared as bright spots. Rhodium crystallites were observed as bright white spots on the grey alumina support for the rhodium sample. A STEM micrograph for the iron sample had a poor resolution because of the small difference in density of iron, iron oxide and alumina which resulted in poor contrast. The average crystallite sizes of the iron promoted alumina-supported rhodium samples catalysts obtained from STEM were similar to those obtained using HRTEM. Iron promoted alumina-supported rhodium crystallites were observed to be small as seen in Figure 4.4 and Table 4.1.

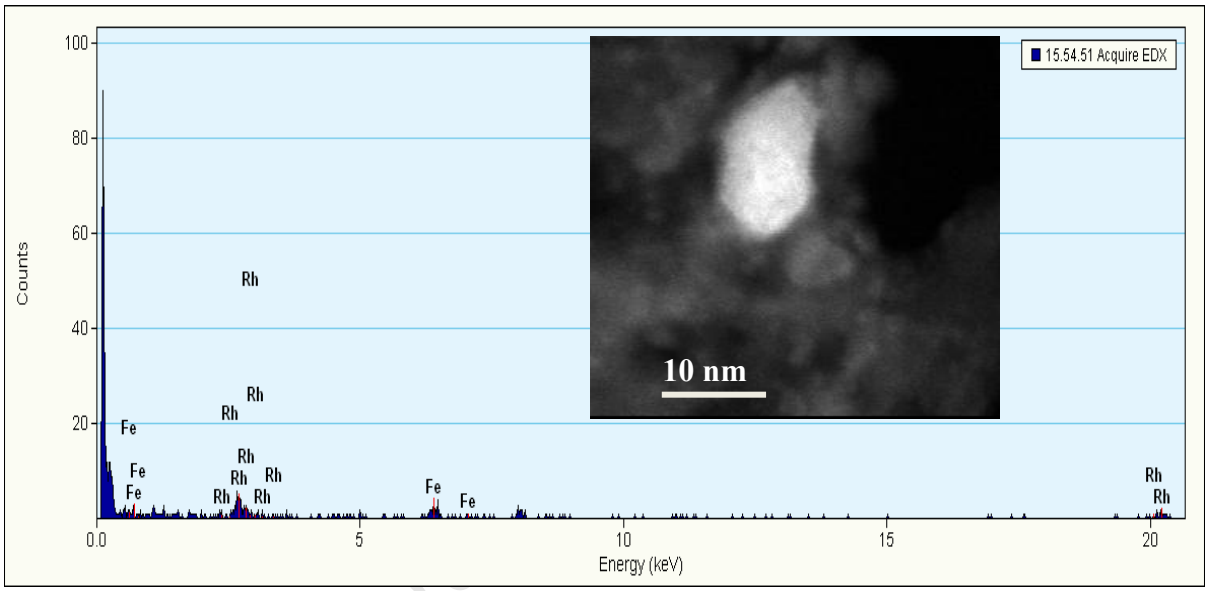

Figure 4.5: STEM-EDX illustrating rhodium and iron on the Rh1Fe1 catalyst

EDX was used for elemental analysis of the Rh-Fe bimetallic catalysts in order to determine whether both Rh and Fe are present in some crystallites. An EDX map of STEM micrograph is shown in Figure 4.5. The white spot was analysed for elemental analysis. In the EDX analysis of the Rh-Fe bimetallic catalyst with low loading of iron (Rh1Fe0.1), only Rh crystallites were detected while in the analyses of the Rh-Fe bimetallic catalysts with high loading of iron (Rh1Fe0.5 and Rh1Fe1), both Rh and Fe were detected in the crystallites. Ichikawa et al. (1986) reported that catalyst of a low Fe/Rh, Fe atoms are mostly present in the state of Fe^{3+} while the fraction of Fe^{0} increases with increase of the Fe/Rh ratio. This implies that truly bimetallic crystallites may only form at high loading of iron.

4.2.2. XRD Analysis of Supported Crystallites

XRD was used to determine the average crystallite sizes and phases of rhodium, iron and iron promoted alumina-supported rhodium at different ratios of Rh:Fe catalysts. XRD patterns of Rh, Fe and alumina-supported iron-promoted rhodium crystallites at various molar ratios of Rh:Fe in the calcined state are shown in Figure 4.6. Only alumina phases were detected using XRD for the calcined catalysts. These results are consistent with the findings obtained via HRTEM analyses for the Rh, iron promoted alumina-supported rhodium catalysts. The crystallite sizes are too small to be detected by XRD and the alumina support peaks dominate the scans. It is therefore difficult to analyse phases that may be present other than alumina. For the calcined iron sample, only the diffraction patterns due to the alumina support were detected. However, from HRTEM analyses the iron crystallites in the calcined state were large enough to be detected by XRD suggesting that amorphous iron phases are present rather than crystalline ones.

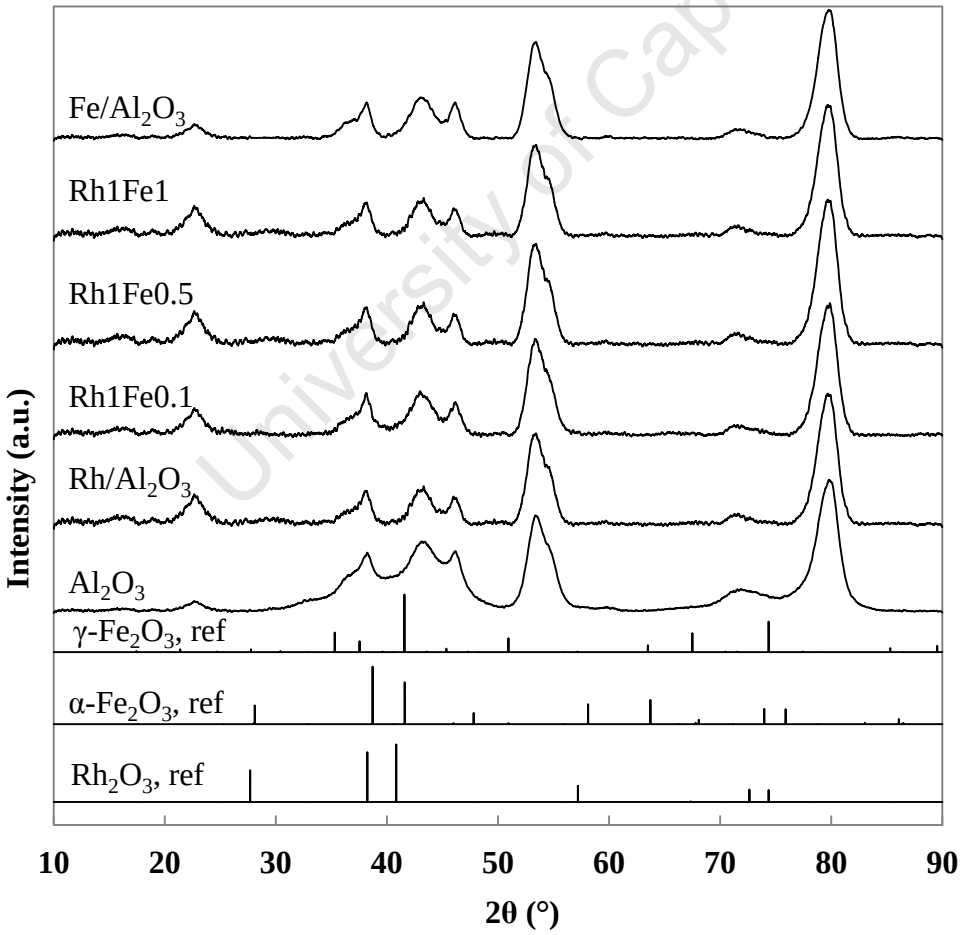

Figure 4.6: XRD patterns of model catalysts in the calcined state and pure alumina support, including reference patterns for rhodium oxide and hematite

XRD analysis was also performed on the reduced and passivated samples. XRD patterns of the model catalysts in the reduced state are illustrated in Figure 4.7. The XRD pattern of the reduced rhodium sample displayed a peak for metallic rhodium (2θ = 48.0°) although the scan was dominated by the diffraction pattern of the γ-alumina support. The reduced iron XRD pattern clearly showed the main peak for metallic iron (2θ = 52.4°) besides the alumina peaks.

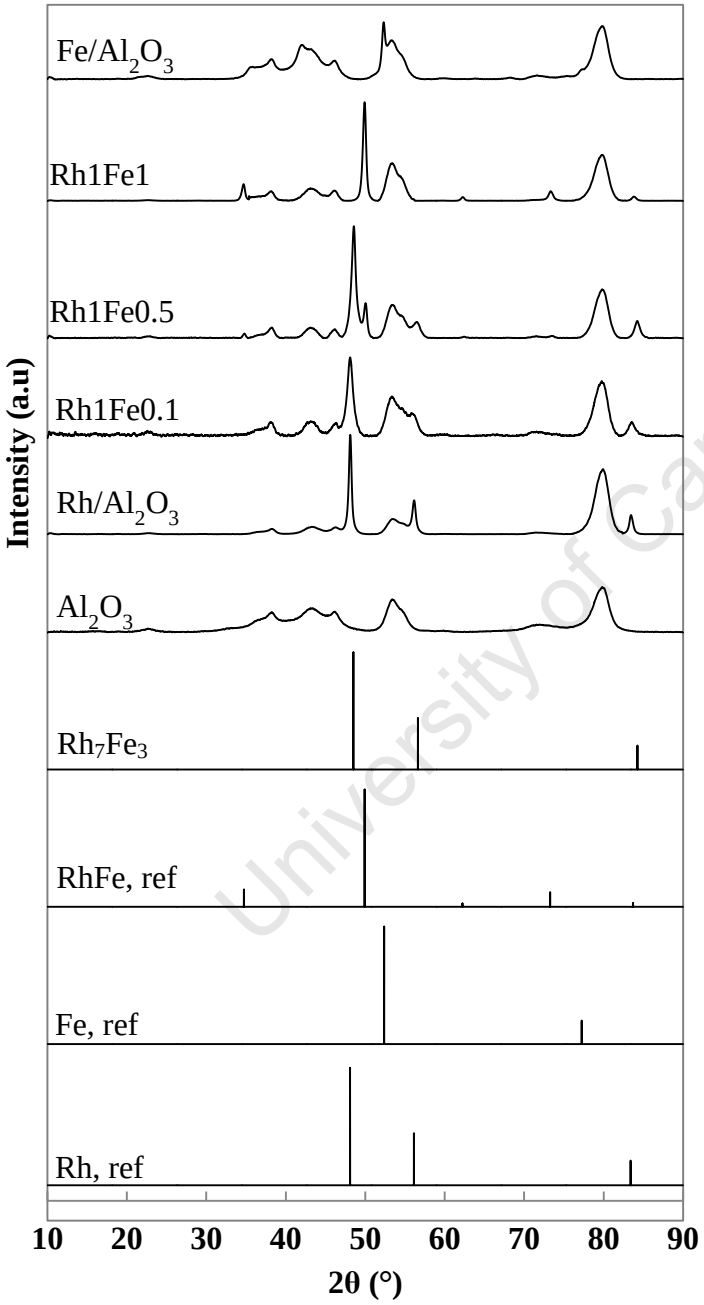

Figure 4.7: XRD patterns of model catalysts in the reduced state and pure alumina support. Reference patterns for metallic rhodium, metallic iron, RhFe and Rh_7Fe_3 alloys are included

It was found that the XRD pattern for the Rh:Fe = 1:0.1 molar ratio catalyst exhibited characteristic peaks for metallic rhodium (2θ = 48.09°, 83.4°). On the basis of these results, it could not be suggested that the Rh:Fe = 1:0.1 bimetallic catalyst contains alloys of rhodium and iron. Only rhodium peaks were detected which could be due to low iron loading in the catalyst. This result is in agreement with Ichikawa et al. (1986) who reported that catalyst of a low Fe/Rh (Fe/Rh = 0.3), Fe atoms are mostly present in the state Fe^{3+}. However, the Rh:Fe bimetallic catalysts with high loading of iron exhibited different results compared with the one with low iron loading.

The characteristic peaks for Rh:Fe = 1:0.5 molar ratio catalyst revealed that it is composed of two different alloy phases (see figure 4.8). The strong peak at the 2θ = 48.5° as well as the peaks at 2θ = 56.6°, 84.3° in the diffraction pattern of Rh:Fe = 1:0.5 bimetallic catalyst correspond to the Rh_7Fe_3 alloy phase while the peaks at 2θ = 34.7°, 50.0° correspond to the RhFe alloy phase. It seems that the Rh:Fe = 1:0.5 molar catalyst consist mostly the Rh_7Fe_3 alloy phase. This implies that the catalyst is composed of alloys rather than a mixture of monometallic rhodium and iron crystallites. Compared with the XRD pattern of Rh:Fe = 1:0.5 bimetallic catalyst, the Rh:Fe = 1:1exhibits the same result, however only one alloy phase (RhFe) was observed. It was established from the observation that the Rh:Fe bimetallic catalysts with high loading of iron exhibit alloy characteristics. These results are in agreement with the findings obtained from the EDX analysis which confirmed that the catalysts with high loading of iron have both Rh and Fe present.

The average crystallite sizes determined using the Scherrer equation and the XRD scans are listed in Table 4.2. The sizes were then compared with volume average crystallite sizes obtained from HRTEM results (see Table 4.2) and a good agreement was found.

Table 4.2: Calculated average crystallite sizes of the reduced model catalysts using the Scherrer equation from XRD scans, peaks used for calculations and volume weighted average crystallite size from HRTEM

Sample Code	d_{red}, nm (XRD)	2θ (°)	d_{vol}, nm (HRTEM)
Rh/Al_2O_3	5.1	48.0	4.2 ± 1.4
Rh1Fe0.1	4.4	48.1	5.3 ± 1.4
Rh1Fe0.5	4.2	48.5	5.1 ± 1.5
Rh1Fe1	3.5	49.9	4.5 ± 1.7
Fe/Al_2O_3	9.0	52.4	8.5 ± 2.3

4.2.3. ICP and SEM-EDX Analysis of Supported Crystallites

Acid digestion was performed of the model catalysts in preparation for ICP analysis which was done to determine the elemental composition of the catalysts. SEM-EDX was also used to determine elemental composition. The calculated and actual loadings obtained using ICP and SEM-EDX of the model catalysts are listed in Table 4.3. The actual loadings were lower than the anticipated value as expected due to loss during the washing step of the catalyst preparation. This loss was expected as the prepared catalysts in the study have small crystallites and it was most difficult to decant during the washing steps.

Table 4.3: Weight loadings of rhodium and iron of the model catalysts using ICP and SEM-EDX

Sample Code	Nominal composition (wt %)	ICP (wt %)	EDX (wt %)
Rh/Al_2O_3	10% Rh/Al_2O_3	8.0% Rh	9.1% Rh
Rh1Fe0.1	10% Rh-0.54% Fe/Al_2O_3	8.1% Rh-0.4% Fe	9.1% Rh-0.5% Fe
Rh1Fe0.5	10% Rh-2.71% Fe/Al_2O_3	7.1% Rh-2.1% Fe	8.5% Rh- 2.5% Fe
Rh1Fe1	10% Rh-5.43% Fe/Al_2O_3	10.6% Rh-5.9% Fe	8.6% Rh-5.5% Fe
Fe/Al_2O_3	10% Fe/Al_2O_3	7.4% Fe	7.6% Fe

4.2.4. Reduction Behaviour of Supported Crystallites

The reduction behaviour of the model catalysts was determined using TPR in a 5% H_2/Argon mixture. TPR profiles of the alumina-supported rhodium, iron as well as iron promoted alumina-supported rhodium catalysts at various ratios of Rh:Fe are shown in Figure 4.8. The reduction of the Rh/Al_2O_3 took place within the temperature range of 60-160°C and was characterised by a single narrow peak which was assigned to the reduction of Rh_2O_3 to metallic rhodium (equation 4.2).

$$Rh_2O_3 + 3H_2 \rightarrow 2Rh + 3H_2O \quad (4.2)$$

The result is in agreement with the findings of van't Blik and Prins (1986) who obtained a similar profile for alumina-supported Rh catalyst dried at 120°C in air.

The reduction of Fe/Al_2O_3 was difficult compared to Rh/Al_2O_3 and was characterised by two broad peaks. The first peak occurred between 170°C and 350°C and may be ascribed to the reduction of Fe_2O_3 to form Fe_3O_4, represented by equation 4.3. The second peak was assigned to the reduction of Fe_3O_4 to metallic Fe and occurred within the temperature range of 400-650°C, represented by equation 4.4.

This result is consistent with the findings by Lin et al. (2003) who reported that the reduction profile of precipitated iron oxide consists of two peaks which correspond to the two steps reduction process of Fe_3O_2 to metallic Fe (see Equations 4.3 and 4.4).

$$3Fe_2O_3 + H_2 \rightarrow 2Fe_3O_4 + H_2O \quad (4.3)$$

$$Fe_3O_4 + 4H_2 \rightarrow 3Fe + 4H_2O \quad (4.4)$$

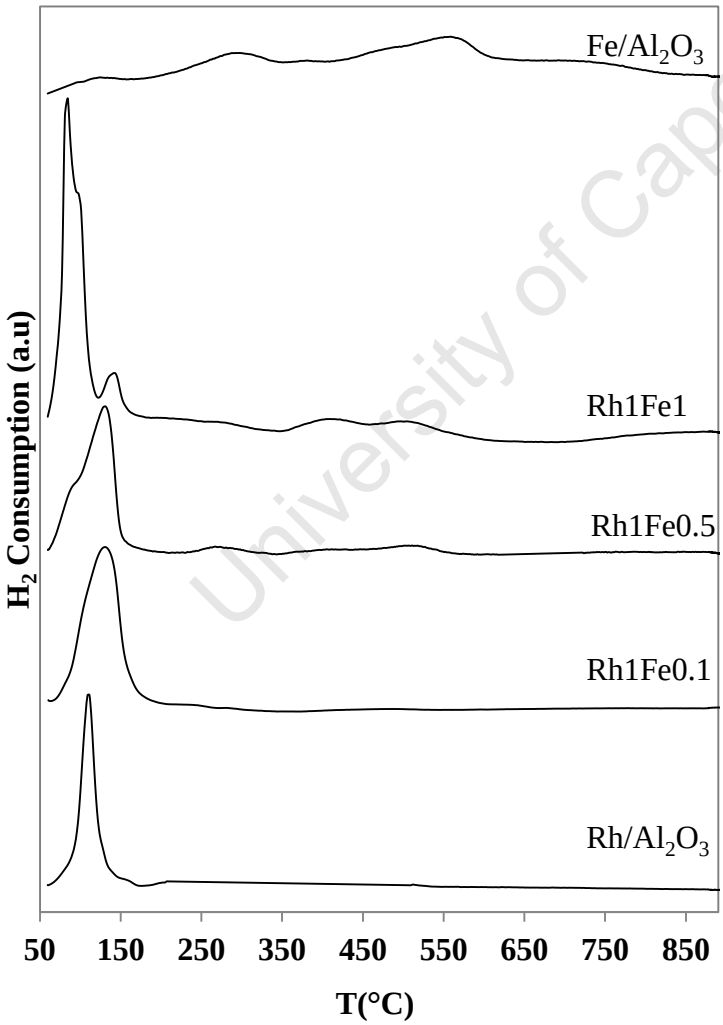

Figure 4.8: TPR profiles of alumina-supported rhodium, iron and Rh-Fe bimetallic at different molar ratios of Rh:Fe

The most interesting results from TPR profiles are the Rh-Fe bimetallic samples. Reduction of all the Rh-Fe bimetallic samples showed a strong large broad peak within the temperature range of 60-200°C. This indicates that both metals are in intimate contact and once rhodium has been reduced to metallic rhodium it is able to assist in the reduction of iron oxide to form Rh-Fe bimetallic ensembles (van't Blik and Niemantsverdriet, 1984; Schunemann et al., 1995; Guglielminotti et al., 1995; Burch and Hayes, 1997; Mo et al., 2009a; Chen et al., 2011). This result is consistent with the findings obtained from XRD analyses that Rh-Fe bimetallic samples with high loading of iron results in alloy formation. Furthermore, it was found that the hydrogen consumption increased with increasing iron loading (see Table 4.4) and was more than the required amount to achieve a complete reduction of Rh_2O_3 to metallic rhodium (1.5 mol H_2:1.0 mol Rh_2O_3). The catalyst with low loading of iron (Fe:Rh = 0.1) was shown to have no peak where reduction in Fe/Al_2O_3 was observed while the catalysts with high loadings of iron were observed to have small broad peaks similar to the reduction peaks of pure iron. This was ascribed to the reduction of isolated iron species (Chen et al., 2011). The Rh1Fe1 sample was also observed to have a shoulder peak at 140°C and it could not be assigned to a compound. The result is consistent with the findings of van't Blik and Niemantsverdriet (1984) who obtained a similar profile for silica-supported RhFe bimetallic catalyst with atomic ratio of Rh:Fe = 1. It was assumed all the catalysts are fully reduced at 500°C.

Table 4.4: Hydrogen consumption results of the model catalysts obtained during temperature reduction programme

Catalyst Code	**Hydrogen consumption**	
	mol H_2/mol Rh	mol H_2/mol Fe
Rh/Al_2O_3	1.43	-
Rh1Fe0.1	1.93	-
Rh1Fe0.5	1.85	-
Rh1Fe1	2.08	-
Fe/Al_2O_3	-	1.4

4.3. CO Hydrogenation Performance of Model Catalysts

In order to investigate the effect of iron on the alumina-supported rhodium catalysts in CO hydrogenation, the model catalysts were tested in a fixed bed reactor. Prior to CO hydrogenation, 1 g of the calcined catalyst was reduced in-situ in 50 ml(NTP)/min pure H_2 at 500°C for 2 hours with a temperature ramp of 1°C/min and then flushed with N_2 for 30 minutes. The model catalysts were tested at a reaction temperature of 180°C, a pressure of 10 bar and a synthesis gas flow of 20 ml(NTP)/min with a H_2/CO ratio of 1. These mild conditions with low conversions were chosen to minimize effects of crystallite sintering. The experiments were run for 25 hours and steady state was reached after 3 hours.

4.3.1. CO Hydrogenation Activity and Characterisation of the Spent Catalysts

Catalytic activity of alumina-supported Rh, Fe and Rh-Fe bimetallic catalysts is expressed in terms of CO conversion. CO conversion of the model catalysts was monitored as a function of time on stream. A Gas Chromatograph equipped with Thermal Conductivity Detectors was used to analyse the amount of CO flowing in and out of the reactor. This enabled the determination of CO conversion using nitrogen as an internal standard. The activity results for the catalysts are shown in Figures 4.9 and 4.10.

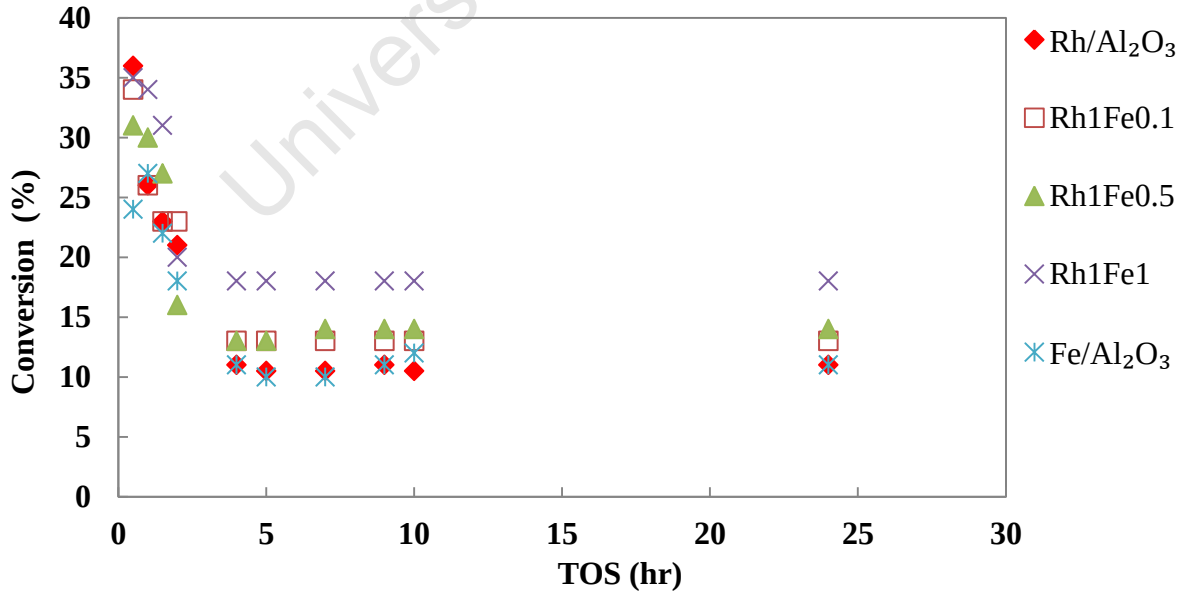

Figure 4.9: CO conversion on model catalysts in CO hydrogenation as a function of time on stream (TOS)

(Reaction conditions: T = 180°C, P = 10 bar, GHSV = 20 ml(NTP)/min.g_{cat}, H_2/CO = 1)

The activity of the rhodium catalyst is high initially at about 35% but falls to a steady state conversion of 12% after 3 hours TOS. This loss in activity may be due to surface reconstruction of the crystallites upon exposure of the catalyst to the synthesis gas (Bezemer et al., 2006; and Schulz et al., 2002).

The iron catalyst was less active as compared to the rhodium catalyst initially and deactivation was observed with time on stream until steady state was reached at around 12 % which is similar to the rhodium catalyst. This result is consistent with the findings by Bligaard et al. (2004) who reported that Rh and Fe have similar activity for methane formation.

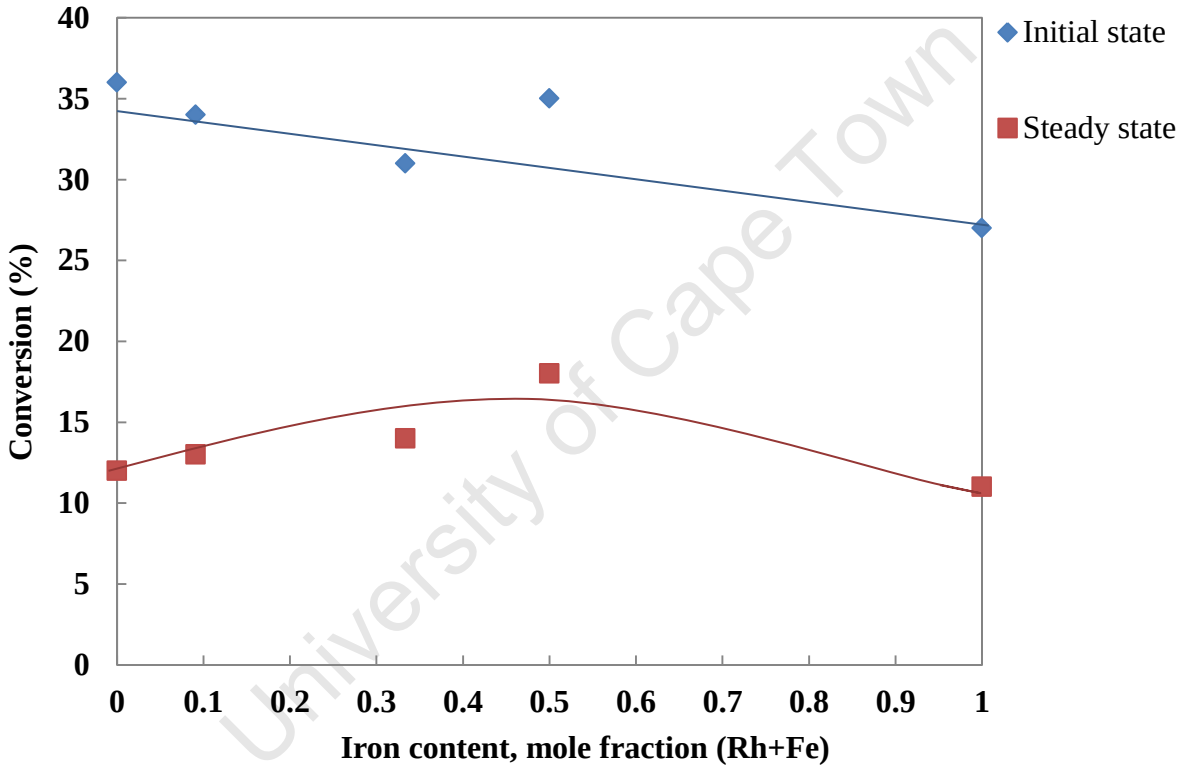

Figure 4.10: CO conversion as a function of iron mole fraction in catalyst at both the initial state (10 minutes) and at steady state (7 hours)
(Reaction conditions: T = 180°C, P = 10 bar, GHSV = 20 ml(NTP)/min.g_{cat}, H_2/CO = 1)

The effect of iron loading on the activity of alumina-supported rhodium catalysts is shown in Figures 4.9 and 4.10. Similar to the mono metallic catalysts all of the modified catalysts underwent initial deactivation. It can be seen that at steady state CO conversion increases with increasing iron loading (or total metal loadings, respectively) which is in agreement with the literature (Fukushima et al., 1985; Burch and Petch, 1992a; Schunemann et al., 1995; Burch and Hayes, 1997; Haider et al., 2009). However, it was reported in literature that there

is an optimum to the loading of iron as a promoter and further increase causes a decrease in CO conversion due to the blockage of sites at the rhodium promoter interface (Burch and Petch, 1992a; Burch and Hayes, 1997; Haider et al., 2009). It has been suggested that the increase in catalytic activity with increase in iron loading is due to the intimate contact between rhodium and iron creating new active sites (Burch and Hayes, 1997). Alternatively, the enhancement in activity with increasing iron loading may be due to the formation of alloys (Schunemann et al., 1995). Schunemann et al. (1995) proposed that Fe^0 alloyed with Rh^0 was responsible for the increase in catalytic activity for CO hydrogenation at 250°C, 10 bar and $H_2/CO = 2$. From the TPR results it was seen that rhodium and iron were in close contact with each other and furthermore from the XRD analyses the Rh-Fe bimetallic catalysts (Rh:Fe = 1:0.5 and Rh:Fe = 1:1) were observed to be composed of alloys.

Furthermore in order to gain more insight on the activity of the model catalysts, the catalytic activity was also reported in terms of turn-over frequency (TOF) which is defined as the moles of CO converted per time unit and exposed rhodium/iron metal atom. The TOF was normalised with respect to both Rh and Fe for the Rh/Fe catalysts. This was done by combining the loading of Rh and Fe on average molecular weight, depending on actual catalyst composition. Figure 4.11 shows turn-over frequency (TOF) as a function of time on stream (TOS) for the model catalysts. In addition, TOF both during the initial state (10 minutes) and steady state (7 hours) as a function of iron mole fraction in catalyst for all the model catalysts are shown in Figure 4.12. It can be noted that pure rhodium and Rh/Fe catalysts display the same behaviour as reported from the conversions results (see Figure 4.10). It has been reported that crystallite size affects specific catalyst activity (TOF) (Ojeda et al., 2004a). However the effects of crystallite sizes was eliminated by preparing the Rh and Rh/Fe catalysts with similar crystallite sizes and therefore the increase in TOF with increased iron loading is mainly due to the effect of iron addition only. Nakamula et al. (2011) reported that the increase in TOF for the Rh/Fe catalysts was due to synergistic electronic effect. However, the pure iron crystallite sizes was larger compared to the other catalysts which would explain the higher TOF for this sample. Some recent studies reported that larger crystallites display higher TOF compared to smaller crystallites and has been attributed to a combination of structural and electron effects (Mabaso, 2005; Barkhuizen et al., 2006; Bezemer et al., 2006; Welker, 2007; Fischer 2011).

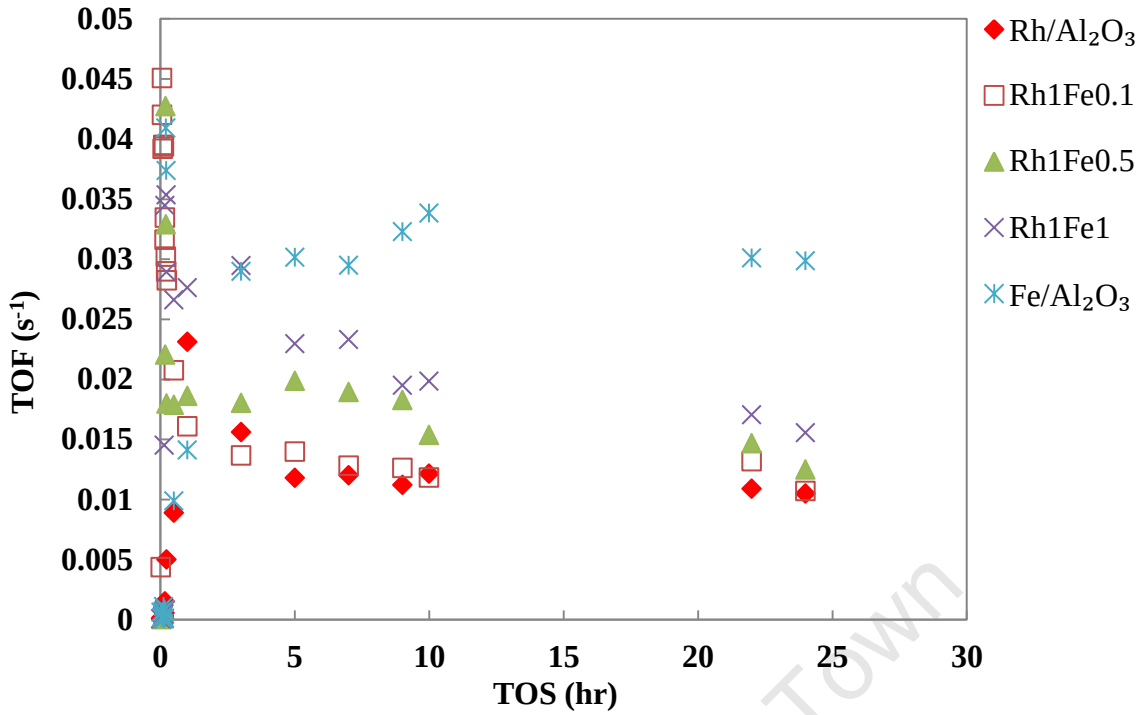

Figure 4.11: Turn-over frequency (TOF) of model catalysts as a function of time on stream (TOS)

(Reaction conditions: T = 180°C, P = 10 bar, GHSV = 20 ml(NTP)/min.g_{cat}, H_2/CO = 1)

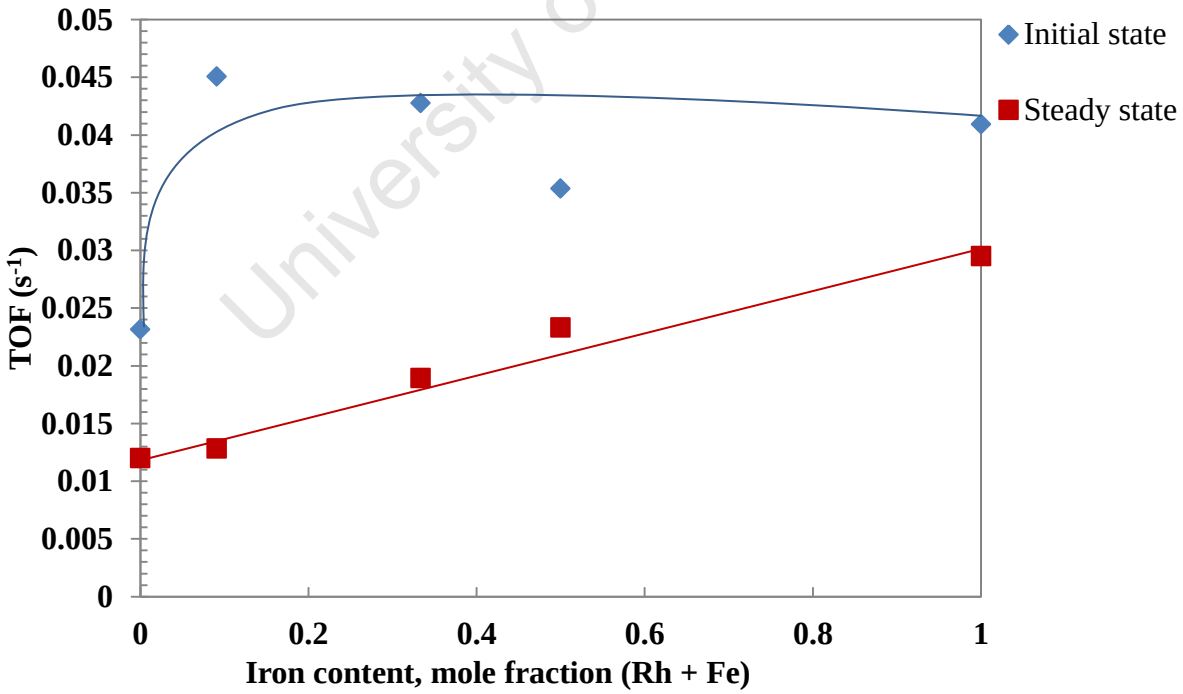

Figure 4.12: Turn-over frequency of model catalysts as a function of iron mole fraction in catalyst at both maximum activity and steady state (7 hours)

(Reaction conditions: T = 180°C, P = 10 bar, GHSV = 20 ml(NTP)/min.g_{cat}, H_2/CO = 1)

It is important to note that the same crystallite sizes were used for calculation of TOF at beginning and end. Strictly, for the latter the sizes of the spent catalysts should have been used. However, the XRD analysis performed for the spent catalysts (see Figure 4.13 and Table 4.5) showed that the Rh-bearing catalysts did not undergo crystallite growth. The average crystallite size of the spent pure iron catalyst decreased. The TOF of the size of the spent iron catalyst was obtained to be 0.0075 s^{-1}.

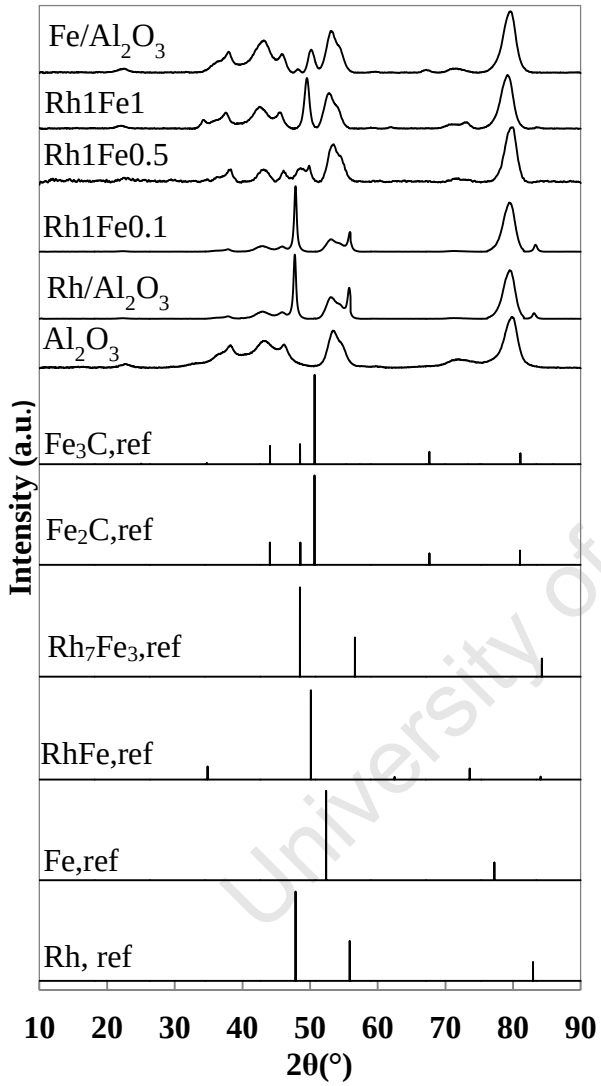

Figure 4.13: XRD patterns of spent model catalysts. The diffraction spectrum of γ-alumina support and reference patterns for metallic rhodium, metallic iron, RhFe, Rh_7Fe_3, Fe_2C (hexagonal) and Fe_3C (cementite) are include

The characterisation of the spent catalysts was performed by means of XRD. It was very important to do post-run analysis of the model catalysts as it would help determine the iron phase in the Rh/Fe catalysts as well as in the pure iron catalyst. This would assist to develop

the idea why the Rh/Fe catalysts are very different from the pure iron catalysts. XRD patterns of Rh, Fe, Rh/Fe catalysts at various molar ratios of Rh:Fe as well as reference patterns for metallic rhodium, metallic iron, RhFe, Rh_7Fe_3, Fe_2C and Fe_3C are shown in Figure 4.13. The XRD patterns of rhodium and Rh1Fe0.1 samples clearly showed the peaks for metallic rhodium. As previously pointed out for the Rh1Fe0.1 reduced catalyst, no alloys formation was observed. According to Ichikawa et al. (1986), Fe atoms are mostly present in the state Fe^{3+} for catalyst of a low Fe/Rh. The XRD pattern for Rh1Fe0.5 sample revealed that it is composed of RhFe alloy as well as little cementite carbide formation while XRD pattern for Rh1Fe1 sample clearly showed peaks for RhFe alloy only. It was found that the XRD pattern for pure iron catalyst exhibited characteristic peaks for mainly cementite and hexagonal carbides. It can be noted from the XRD analysis that the pure iron catalyst mainly result to carbide formation while the Rh1Fe0.5 and Rh1Fe1 samples resulted to the formation of alloys and very little carbide formation.

Table 4.5: Calculated average crystallite sizes of the model catalysts in the spent state using the Scherrer equation from XRD scans and peaks used for calculations

Sample Code	d_{spent}, nm (XRD)	$d_{red,}$ nm (XRD)	2θ (°)
Rh/Al_2O_3	5.4	5.1	47.8
Rh1Fe0.1	4.6	4.4	47.9
Rh1Fe0.5	4.1	4.2	50.0
Rh1Fe1	2.0	3.5	49.9
Fe/Al_2O_3	1.6	9	50.1

Table 4.5 shows the average crystallite sizes of the spent model catalysts as well as sizes of the freshly reduced model catalysts for comparison. It is evident that the Rh-bearing catalysts did not undergo crystallite growth. However the average crystallite size of iron catalyst decreased from 9 nm (freshly reduced) to 1.6 nm (spent) which is suggested to be due to phase changes. The iron catalyst prior to the reaction contained α-Fe assuming full reduction and after 25 hours under CO hydrogenation conditions carbides formation occurred (see Figure 4.13).

4.3.2. Product Formation

Organic products collected using the ampoule sampling procedure were analysed using an offline GC equipped with Flame Ionisation Detector (FID). The methane selectivity was calculated using the offline FID analysis because no methane or carbon dioxide could be detected using the online TCD under the reaction conditions of the study. Selectivities reported here are those of the organic product compounds (C_1-C_7) which are volatile at reaction conditions. Very small amounts of longer chained organic products were present in the FID chromatograph, in particular with the Rh-bearing catalysts. The methane and organic products selectivity during the initial state of the experiment (10 minutes) and at steady state (7 hours) for the model catalysts are reported below. Analysis of the organic products was also performed using an offline two-dimensional gas chromatography coupled with a mass spectrometer (GCxGC-TOF) in order to identify oxygenates peaks.

GC x GC-TOF chromatography was also used to confirm the acetic acid peak as it was very difficult to detect on the offline FID because it co-elute with some of the major hydrocarbon compounds (butene-1). Figures 4.14-4.17 show the spectra of pure rhodium catalyst, Rh/Fe catalysts and pure iron catalyst. The presence of oxygenates including ethanol, acetaldehyde, methanol, propanol and acetic acid were observed. The GC x GC spectrum obtained with the pure iron catalyst (see Figure 4.17) was very different from that obtained for the pure rhodium and the Rh/Fe catalysts. It is very important to note that Rh and Rh/Fe catalysts mostly formed oxygenated compounds while the pure iron catalyst resulted to the formation of mainly hydrocarbons. Corresponding FID chromatograms confirming this trend are shown in the appendix B (see figures B.2-B.6).

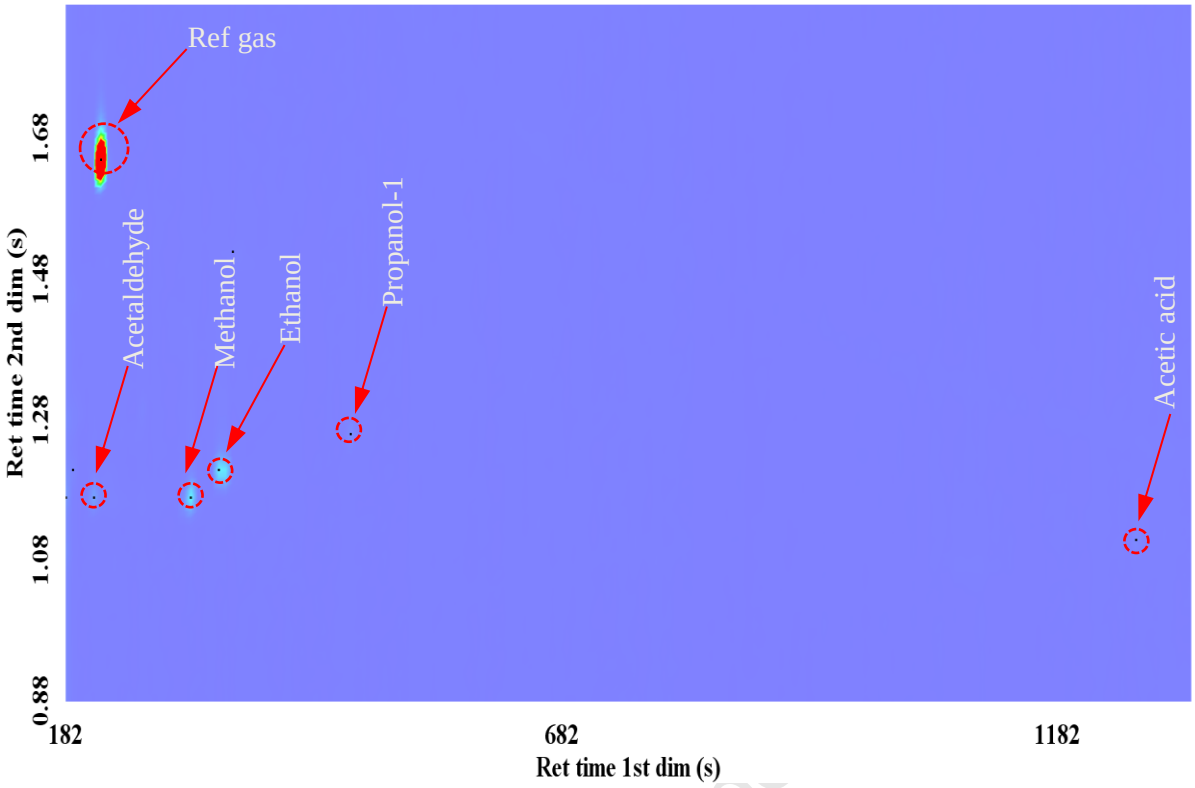

Figure 4.14: Offline GCxGC-TOFMS chromatograph contour plot for the pure rhodium sample

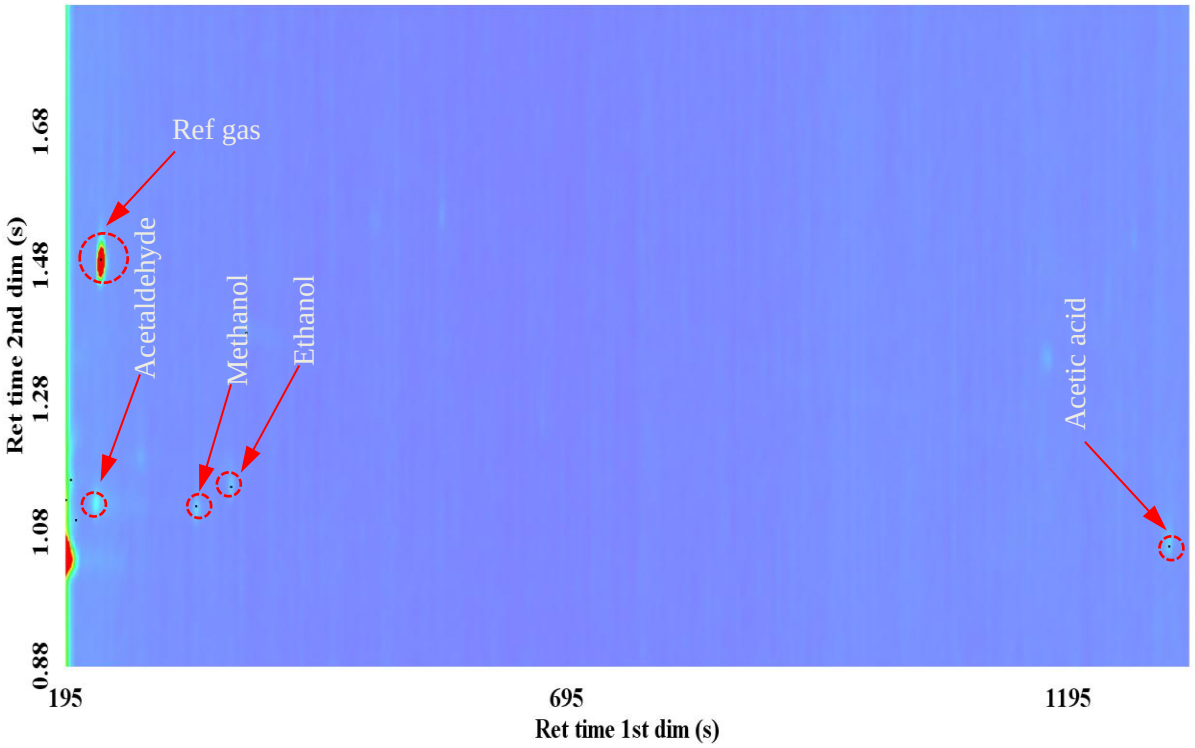

Figure 4.15: Offline GCxGC-TOFMS chromatograph contour plot for the RhFe bimetallic sample with Fe:Rh molar ratio of 0.1

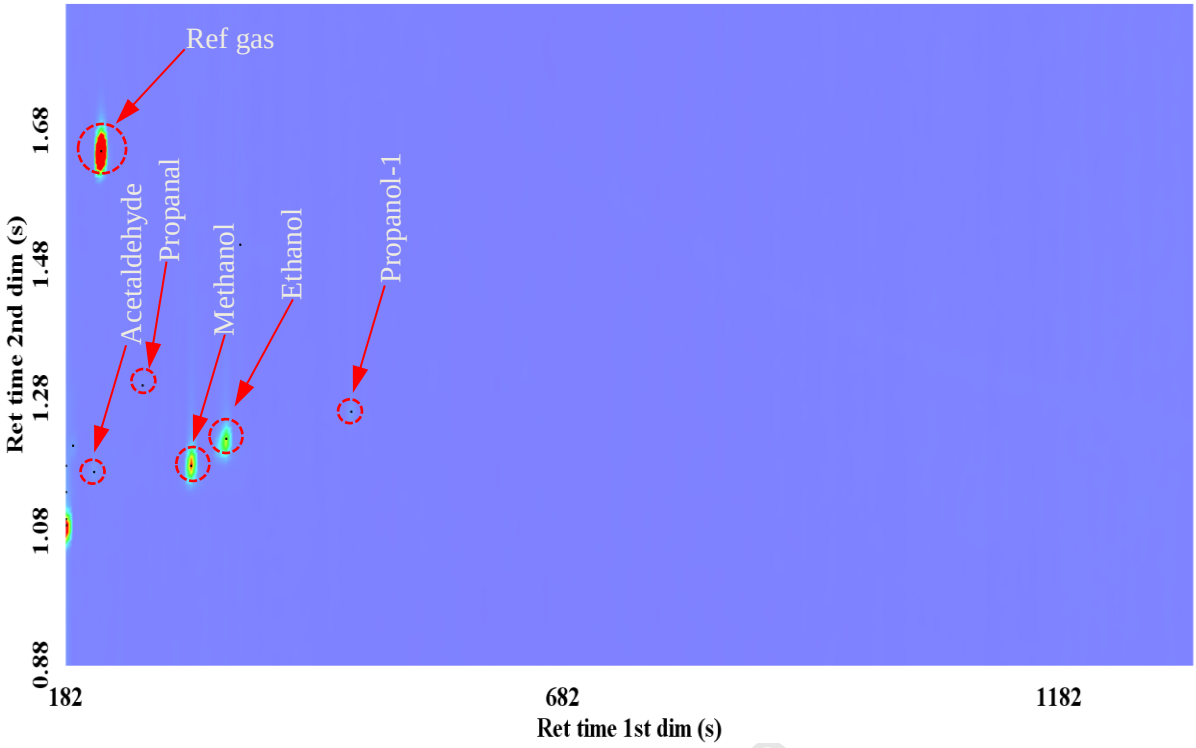

Figure 4.16: Offline GCxGC-TOFMS chromatograph contour plot for the RhFe bimetallic sample with Fe:Rh molar ratio of 1

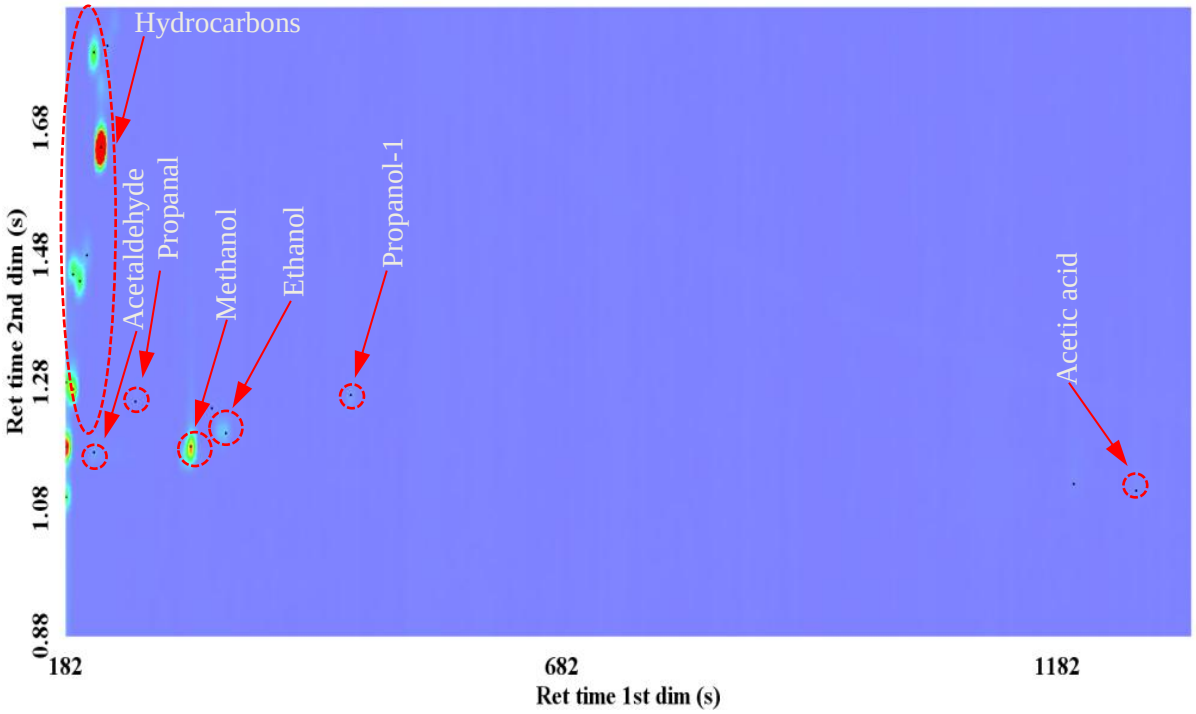

Figure 4.17: Offline GCxGC-TOFMS chromatograph contour plot for the pure iron sample

4.3.2.1. Methane Selectivity

Methane is the most thermodynamically stable product in Fischer-Tropsch synthesis (Anderson, 1984). However, methane is the least valuable product of the Fischer-Tropsch synthesis, therefore inhibition of methane formation is essential (Schulz, 2003). It is formed through associative desorption of a methyl species and activated surface hydrogen. Alternatively, the methyl species can act as a chain starter leading to chain growth. Methane is also believed to form on additional sites which are not capable of supporting FT-chain growth (Schulz, 2003).

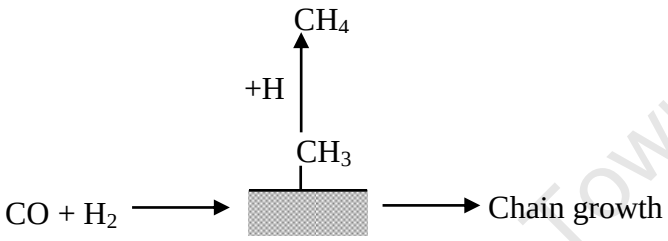

Figure 4.18: Schematic representation of the formation of methane or chain growth in the FT synthesis (adapted from Claeys and van Steen, 2004)

Methane selectivities obtained in the experimental runs for the model catalysts as a function of time on stream are shown in Figure 4.19. In addition, methane selectivities both during the initial state (10 minutes) and steady state (7 hours) as a function of iron mole fraction in catalyst for all the model catalysts are shown in Figure 4.20.

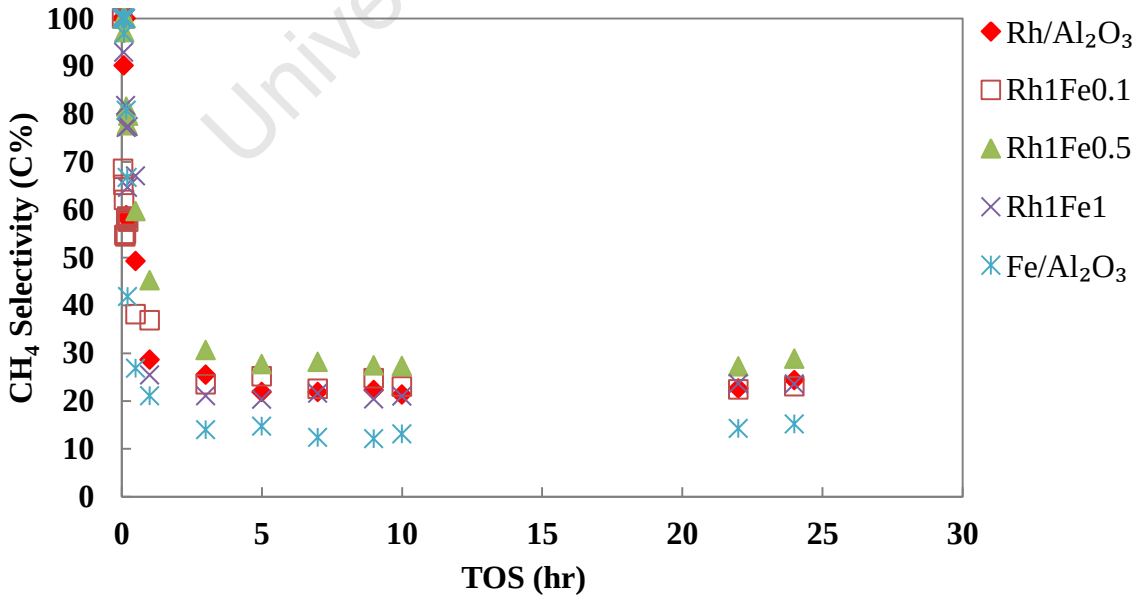

Figure 4.19: Methane selectivity of model catalysts as a function of time on stream (Reaction conditions: T = 180°C, P = 10 bar, GHSV = 20 ml(NTP)/min.g_{cat}, H_2/CO = 1)

Methane selectivities of 60-80 C% for the model catalysts were obtained during the initial state of the runs which rapidly decreased to steady state values of 12-28 C%. Addition of iron to alumina-supported rhodium catalysts led to slightly higher methane selectivities compared to the unpromoted alumina-supported rhodium catalyst. These results are consistent with the findings by Mo et al. (2009a and b) who observed a slight increase in methane selectivity with addition of iron in CO hydrogenation for silica-supported rhodium catalysts. The increase in methane selectivity is attributed to the enhancement of the hydrogenation step during CO hydrogenation by iron which in turn leads to increase in methane formation.

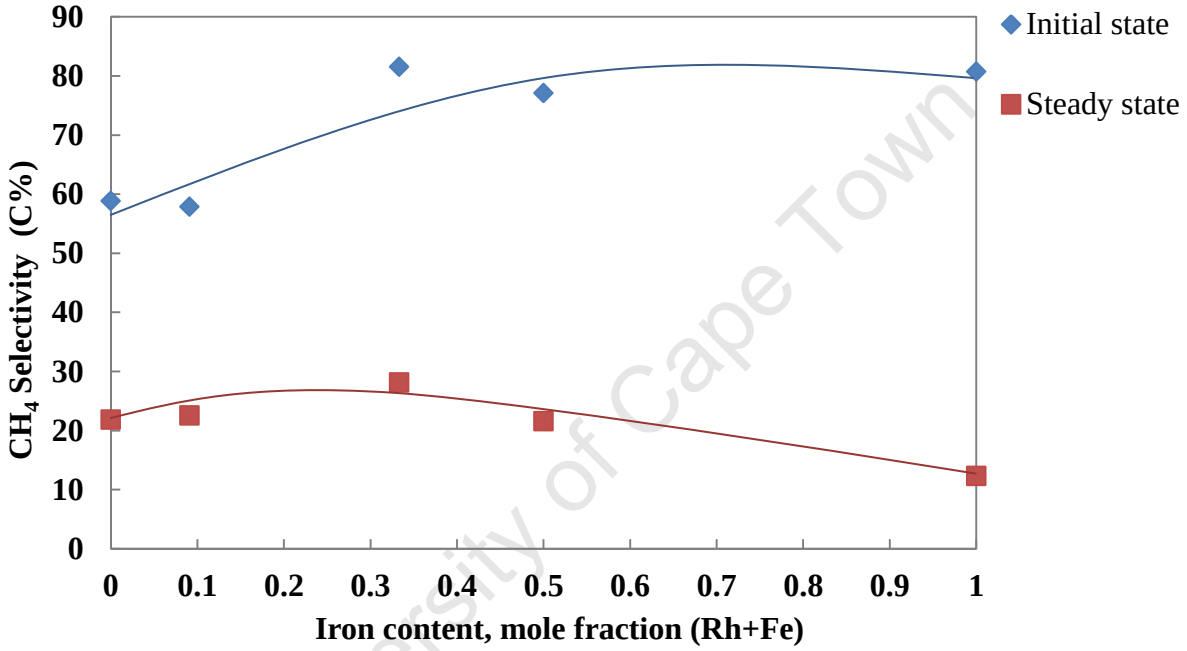

Figure 4.20: Methane selectivity as a function of iron mole fraction in catalyst at both the initial state (10 minutes) and steady state (7 hours)
(Reaction conditions: T = 180°C, P = 10 bar, GHSV = 20 ml(NTP)/min.g_{cat}, H_2/CO = 1)

The methane selectivity for the iron catalyst was higher in the initial state of the run and drastically decreased from 80 C% during the initial stage to steady state value of 12 C%. The methane selectivity obtained in the study was slightly higher than methane selectivies in commercial processes. In commercial processes methane selectivity is 4 C% for Low Temperature Fischer-Tropsch synthesis and 8 C% for High Temperature Fischer-Tropsch synthesis (Dry, 2004b). The methane selectivity may be slightly higher because the value obtained was a slight overestimate of the actual methane selectivity as long chain products were not taken into account in the calculations. Also the conversion levels here are very low and it is known that this and the corresponding low water partial pressures contribute to high

methane selectivity (Claeys and van Steen, 2002). The pure iron catalyst resulted to less methane as compared to Rh/Fe catalysts and ascribed to phase changes of the catalyst which, in this case, formation of carbides. Riedel et al. (1999) reported that carbiding of iron catalysts is of great importance and formation of carbides inhibits methane formation. However, little carbide formation was observed in Rh/Fe catalysts (see Figure 4.13), which might explain why pure iron catalyst gives less methane than Rh/Fe catalysts. Furthermore, as shown in the section below, with Fe much higher chain growth probabilities are obtained therefore resulting in lower methane selectivity. Also there is more CH_4 formation with Rh in general and is due to low chain growth.

4.3.2.2. Chain Growth

Chain growth is the essential feature of Fischer-Tropsch synthesis (Schulz, 2003). Inhibition of product desorption is very important allowing for chain growth (Schulz, 2003). The chain growth probability (α) is an indication of the probability of the catalysts to form longer chain hydrocarbons. Higher chain growth probabilities indicate formation of higher molecular weight products.

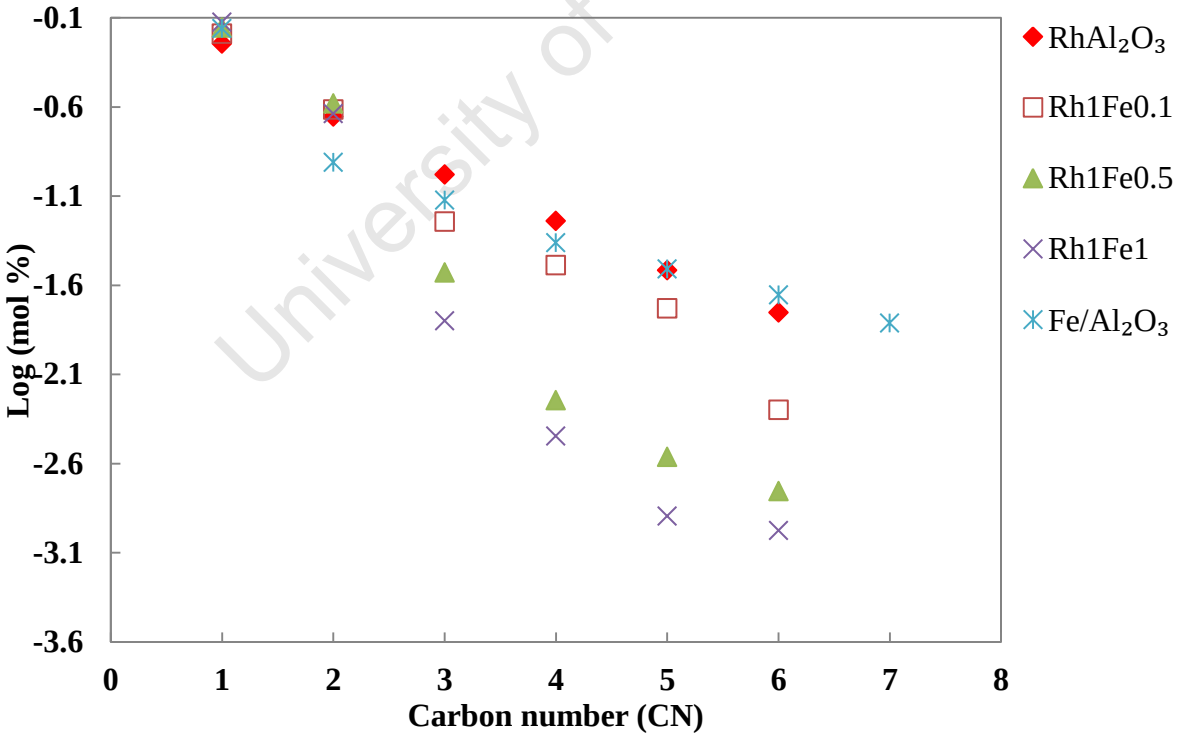

Figure 4.21: Logarithmic molar product distributions of the hydrocarbons and oxygenates as a function of carbon number in CO hydrogenation at steady state (7 hours)
(Reaction conditions: T = 180°C, P = 10 bar, GHSV = 20 ml(NTP)/min.g_{cat}, H_2/CO = 1)

Assuming carbon number independence, the chain growth probabilities for the model catalysts were extracted from the slopes (C_3-C_7 carbon number range) of the straight line of the Anderson-Schulz-Flory distributions (i.e. logarithmic plots of mole fractions of hydrocarbons and oxygenates as a function of carbon number).

The logarithmic molar product distributions of the hydrocarbons and oxygenates as a function of carbon number at steady state (7 hours) for the model catalysts are shown in Figure 4.21. It can be seen in Figure 4.21. that all curves of the model catalysts approximately show the often obtained deviations from ideal distributions with relatively high values at C_1 and a slight curvature with increasing carbon number (Schulz and Claeys, 1999). However, instead of obtaining relatively low values at C_2 as is usually reported in literature, the values at C_2 were relatively high. The result is consistent with the findings of Lin et al. (1995) who obtained similar results for the distribution of oxygenated and hydrocarbon products on a Rh-Mn/SiO_2 catalyst. An explanation for this result may be that after CO dissociation and hydrogenation to produce CH_x species over the catalyst surface, the rate of chain growth is lower than that of CO insertion into the CH_x species resulting in an increase in the formation of oxygenated compounds. In addition, it is well known that rhodium favours the formation of short chain products with C_2 oxygenates generally observed as the major products of oxygenates (Bhasin et al., 1978), therefore explaining why the C_2 values are relatively high.

In order to prove that the values at C_2 are high due to the oxygenated compounds, the logarithmic molar production of the linear hydrocarbons as a function of carbon number at steady state (7 hours) for the model catalysts is shown in Figure 4.22. It was observed that all model catalysts have low C_2 content following ASF distribution of Fischer-Tropsch synthesis. The relatively low C_2 content was attributed to the readsorption of ethene to undergo secondary reactions in particular incorporation. Ethene is very reactive as compared to the other α-olefins. An extrapolation of the slope obtained between C_3 and C_7 towards C_1 suggest a relatively high methane content, i.e. higher than expected assuming ideal ASF kinetics. This has been ascribed by Schulz (2003) as “extra methane” which is formed on non FT sites.

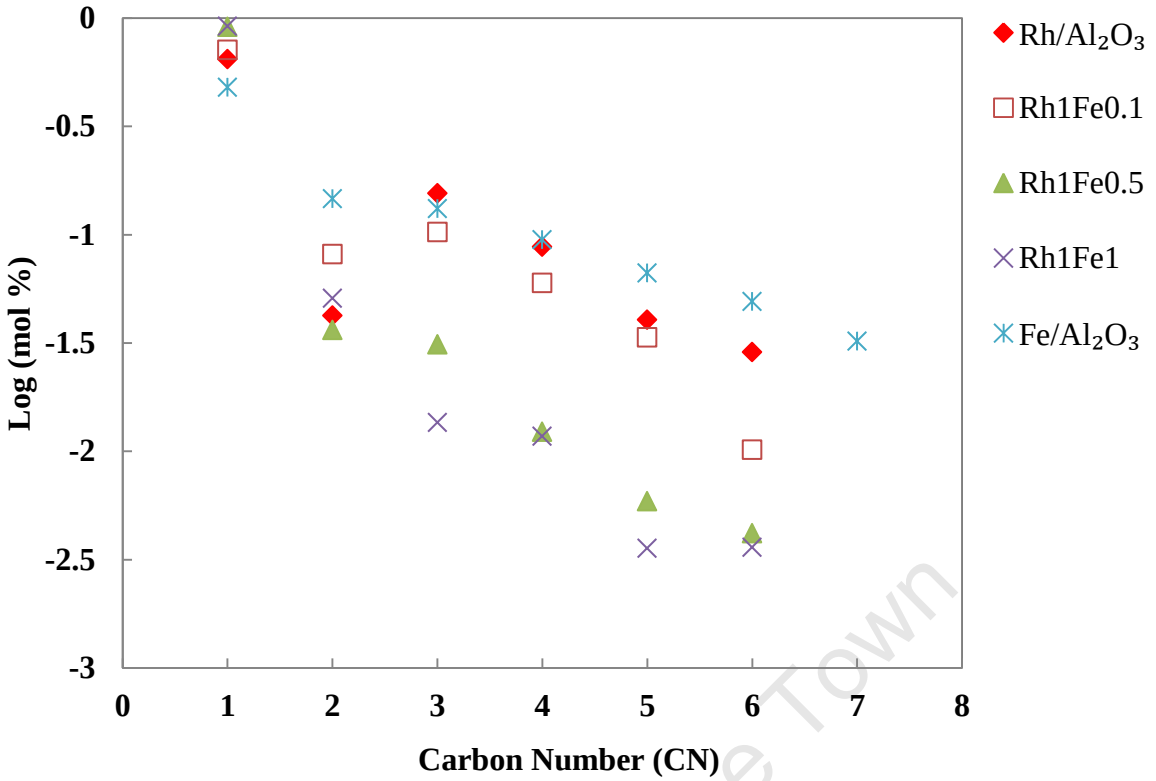

Figure 4.22: Logarithmic molar product distributions of the linear hydrocarbons as a function of carbon number in CO hydrogenation at steady state (7 hours)

(Reaction conditions: T = 180°C, P = 10 bar, GHSV = 20 ml(NTP)/min.g_{cat}, H_2/CO = 1)

The chain growth probabilities of the model catalysts were obtained from Anderson-Schulz-Flory distributions (hydrocarbons and oxygenates distributions) in the carbon number range C_3 to C_7 as shown in Figure 4.23. Chain growth probability and methane selectivity are inversely related. However, there may be sites which only promote methane formation and no chain growth. Deviations of methane in the ASF plot are a good indication for this. Just looking at this, quantitatively, this seems to be more pronounced for the Rh, Rh/Fe catalysts. The chain growth probabilities decrease, while methane selectivities increase with increasing iron loading of the alumina-supported rhodium catalysts. The chain growth probability of the pure alumina-supported rhodium catalyst was 55% and with increasing iron loading the chain growth probability decreased to a minimum value of 40% for the catalyst with the highest loading of iron. The chain growth probabilities for all model catalysts were very low except for the pure alumina-supported iron catalyst which was relatively high (68%).

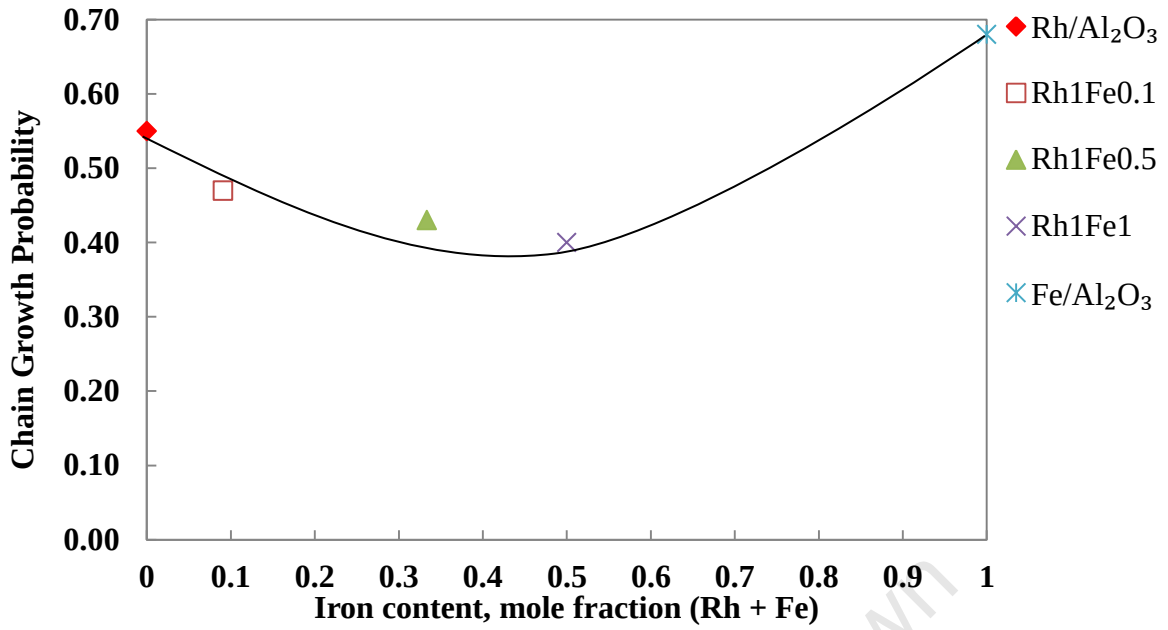

Figure 4.23: Chain growth probability (C_3-C_7) of the model catalysts as a function of iron mole fraction in catalyst at steady state (7 hours)
(Reaction conditions: T = 180°C, P = 10 bar, GHSV = 20 ml(NTP)/min.g_{cat}, H_2/CO = 1)

Rhodium favours the formation of short chain products and the major products observed for the Rh-based catalysts are methane, C_2 oxygenates and a small fraction of C_{2+} hydrocarbons (Chuang et al., 2005) which results in low chain growth probability. The addition of iron to the Rh-based catalysts has been found to result in a significant decrease in hydrocarbons especially olefins (Burch and Petch, 1992a; Mo et al., 2009a). Furthermore, it has been suggested that the presence of iron on the rhodium-based catalyst results in the creation of new sites which selectively produce C_2 oxygenates (Burch and Hayes, 1997) resulting in low chain growth probability. Also, the addition of iron to the rhodium-based catalysts has been proposed to enhance hydrogenation resulting in an increase in the hydrogen availability on the catalyst surface leading to more saturated hydrocarbons and low chain growth probability (Burch and Petch, 1992a; Mo et al., 2009a). It seems that Rh containing catalyst display a completely different behaviour, in other words the Rh/Fe catalysts do not behave like a Rh and a Fe type spectrum but rather a modified Rh type spectrum. This is also an indication that Rh and Fe interact very closely in Rh/Fe catalysts, i.e. the two metals are not segregated in these catalysts.

4.3.2.3. Olefin Formation

The primary organic products of the FT synthesis are α-olefins and n-paraffins (Schulz, 1999). Olefins are formed via the dissociative β-H-elimination from a surface alkyl species while paraffins are formed via hydrogenation of a surface alkyl species. A primary carbon number independent olefin content of 70-90 mol% can be obtained in FT products (Schulz and Claeys, 1999). However, olefin desorption is reversible as olefins can readsorb and undergo secondary reactions such as hydrogenation to the corresponding paraffin, isomerisation via double bond shift and incorporation into further chain growth (Schulz and Claeys, 1999).

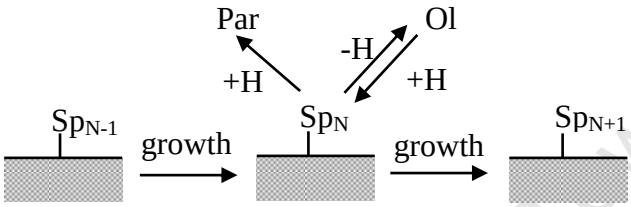

Figure 4.24: Surface polymerisation with chain growth, chain termination step to form n-paraffin or α-olefins and readsorption of α-olefins (adapted from Claeys and van Steen, 2004)

Figure 4.25 shows molar olefin contents in the linear hydrocarbons as a function of carbon number for the model catalysts and was used to obtain information on the extent to which olefins underwent secondary reactions.

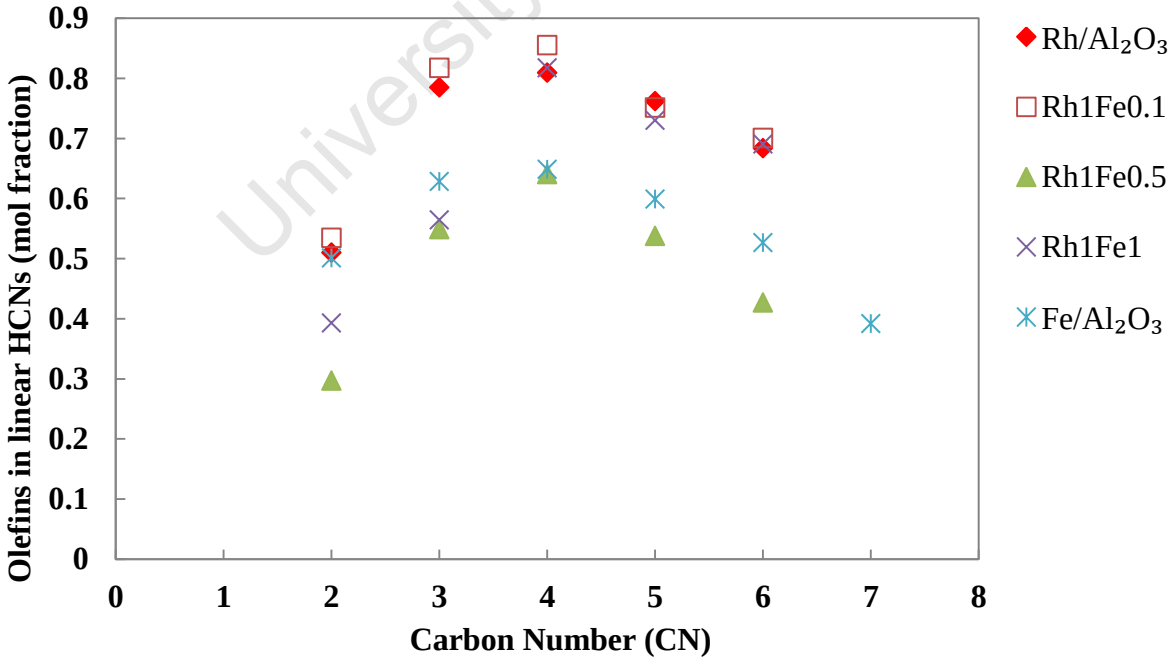

Figure 4.25: Molar content olefin fraction in the linear hydrocarbons as a function of carbon number

(Reaction conditions: T = 180°C, P = 10 bar, GHSV = 20 ml(NTP)/min.g_{cat}, H_2/CO = 1)

These curves typically show relatively low olefin contents in C_2 fraction and a decrease in olefin content from carbon number C_3 onwards. The low C_2 olefin content is attributed to the high reactivity of ethene compared to longer chain olefins. The decrease in olefin content with increasing carbon number is believed to be a result of carbon number dependent solubility (Schulz and Claeys, 1999), or carbon number dependent diffusion rates (Iglesia et al, 1993) which lead to higher residence times of the longer chained olefins, therefore increasing the probability to undergo secondary reactions.

The pure rhodium catalyst was observed to have low olefin content in C_2, however from C_3 onwards the olefin content was between 70-80 mol% which is the expected olefin content for primary olefin selectivity implying that almost no secondary olefin reactions took place. The pure iron catalyst was shown to have relatively low olefin content in C_2 and a decrease in olefin content with increasing carbon number. It is evident that secondary olefin reactions took place during CO hydrogenation using this catalyst. The olefin content in linear hydrocarbons decreased with increasing iron content for the Rh-Fe bimetallic catalysts as well as for pure rhodium catalyst. The addition of iron to the alumina-supported rhodium catalyst has been found to improve hydrogenation resulting in an increase in the hydrogen availability on the surface which in turn favours the formation of paraffins (Mo et al., 2009a). An alternative explanation for the decrease in olefin content in linear hydrocarbons with increasing iron content could be that iron added to rhodium catalyst exerts a modifying effect to stabilize an alkyl species leading to the formation of paraffins (Fukushima et al., 1985) and thus resulting in low chain growth probability.

Figure 4.26 shows the molar amount of propene in C_3 hydrocarbons for the model catalysts as a function of time on stream. Generally, low olefin contents were obtained in the initial state which increased until reaching a steady state. It can be noted that the propene fraction in C_3 hydrocarbons decreases with increasing iron content as shown in Figure 4.27. This is indeed as expected since the addition of iron has been proposed to improve hydrogenation. However, the catalyst with the highest iron content was found to have higher propene content as compared to the catalyst with the intermediate iron loading. It appears that too much iron decreases secondary olefin hydrogenation. It is proposed that the presence of high concentration of iron on the surface may inhibit olefin re-adsorption to the corresponding paraffin. The Rh1Fe1 catalyst may start to approach pure Fe behaviour. Furthermore, the pure iron catalyst gives higher propene content in C_3 hydrocarbons as compared to Rh1Fe0.5 and Rh1Fe1 catalysts. This is attributed to the formation of iron carbide in pure iron while little

carbide formation was observed in Rh1Fe0.5 and Rh1Fe1 catalysts (see Figure 4.13). Riedel et al. (1999) reported that iron carbide formation inhibits hydrocarbon C_{2+} product desorption and also secondary olefin hydrogenation.

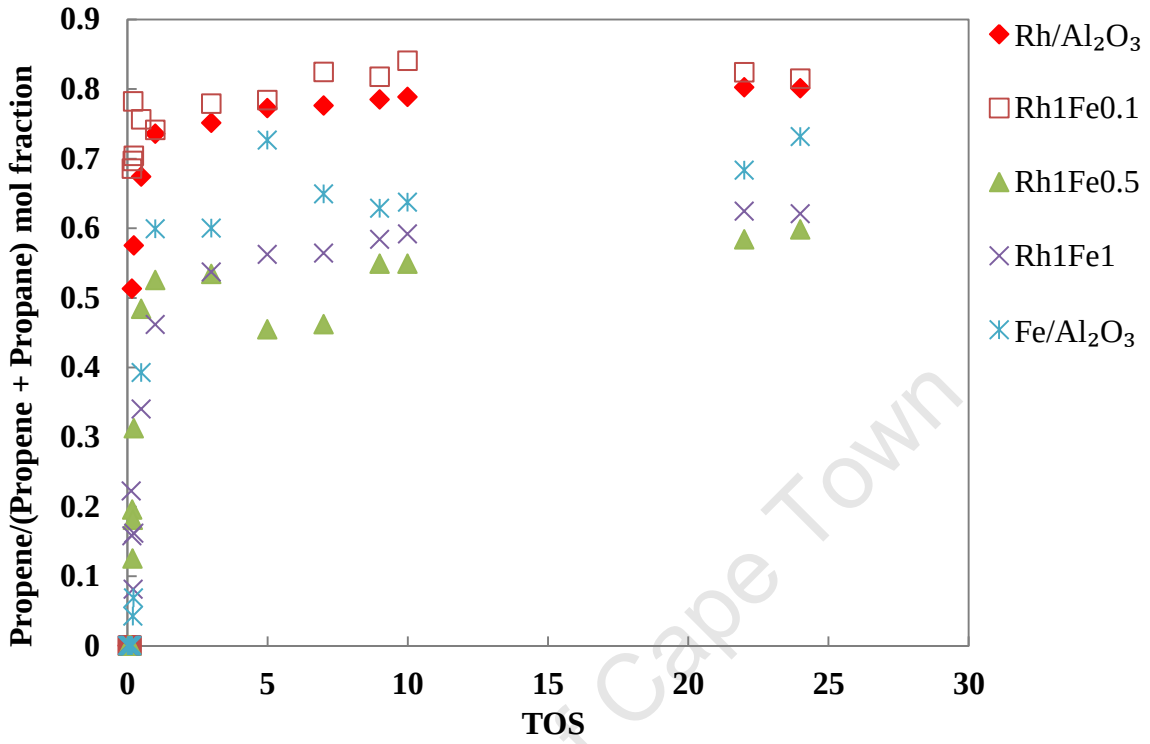

Figure 4.26: Propene mole fraction in C_3 hydrocarbon fraction (propene and propane) for the model catalysts as a function of time on stream
(Reaction conditions: T = 180°C, P = 10 bar, GHSV = 20 ml(NTP)/min.g_{cat}, H_2/CO = 1)

In addition to hydrogenation and incorporation into further chain growth, α-olefins can also readsorb non-terminally to form olefins with internal double bonds. This reaction is known to occur on metal sites in the presence of hydrogen as well as on acid sites which may be present on support material (Germain, 1969).

As mentioned earlier, 70-90 mol% of the primary FT product is expected to consist of α olefins (Schulz and Claeys, 1999) and only small amounts (i.e. less than 5 %) of olefins with internal double bond is believed to be formed as a primary product. Therefore the contents of α olefins in the linear olefins would give an indication as to the extent to which this secondary reaction had occurred.

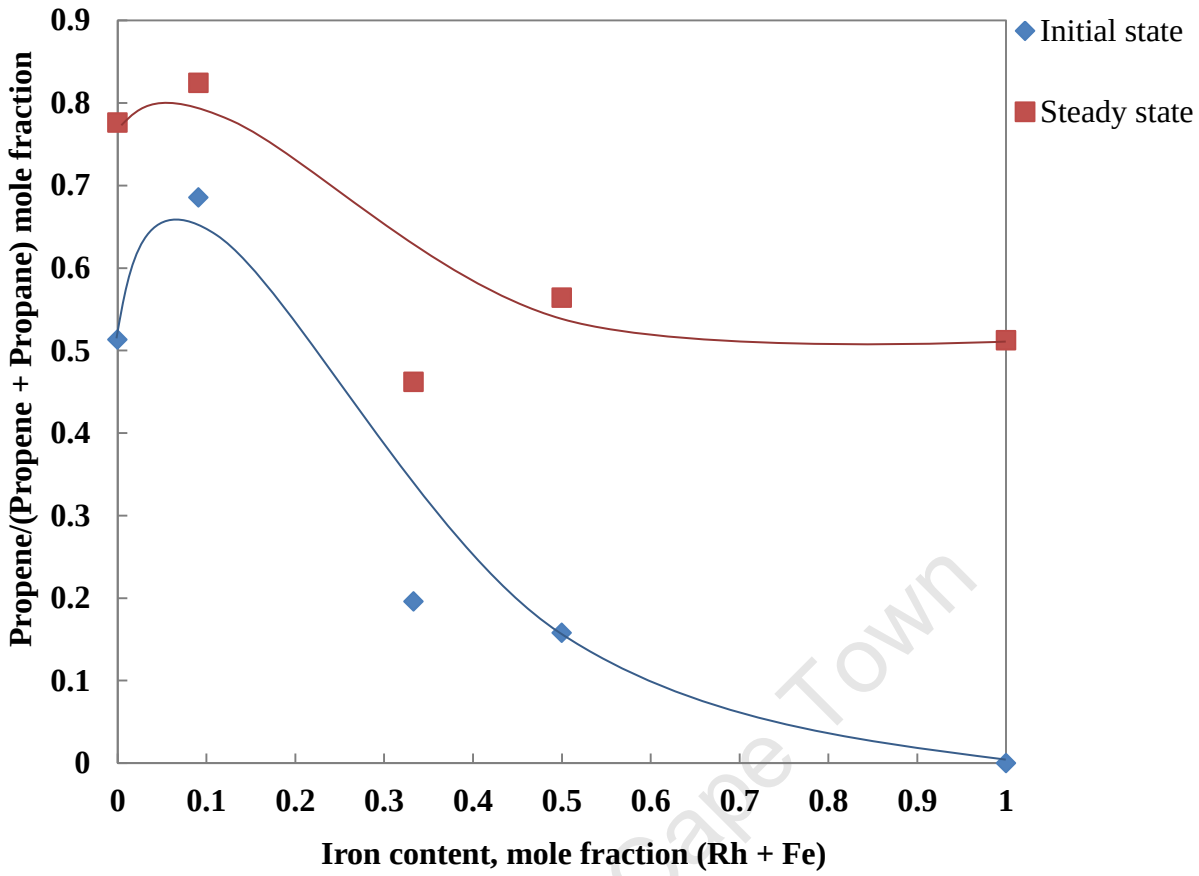

Figure 4.27: Propene mole fraction in C_3 hydrocarbon fraction for the model catalysts as function of iron mole fraction in catalyst at both the initial state (10 minutes) and steady state (7 hours)

(Reaction conditions: T = 180°C, P = 10 bar, GHSV = 20 ml(NTP)/min.g_{cat}, H_2/CO = 1)

Figure 4.28 shows the molar content of α-olefins in the linear olefins as a function of carbon number. It can be seen that α-olefins in linear olefins decrease with increasing iron content. The addition of iron to rhodium catalysts seems to favour the formation of olefins with internal double bond instead of α olefins. The lower α olefins content indicates that the addition of iron to rhodium catalysts improves hydrogen availability on the surface. Thus an increase in olefins with internal double bond is observed as this reaction requires the presence of hydrogen on the surface. The catalyst with the highest iron content was found to favour the secondary reaction to form olefins with internal double bond instead of hydrogenation to paraffins. Interestingly, on the pure iron catalyst much less double bond isomerisation was obtained.

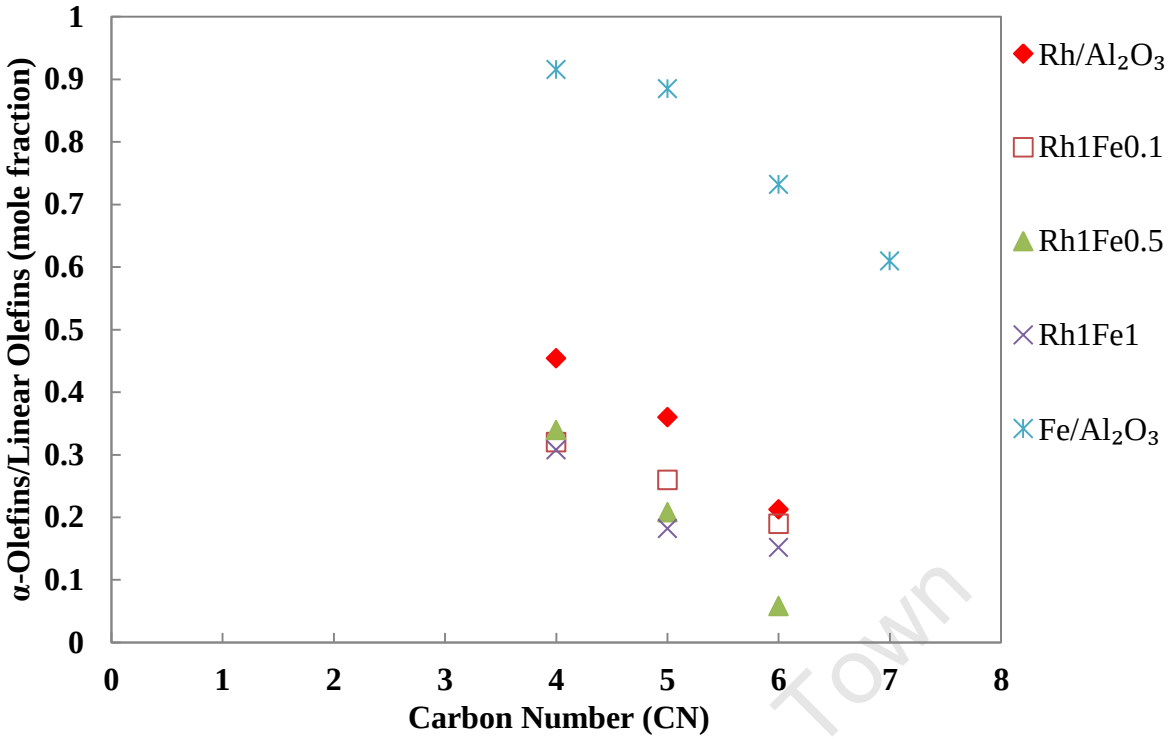

Figure 4.28: Molar content α-olefin in the linear olefins as a function of carbon number (Reaction conditions: T = 180°C, P = 10 bar, GHSV = 20 ml(NTP)/min.g_{cat}, H_2/CO = 1)

4.3.2.4. Formation of Oxygenates

Oxygenates are important chemicals especially C_2-oxygenates. Typically oxygenates in FT synthesis include aldehydes, alcohols, acids and ketones. FT catalysts (Fe, Co and Ru) favour the formation of hydrocarbons and oxygenates (mainly alcohols and aldehydes) are formed as minor products. There is controversy about the exact mechanism for the formation of oxygenates, however there are two common mechanisms that have been proposed. Johnston and Joyner (1993) proposed that an oxygen containing surface species can be formed by addition of a surface hydroxyl species into an alkylidene species. However, the most accepted route for the formation of oxygenates is the CO-insertion mechanism proposed by Pichler and Schulz (1970). In this mechanism, an oxygen containing surface species is formed via CO-insertion to a surface alkyl group. In both mechanisms, desorption of this species by hydrogen addition or elimination leads to the formation of alcohols or aldehydes. Furthermore, Cairns (2008) has shown that the oxygenates formed with iron based Fischer-Tropsch synthesis include carboxylic acids and that alcohols, aldehydes as well as carboxylic acids have the ability to readily interact with each other. Cairns (2008) proposed that the addition of an OH group to the acyl species yields the formation of carboxylic acids (see scheme 4.29).

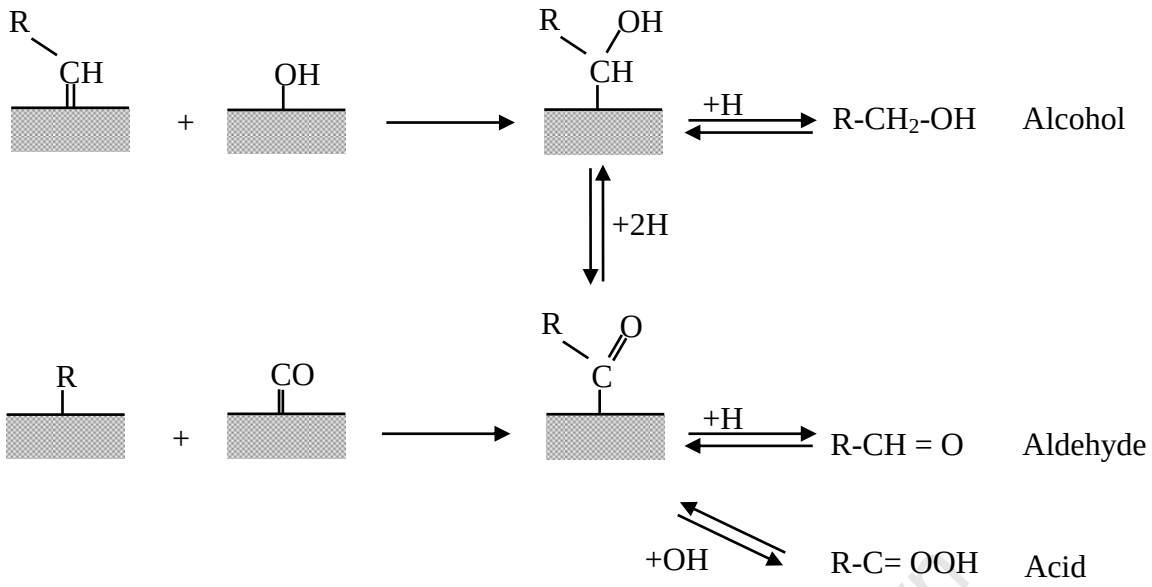

Figure 4.29: Kinetic scheme of oxygenate formation and interaction (adapted from Claeys and van Steen, 2004; Cairns, 2008)

Importantly it was also concluded that some of the reaction steps were affected by addition of copper leading to the more hydrogenated product. These observations were obtained from studies where oxygenates were co-fed during synthesis. In these studies no hydrogenation of the oxygenates to the corresponding hydrocarbon was obtained, suggesting that the formation of oxygenates (via OH addition) or 'terminal' steps in the synthesis and the oxygenates precursors do therefore not contribute to chain growth.

Rhodium catalysts are of interest because so far they have been found to be the most selective catalysts for the formation of mainly C_2 oxygenates (Chuang et al., 2005). This is attributed to the fact that rhodium has the ability to catalyse CO dissociation and CO-insertion (Chuang et al., 2005). The activity and selectivity of rhodium catalysts can be significantly altered by the presence of promoters. The addition of promoters to rhodium catalysts such as Fe, Mn and Li can change the product distributions (Burch and Petch, 1992b, Trevino et al., 1995).

The addition of iron exhibits significant effects which modify selectivity for oxygenates in CO hydrogenation on supported rhodium catalysts (Fukushima et al., 1985). Figure 4.30 illustrates the total oxygenates selectivity as a function of time on stream and was used to explain the effect of iron on supported Rh catalysts. Initially very low oxygenates contents were observed (see Figure 4.31), again highlighting the strongly hydrogenating regime in the early stages of the experiment. Methane was a major product with minor C_{2+} hydrocarbons in the initial state of the runs. Furthermore Figure 4.32 shows the C_{2+} hydrocarbons as a

function of time on stream. It can be observed in Figure 4.30 that the unmodified alumina-supported rhodium catalyst only produced total oxygenates with 35 C% selectivity at steady state while the selectivity towards C_{2+} hydrocarbons was 45 C% (see Figure 4.32). The formation of total hydrocarbons made up the majority of the total products for the unmodified alumina supported rhodium catalyst.

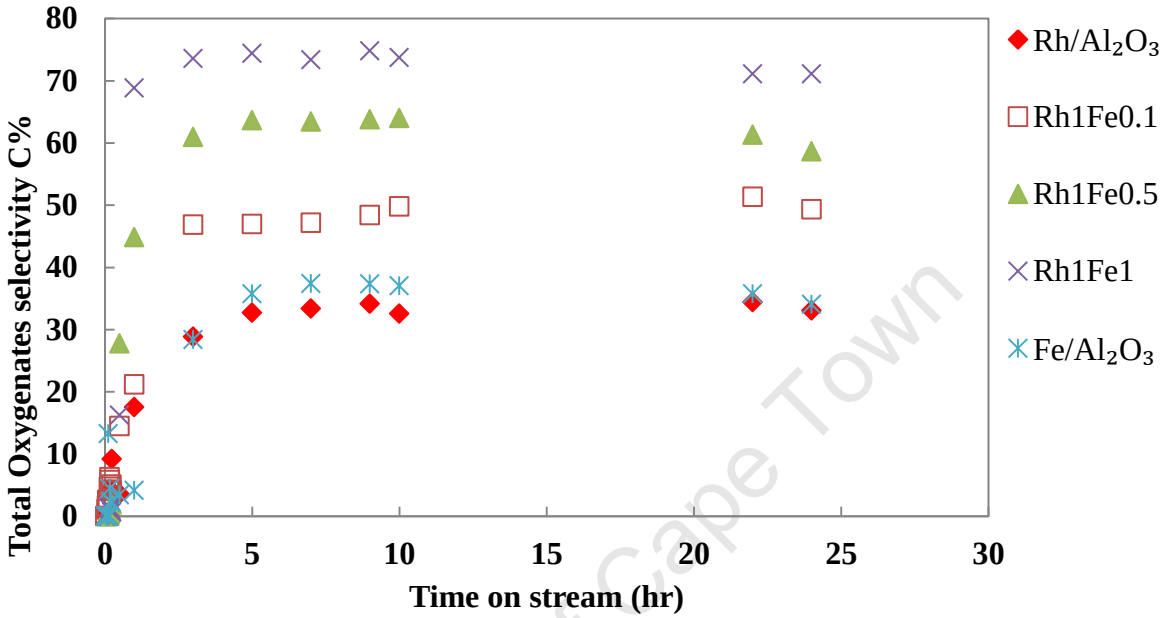

Figure 4.30: Total oxygenates selectivity of model catalysts as a function of time on stream (Reaction conditions: T = 180°C, P = 10 bar, GHSV = 20 ml(NTP)/min.g_{cat}, H_2/CO = 1)

The iron catalyst (no rhodium in the catalyst) resulted in a high selectivity for C_{2+} hydrocarbons of 50 C% which is in agreement with the results in the literature for the iron-based catalysts (Bhasin et al., 1978). However, it is very interesting to note the selectivity to total oxygenates of the iron catalyst (see Figure 4.30). This catalyst exhibited a high selectivity to oxygenates of 37% while usually iron catalysts in the Fischer-Tropsch synthesis produce mainly hydrocarbons and minor oxygenates (Mabaso, 2005; Cheang, 2009). This could be attributed to the conditions used in the study with low reaction temperature and a low H_2:CO ratio.

It can be seen in Figures 4.30 and 4.31, that the total oxygenates selectivity increases with increasing iron loading on the Rh/Fe catalysts. Furthermore, it is very interesting to note that the selectivity to C_{2+} hydrocarbons was significantly reduced from 45 C% for the unmodified rhodium catalyst to 5 C% for the catalyst with the large content of iron (see Figure 4.32). This is in agreement with results by Bhasin et al. (1978); Burch and Petch (1992) and Mo et

al. (2009b) who observed a decrease in hydrocarbons selectivity and sharp increase in the oxygenates selectivity.

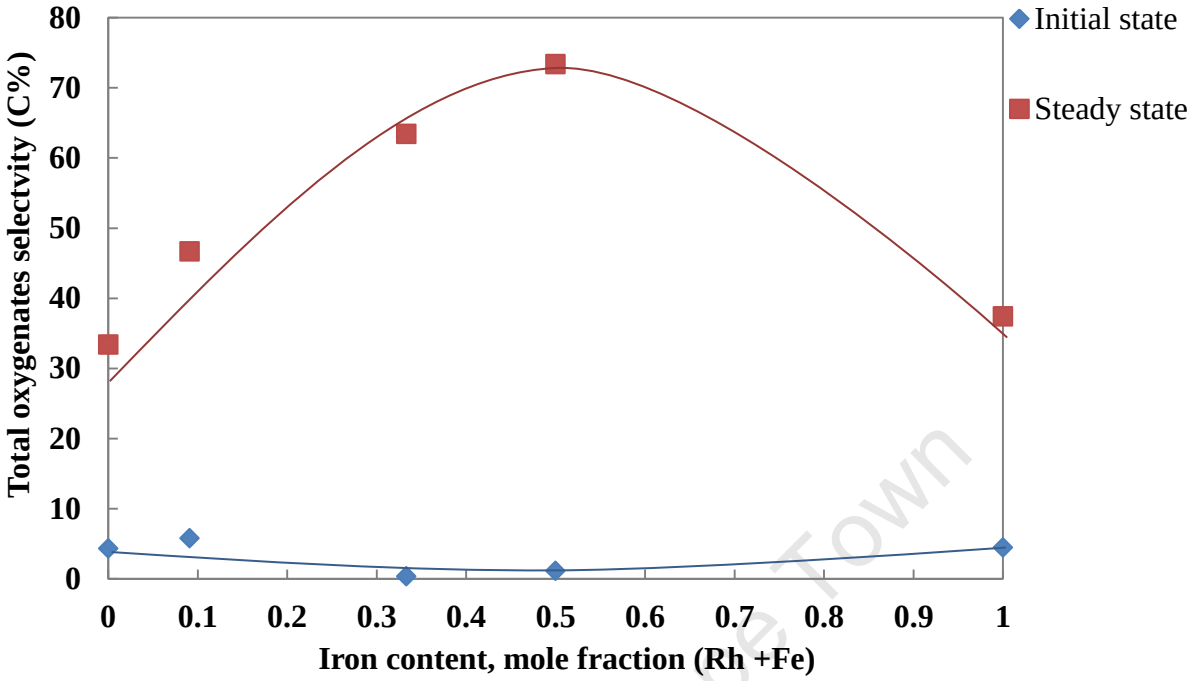

Figure 4.31: Total oxygenates selectivity as a function of iron mole fraction in catalyst both the initial state (10 minutes) and steady state (7 hours)

(Reaction conditions: T = 180°C, P = 10 bar, GHSV = 20 ml(NTP)/min.g_{cat}, H_2/CO = 1)

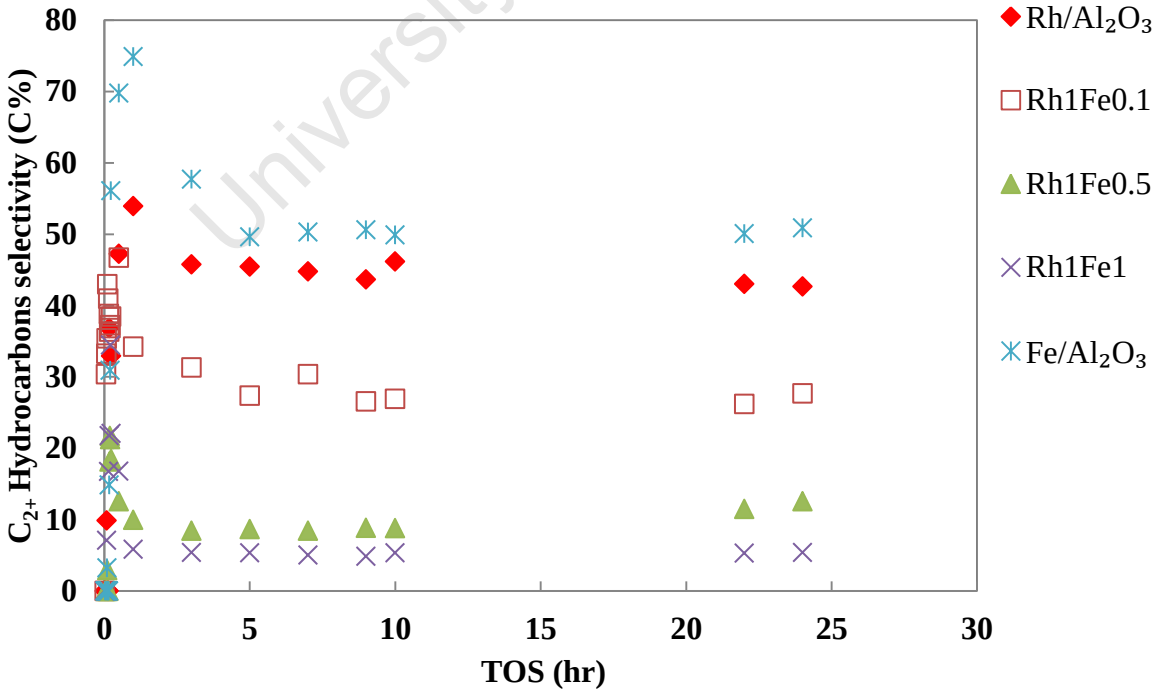

Figure 4.32: C_{2+} hydrocarbons selectivity of model catalysts as a function of time on stream

(Reaction conditions: T = 180°C, P = 10 bar, GHSV = 20 ml(NTP)/min.g_{cat}, H_2/CO = 1)

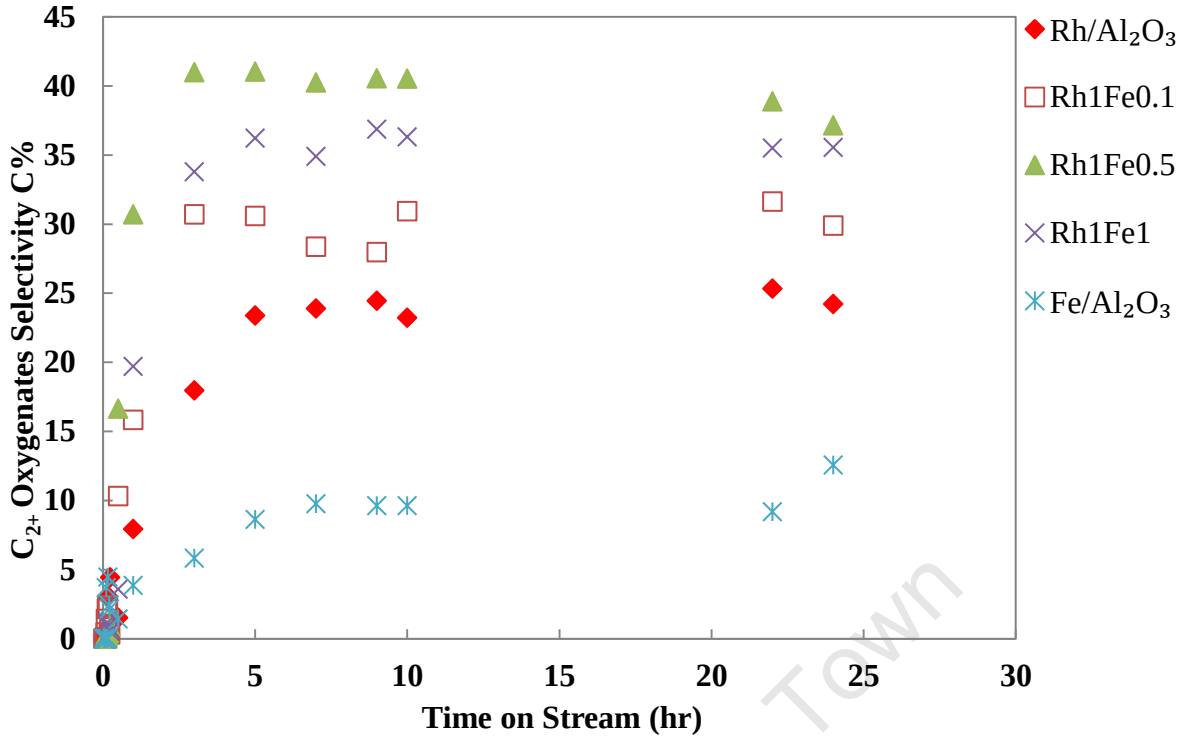

Figure 4.33: C_{2+} oxygenates selectivity of model catalysts as a function of time on stream (Reaction conditions: T = 180°C, P = 10 bar, GHSV = 20 ml(NTP)/min.g_{cat}, H_2/CO = 1)

In order to obtain more information on the effects of iron on alumina supported rhodium catalysts towards the formation of oxygenates, C_{2+} oxygenates selectivity of model catalysts as a function of time on stream are shown in Figure 4.33. In addition, the oxygenate product distribution is shown in Figure 4.34. The selectivity towards C_{2+} oxygenates for the unmodified rhodium catalyst was 25 C%. The oxygenate product distribution (see Figure 4.34) shows that the unmodified rhodium catalyst is selective mainly to methanol, ethanol and acetaldehyde which implies that C_2 oxygenates were the major products with ethanol being the dominant product. These results are similar to the findings obtained by Ojeda et al. (2004a) in which C_2 oxygenates with a 21.9 C% selectivity for alumina-supported Rh catalyst with crystallite size less than 5 nm prepared using microemulsion was observed.

The iron catalyst was selective to the formation of alcohols (see Figure 4.34) mainly consisting of methanol. The C_{2+} oxygenates selectivity of this catalyst was only 10 C%. These results were surprising because iron typically does not catalyse the production of significant amounts of methanol (Mabaso, 2005; Cheang, 2009). This may be due to the conditions used in the study with low reaction temperature and a low H_2:CO ratio. However, Hayashi et al. (2002a) showed that the Fe/SiO_2 catalysts prepared by microemulsion method exhibit high selectivity towards oxygenates, mainly alcohols while catalysts prepared by

impregnation gave high selectivity towards hydrocarbons. This was attributed to the electronic state of iron metals existing in microemulsion and impregnation catalysts. The density of Fe^{+} species was higher for the microemulsion catalyst, as a result promoted the insertion of CO into alkyl group leading to a high selectivity of oxygenates.

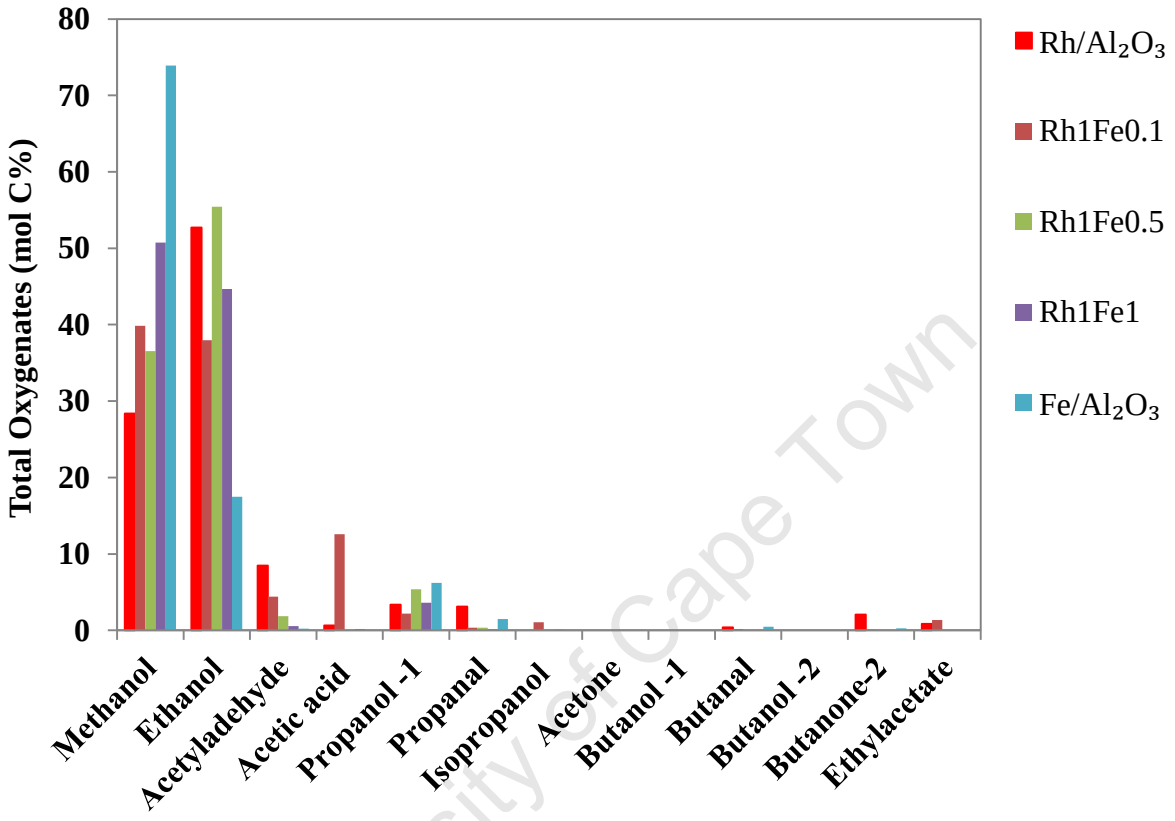

Figure 4.34: Oxygenate Product Distribution of model catalysts

(Reaction conditions: T = 180°C, P = 10 bar, GHSV = 20 ml(NTP)/min.g_{cat}, H_2/CO = 1)

With the addition of iron to the rhodium catalysts, the selectivity to C_{2+} oxygenates increased as compared to the unmodified rhodium catalyst and C_2 oxygenates were formed as major products. Furthermore, iron addition to the rhodium catalysts changes the product distribution from a mixture of methanol, acetaldehyde and ethanol on unmodified rhodium catalyst to a mixture of ethanol and methanol on Rh/Fe catalysts (see Figure 4.34). According to Schunemann et al. (1995) the effect of iron on rhodium may be related to the iron phase present in the catalyst. As shown from XRD analysis of spent catalysts (see Figure 4.13), the iron phase in the Rh/Fe catalysts is very different from the carbide type phases in the pure iron catalyst which might explain the improved selectivity towards oxygenates when iron is added to the rhodium catalysts.

The catalyst sample of alumina supported Rh-Fe bimetallic (Fe:Rh molar ratio = 0.1) exhibited a selectivity of 30 C% towards C_{2+} oxygenates. From the oxygenate product distribution it can be seen that the catalyst sample (Fe:Rh molar ratio = 0.1) was selective mainly to methanol and ethanol while the acetaldehyde selectivity decreased as compared to alumina supported rhodium. Interestingly, the catalyst sample (Fe:Rh = 0.1) was also found to selectively produce acetic acid. This result was quite surprising because the unpromoted alumina-supported rhodium catalyst produced small traces of acetic acid, therefore as previously reported in the literature Fe:Rh = 0.1 sample should produce virtually no acetic acid (Bhasin et al., 1978; Fukushima et al., 1985; Burch and Petch, 1992a).

As the molar ratio of Fe:Rh was increased to 0.5, the selectivity to C_{2+} oxygenates changed to 40 C% with ethanol being the dominant C_2 oxygenate followed by methanol. The formation of acetaldehyde dramatically declined with this catalyst. With a large content of iron (Rh1Fe1), the selectivity to C_{2+} decreased to 36 C%. Moreover, the sample with a large content of iron, was substantially selective to methanol, even compared with the increase of ethanol. It is very important to note that the addition of too much iron led to higher selectivity of methanol which is an undesired product and decreases the formation of ethanol which is the desired product. It is therefore evident that there is a limit to the loading of iron as a promoter since high loading no longer selectively produce valuable oxygenates. Note again the formation of acetaldehyde was almost completely eliminated with the sample containing a large amount of iron. The results obtained on alumina supported Rh-Fe catalysts are consistent with literature (Bhasin et al., 1978; Fukushima et al., 1985; Burch and Petch, 1992a; Schunemann et al., 1995; Mo et al., 2009a).

Figure 4.35 illustrate ethanol, acetaldehyde and acetic acid content in C_2 oxygenate as function of iron loading. Cairns (2008) observed the formation of alcohols, aldehydes and carboxylic acids with iron based catalysts in the Fischer-Tropsch synthesis and that these readily interact with each other. It was reported that these oxygenates were affected by addition of copper leading to more hydrogenated product. These observations seem to apply to the Rh/Fe system in the study. As shown in Figure 4.35, iron addition leads to the more hydrogenated product. It can be seen in Figure 4.35, that acetaldehyde decreases with increase in iron loading on the Rh/Fe catalysts. The sample with a large content of iron (Rh1Fe1) produced virtually no acetaldehyde as compared to alumina supported rhodium. Acetaldehyde was hydrogenated to ethanol rather than desorbed as acetaldehyde. It was very

difficult to deduce the same results with acetic acid as virtually no acetic acid was produced with the model catalysts.

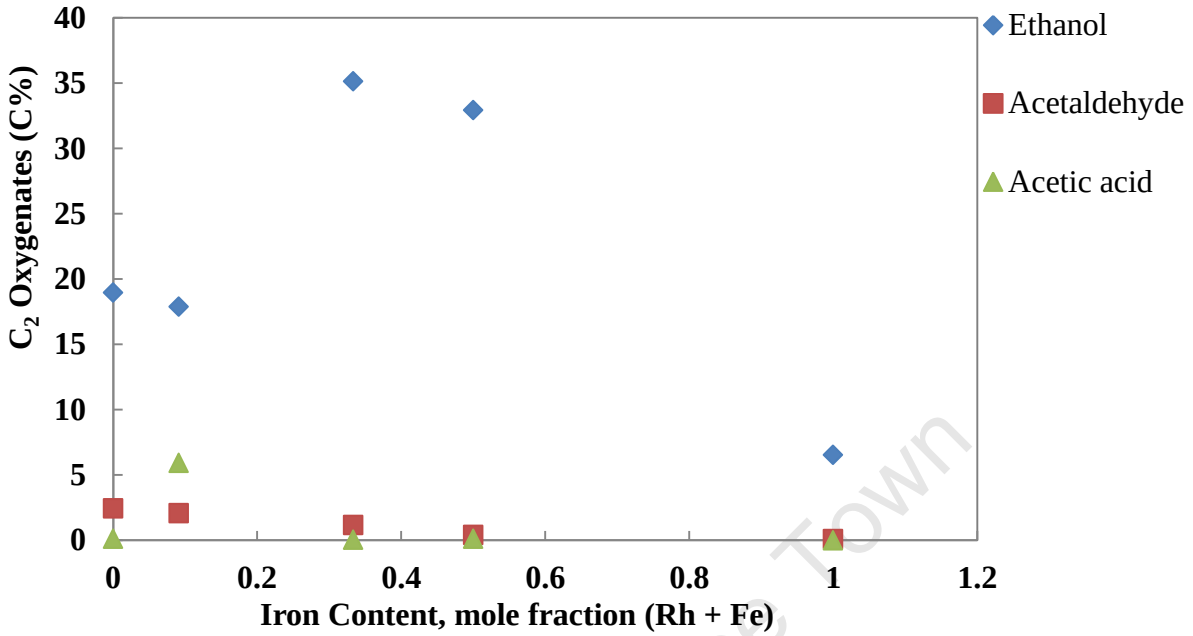

Figure 4.35: Ethanol, acetaldehyde and acetic acid content in C_2 oxygenates fraction as a function of iron mole fraction in catalyst

(Reaction conditions: T = 180°C, P = 10 bar, GHSV = 20 ml(NTP)/min.g_{cat}, H_2/CO = 1)

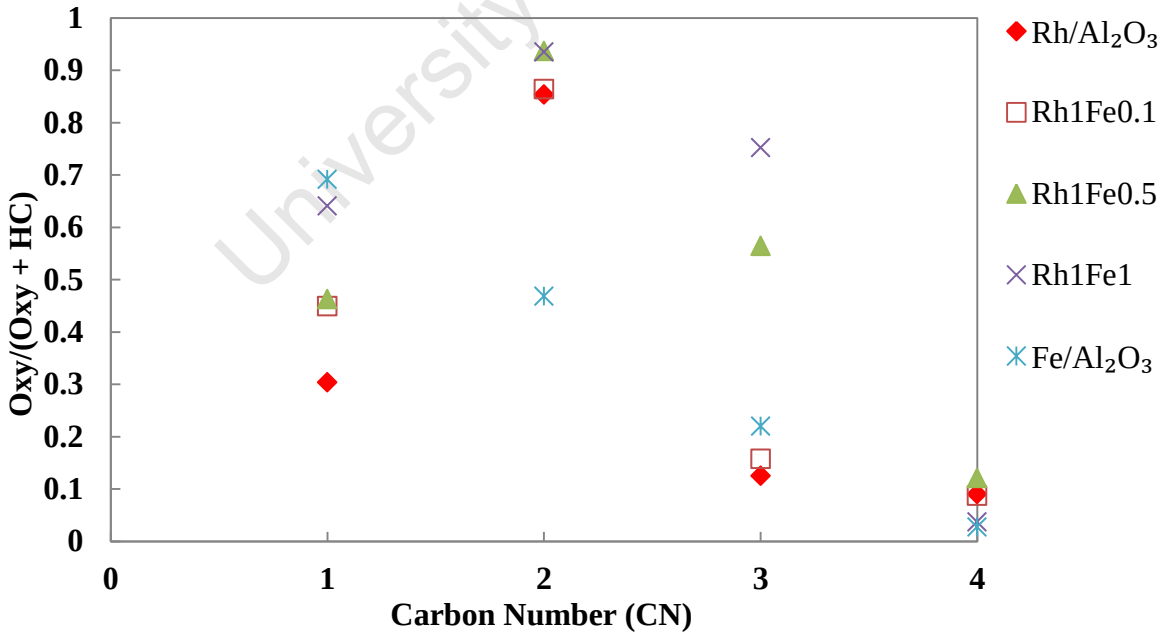

Figure 4.36: Mole fraction of oxygenate in the oxygenates and hydrocarbons fraction as a function of carbon number at steady state (7 hours)

(Reaction conditions: T = 180°C, P = 10 bar, GHSV = 20 ml(NTP)/min.g_{cat}, H_2/CO = 1)

Figure 4.36 shows the mole fraction of oxygenate in the oxygenates and hydrocarbons fraction as a function of carbon number. It can be observed also that oxygenates fraction increases with increase in iron loading for Rh and Rh/Fe catalysts with each carbon number. However the pure iron sample was shown to behave different from the Rh and Rh/Fe catalysts, the oxygenate fraction decreased with increase in carbon number and relatively high oxygenate content in C_1 was observed.

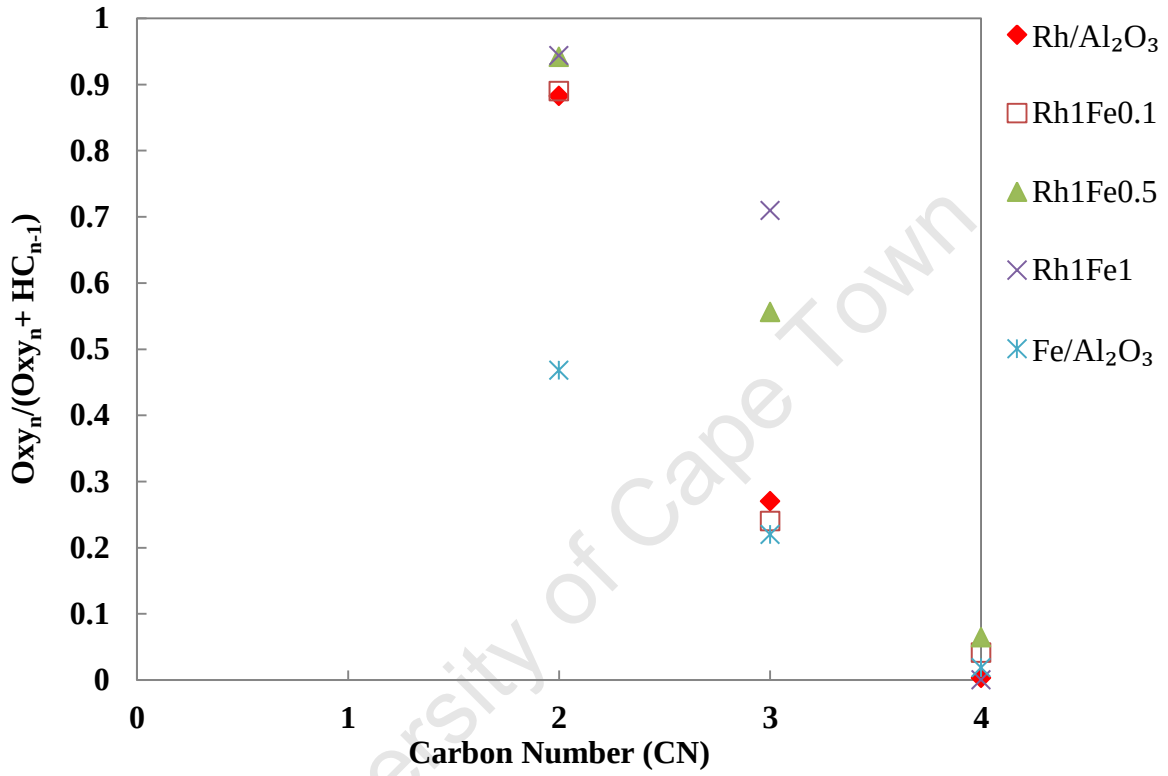

Figure 4.37: Mole fraction of straight oxygenate in the straight oxygenates and straight hydrocarbons fraction as a function of carbon number at steady state (7 hours)
(Reaction conditions: T = 180°C, P = 10 bar, GHSV = 20 ml(NTP)/min.g_{cat}, H_2/CO = 1)

Figure 4.37 shows the mole fraction of n-oxygenate (straight) in the fraction of n-oxygenate plus straight hydrocarbons as a function of time. It was observed that n-oxygenates fraction increases with increase in iron loading for Rh and Rh/Fe catalysts with each carbon number. It can be deduced that addition of iron to rhodium catalysts decreases the likelihood of n-oxygenates undergoing secondary reaction.

It is crucial to explain the enhanced selectivity to oxygenates with iron promoted catalysts as well as the high selectivity to ethanol and methanol coupled with almost complete elimination of acetaldehyde. Firstly, the increase selectivity towards oxygenates at the

expense of the hydrocarbons was attributed to a decrease in the rate of chain growth as compared to the CO insertion into the CH_x (Burch and Petch, 1992a; Lin et al., 1995). Another explanation for the enhanced selectivity to oxygenates is that the presence of iron seems to result in the creation of new sites at the interface between rhodium and iron which may selectively produce oxygenates (Burch and Petch, 1992a; Burch and Hayes, 1997).

A considerable amount of work has been undertaken to gain insight into the mechanism for the formation of acetaldehyde and ethanol. It has been proposed that ethanol is formed as a secondary product by hydrogenation of acetaldehyde (Burch and Hayes, 1992 a and b; Burch and Hayes, 1997; Haider et al., 2009; Mo et al., 2009a).

Burch and Petch, 1992b conducted an experiment to investigate reactions of acetaldehyde over promoted rhodium catalysts in order to determine the extent to which acetaldehyde was converted to ethanol. They found that on promoted rhodium catalysts ethanol was produced from acetaldehyde even under very mild conditions.

Addition of iron to alumina-supported rhodium catalysts seemed to increase the stability of the acetyl intermediate, which is eventually converted with hydrogen to ethanol rather than desorbed as acetaldehyde (Fukushima et al., 1985; Burch and Petch, 1992a and b; Burch and Hayes, 1997; Mo et al., 2009a; Haider et al., 2009). This explains the increased selectivity to ethanol at the expense of acetaldehyde. An alternative explanation for the enhanced selectivity to ethanol when iron was added to alumina-supported rhodium catalysts is that iron increases the availability of hydrogen by acting as a hydrogen reservoir (Burch and Petch, 1992a and b; Mo et al., 2009a). Furthermore, addition of iron lead to the more hydrogenated oxygenates as reported by Cairns (2008), who observed that addition of copper on iron based catalysts lead to the more hydrogenated product.

Likewise, iron added to alumina-supported rhodium catalysts seems to stabilise the formyl species which is the proposed intermediate in the methanol synthesis leading to its high concentration on the surface allowing enough time for their hydrogenation to methanol (Fukushima et al., 1985; Burch and Petch, 1992a). This explains the increase in methanol selectivity. It also important to note that as with methane, methanol formation requires few sites or less number of atoms to take place.

5. Conclusions

This study presents an investigation on the effects of iron added to alumina-supported rhodium crystallites on the activity and selectivity for CO hydrogenation. This study can be divided into three parts:

- Preparation of alumina supported model catalysts using reverse micelle method.
- Characterisation of the model catalysts in the calcined state as well as after reduction.
- Fischer-Tropsch testing of the prepared model catalysts as well as characterisation of the spent samples using XRD.

Catalyst Preparation

The first main objective of the study was the preparation of alumina supported nano-sized crystallites with narrow crystallite size distributions as well as a good dispersion of the crystallites onto the support material. This was successfully achieved by using a reverse micelle technique. Size control of the crystallites was very important as the model catalysts were required to have similar crystallite sizes. The sizes of the crystallites could be tuned by the reverse micelle composition, particularly varying the weight water to surfactant ratios and therefore in order to prepare model catalysts with similar crystallite sizes the water to surfactant ratio was kept constant at 0.2 (g/g). This eliminated the effects of crystallite sizes and making the iron effect on the alumina-supported rhodium catalyst being the only parameter investigated in the study.

Reduction model catalysts with similar average crystallite sizes no larger than 5 nm were successfully prepared with the exception of pure iron catalyst which had the crystallite size of 8.5 nm. All model catalysts were assumed to be fully reduced to metallic metals. All the alumina supported model catalysts had a 10 wt % rhodium loading and the iron loading depended on the molar ratio of rhodium to iron in that sample.

It is vital to take note that no work has been previously reported in literature on attempts to apply the reverse micelle approach to prepare model catalysts when investigating the effect of iron on supported rhodium catalyst on the activity and selectivity for CO hydrogenation. Mostly in literature the impregnation method is used to prepare model catalysts. However, this method is not suitable because crystallite size is not easily tunable and it is quite difficult to obtain a narrow crystallite size distribution. Therefore the presence of different crystallite

sizes would influence the activity of the catalyst and would be difficult to determine the effect of iron on the supported rhodium catalysts during CO hydrogenation.

Characterisation

The HRTEM and STEM analyses revealed that the alumina supported nano-sized crystallites were well dispersed on the support with narrow distribution. EDX analysis confirmed the formation of bimetallic crystallites with the samples with high loading of iron (Rh1Fe0.5 and Rh1Fe1). In addition, XRD patterns for the bimetallic samples with high loadings of iron (Rh1Fe0.5 and Rh1Fe1) revealed the formation of alloys. Promotion of rhodium with iron affected the reduction behaviour of the catalyst. TPR provided evidence of a close interaction between rhodium and iron. It was observed that the hydrogen consumption increased with increasing iron loading and was more than the required amount to achieve complete reduction of Rh_2O_3 to metallic rhodium.

Fischer-Tropsch Testing

Fischer-Tropsch testing of the model catalysts was carried out to investigate the effect of iron on alumina-supported rhodium catalysts. The testing was carried out using a u-tube fixed bed reactor operated at 180°C, 10 bar, H_2/CO ratio = 1 and space velocity = 20 ml/$g_{catalyst}$.min. These conditions were very mild and relatively low conversions were targeted (<20 %) so as to minimise/exclude effects of crystallite sintering. Catalyst activity and product selectivity were monitored employing on-line TCD and off-line FID chromatograph.

Catalytic activity based on conversion was observed to increase upon addition of iron to the rhodium catalysts. The conversion of CO increased from 12% with pure rhodium to 18% for bimetallic sample with highest iron loading (Rh1Fe1). The increase in catalytic activity with increase in iron loading was attributed to be due to the intimate contact between rhodium and iron creating new active sites as well as due to the formation of alloys. Furthermore the catalytic activity was also expressed in terms of turn-over frequency (TOF) and it was noted as well that TOF increased with increase in iron loading to the rhodium-based catalysts. However, the iron catalyst was observed to have higher TOF as compared to the rhodium and Rh/Fe catalysts. This was attributed to the effect of crystallite sizes as iron has larger crystallites compared to the other samples. Furthermore when determining the TOF for the Rh/Fe catalysts only rhodium atoms were taken into account when calculating the total number of exposed surface atoms. Through the characterisation of the spent samples using

XRD, it was observed that rhodium and Rh/Fe catalysts are very different from pure iron catalysts. The iron phase in the Rh/Fe catalysts was very different from the carbide type phases in the iron catalyst. It was observed that Rh1Fe0.5 and Rh1Fe1 samples contained RhFe alloy and little cementite carbide while the pure iron resulted to the formation of mainly cementite carbide.

In terms of product formation, the chain growth probabilities decrease, while methane selectivities increase with increasing iron loading on the alumina-supported rhodium catalysts. This was attributed to iron enhancing hydrogen availability on the surface leading to more saturated hydrocarbons therefore low chain growth probability and high methane selectivity. The olefin content in linear hydrocarbons as well as α olefins in the linear olefins decreased with increasing iron content for the Rh-Fe bimetallic catalysts. This was attributed to iron improving the hydrogenation thus favouring the formation of paraffins and olefins with internal double bond. The pure iron sample resulted to less methane, high chain growth probability as well as high α olefins in the linear olefins compared to rhodium and Rh/Fe catalysts. This was ascribed to the formation of carbides in pure iron and it is reported that carbides inhibit methane formation as well as hydrocarbon C_{2+} product desorption and secondary olefin hydrogenation.

Lastly, it was observed that the total oxygenates selectivity increase with increasing iron loading and it was interesting to note in particular the selectivity to C_{2+} hydrocarbons was significantly reduced. Furthermore, with iron promoted rhodium catalysts, a high selectivity to methanol and ethanol coupled with a low selectivity to acetaldehyde was observed as compared to pure rhodium catalyst. Addition of iron to alumina-supported rhodium was proposed to increase the stability of the acetyl and formyl intermediates, which are converted with hydrogen to ethanol and methanol, respectively explaining the increased selectivities. It was shown that ethanol and acetaldehyde readily interact with each other. Addition of iron to the rhodium based catalysts lead to the more hydrogenated product as reported by Cairns (2008) who observed that addition of copper to iron based catalysts led to the more hydrogenated product. The pure iron catalyst was very different from Rh and Rh/Fe catalysts and resulted in a high selectivity towards C_{2+} hydrocarbons and was selective mainly to the formation of methanol.

It was observed that the Rh/Fe sample (Rh1Fe0.5) with iron loading of 2.7 wt % was the limiting value of iron loading and further increase in iron loading resulted in substantially

higher methanol selectivity, even compared with the increase in ethanol selectivity. It was shown that C_{2+} oxygenates selectivity of up to 40 C% with ethanol the dominant C_2 oxygenates could be achieved with an alumina-supported rhodium catalyst containing 10 wt % rhodium and 2.7 wt% iron. These results have not been previously reported in literature under the conditions of the study and employing reverse micelle approach to prepare model catalysts.

6. Recommendations

In order to fully understand the function of the iron promoter on the alumina-supported rhodium catalyst on the activity and selectivity in the CO hydrogenation, it is recommended that future work built on this study should investigate:

- More extensive EDX analysis should be carried in order to analyse the small crystallites and therefore confirming both rhodium and iron are detected on all crystallites on Rh-Fe catalysts.
- In-situ XRD should be investigated in order to determine the phases of rhodium and iron present during Fischer-Tropsch reaction.
- (In-situ) Mössbauer analysis should be investigated in order to obtain information about the iron phases presents on Rh-Fe bimetallic catalysts during FT reaction.
- XPS studies should be performed in order to gain information on the oxidation state of iron and rhodium on the surface. Both XPS and in-situ Mössbauer analyses will show evidence for the formation of alloys.
- Finally Fischer-Tropsch testing should be performed at high temperature to determine the effect of iron on alumina-supported rhodium catalysts at high activity levels.

7. References

Alayoglu, S., Zavalij, P., Eichhorn, B., Wang, Q., Frenkel, A.I. and Chupas, P., (2009). 'Structural and architectural evaluation of bimetallic nanoparticles: A case study of Pt-Ru core-shell and alloy nanoparticles'. *ACS Nano* 3, 3127-3137.

Anderson, R. B., (1984). *The Fischer-Tropsch Synthesis*. Academic Press, New York, USA.

Barkhuizen, D., Mabaso, E., Viljoen, E., Welker, C., Claeys, M., van Steen, E., and Fletcher, J., (2006). 'Experimental approaches to the preparation of supported metal nanoparticles'. *Pure and Applied Chemistry* 78, 1759–1769.

Bergeret, G., and Gallezot, P., (1997). 'Particle size and dispersion measurements'. *Handbook of Heterogeneous Catalysis* 2. VCH, Weinheim, Federal Republic of Germany, Chapt. 3, pp. 439-464.

Bezemer, G. L., Bitter, J. H., Kuipers, H. P. C. E., Oosterbeek, H., Holewijn, J. E., Xu, X., Kapteijn, F., van Dillen, A. J., and de Jong, K. P., (2006). 'Cobalt particle size effects in Fischer-Tropsch reaction studied with carbon supported catalysts'. *Journal of the American Chemical Society.* 128, 3956-3964.

Bhasin, M.M. and O'Connor, G.L., (1975). 'Procede de preparation selective de derives hydrocarbones oxygenes a deux atomes de carbone'. *Belgian Patent* 8,248,22.

Bhasin, M.M., (1975). *Belgian Patent* 8,248,23.

Bhasin, M.M., Bartley, W.J., Ellgen, P.C., and Wilson, T.P., (1978). 'Synthesis gas conversions over supported rhodium and rhodium-iron catalysts'. *Journal of Catalysis* 54, 120-128.

Bligaard, T., Nørskov, J.K., Dahl, S., Matthiesen, J., Christensen, C.H., and Sehested, J., (2004). 'The Brønsted-Evans-Polanyi relation and the volcano curve in heterogeneous catalysis'. *Journal of Catalysis* 224, 206-217.

Boutonnet, M., Kizling, J., and Stenius, P., (1982). 'The preparation of monodisperse colloidal metal particles from microemulsions'. *Colloids and Surfaces* 5, 209–225.

Boutonnet, M., Kizling, J., Mintsa-Eya, V., Choplin, A., Touroude, R., Maire, G., and Stenius, P., (1987) 'Monodisperse colloidal metal particles from nonaqueous solutions:

catalytic behavior in hydrogenation of but-1-ene of platinum, palladium, and rhodium particles supported on pumice'. *Journal of Catalysis* 103, 95-104.

Burch, R., (1982). 'Importance of electronic ligand effects in metal alloy catalysts'. *Accounts of Chemical Research* 15, 24-31.

Burch, R., and Hayes, M.J., (1997). 'The preparation and characterisation of Fe-promoted Al_2O_3-supported Rh catalysts for the selective production of ethanol from syngas'. *Journal of Catalysis* 165, 249-261.

Burch, R., and Petch, M.I., (1992a). 'Investigation of the synthesis of oxygenates from carbon monoxide/hydrogen mixtures on supported rhodium catalysts'. *Applied Catalysis A: General* 88, 39-60.

Burch, R., and Petch, M.I., (1992b). 'Investigation of the reactions of acetaldehyde on promoted rhodium catalysts'. *Applied Catalysis A: General* 88, 61-76.

Burch, R., and Petch, M.I., (1992c). 'Kinetic and transient kinetic investigations of the synthesis of oxygenates from carbon monoxide/hydrogen mixtures on supported rhodium catalysts'. *Applied Catalysis A: General* 88, 77-99.

Cairns, P., (2008). 'Oxygenates in iron Fischer-Tropsch synthesis: is copper a selectivity promoter?'. *Ph.D. thesis, University of Cape Town, Cape Town.*

Capek. I., (2004). 'The preparation of metal particles in water-in-oil (w/o) microemulsions'. *Advances in Colloid and Interface Science* 110, 49-74.

Cheang, V., (2009). 'Effect of crystallite size and water partial pressure on the activity and selectivity of low temperature iron-based fischer-tropsch catalysts'. *Ph.D. thesis, University of Cape Town, Cape Town.*

Chen, D-H., and Chen, C-J., (2002). 'Formation and characterization of Au-Ag bimetallic nanoparticles in water-in-oil microemulsions'. *Journal of Materials Chemistry* 12, 1557-1562.

Chen, W., Ding, Y., Jiang, D., Wang, T., and Luo, H., (2006). 'A Selective synthesis of acetic acid from syngas over a novel Rh nanoparticles/nanosized SiO_2 catalysts'. *Catalysis Communications* 7, 559-562.

Chen, W., Ding, Y., Song, X., Wang, T., and Luo, H., (2011). 'Promotion effect of support calcination on ethanol production from co hydrogenation over $Rh/Fe/Al_2O_3$ catalysts'. *Applied Catalysis A: General* 407, 231-237.

Chuang, S.S.C., Stevens, R.W., and Khatri, R., (2005). 'Mechanism of C_{2+} oxygenate synthesis on Rh catalyts'. *Topics in Catalysis* 32, 225-232.

Claeys, M., (1997). 'Selektivituat, Elementarschritte und Kinetische Modellierung bei der Fischer-Tropsch-Synthese'. *PhD thesis, Universituat Fridericiana Karlsruhe, Germany.*

Claeys, M., and van Steen, E., (2002). 'On the effect of water during Fischer-Tropsch synthesis with a ruthenium catalyst'. *Catalysis Today* 71, 419-427.

Claeys, M., and van Steen, E., (2004). 'Basic studies'. In: Steynberg, A. and Dry M.E.: Fischer-Tropsch Technology, *Studies in Surface Science and Catalysis* 152. Elsevier: Amsterdam, Chapt8, 601-680.

Clapham, B. (2012). 'The development of an In-Situ X-Ray Diffraction Cell for Fischer-Tropsch catalyst characterisation'. *MSc. thesis, University of Cape Town, Cape Town.*

de Smit, E., Beale, A.M., Nikitenko, S., and Weckhuysen, B.M., (2009). 'Local and long range order in promoted iron-based Fischer–Tropsch catalysts: A combined in situ X-ray absorption spectroscopy/wide angle X-ray scattering study'. *Journal of Catalysis* 262, 244-256.

de Smit, E., de Groot, F.M.F., Blume, R., Havecker, M., Knop-Gericke, A., and Weckhuysen, B.M., (2010). 'The role of Cu on the reduction behaviour and surface properties of Fe-based Fischer-Tropsch catalysts'. *Physical Chemistry Chemical Physics* 12, 667-680.

Dry, M. E., (1981). *Catalysis Science and Technology,* Vol. 1, p. 159. Springer Verlag, New York, USA.

Dry, M.E., (1996). 'Practical and theoretical aspects of the catalytic Fischer-Tropsch Process'. *Applied Catalysis. A: General* 138, 319–344.

Dry, M.E., (1999). 'Fischer-Tropsch reactions and the environment'. *Applied Catalysis A: General* 189, 185–190.

Dry, M.E., (2001). 'High quality diesel via the Fischer-Tropsch process- a review'. *Journal of Chemical Technology and Biotechnology* 77, 43-50.

Dry, M.E., (2002). 'The Fischer-Tropsch process: 1950 - 2000'. *Catalysis Today* 71, 227–241.

Dry, M.E., (2004a). 'Present and future applications of the Fischer-Tropsch process'. *Applied Catalysis A: General* 276, 1-3.

Dry, M. E., (2004b). 'FT catalysts'. In Steynberg, A. and Dry, M., editors, *Fischer-Tropsch Technology*, volume 152. Elsevier, Amsterdam, The Netherlands.

Egbebi, A., Schwartz, V., Overbury, S.H., Spivey, J.J., (2010). 'Effect of Li promoter on titania-supported Rh catalyst for ethanol formation from CO hydrogenation'. *Catalysis Today* 149, 91-97.

Eriksson, S., Nylén, U., Rojas, S., and Boutonnet, M., (2004) 'Preparation of catalysts from microemulsions and their applications in heterogeneous catalysis'. *Applied Catalysis* A: General 265, 207–219.

Fischer, N., (2011). 'Preparation of nano and ångstrøm sized cobalt ensembles and their performance in the Fischer-Tropsch synthesis'. *Ph.D. thesis, University of Cape Town, Cape Town.*

Fischer, N., van Steen, E., and Claeys, M., (2013). 'Structure sensitivity of the Fischer-Tropsch activity and selectivity on alumina supported cobalt catalysts'. *Journal of Catalysis* 299, 67-80.

Fukushima, T., Arakawa, H., and Ichikawa, M., (1985). 'In situ high-pressure FT-IR studies on the surface species formed in CO hydrogenation on SiO_2-supported Rh-Fe catalysts'. *The Journal of Physical Chemistry* 89, 4440-4443.

Germain, J.E., (1969). *Catalytic Conversion of Hydrocarbons*. Academic Press, London and New York.

Guglielminotti, E., Pinna, F., Rigoni, M., Strukul, G., and Zanderighi, L., (1995). 'The effect of iron on the activity and the selectivity of Rh/ZrO_2 catalysts in the CO hydrogenation'. *Journal of Molecular Catalysis A: Chemical* 103, 105-116.

Haider, M.A., Gogate, M.R., and Davis, R.J., (2009). 'Fe-promotion of supported Rh catalysts for direct conversion of syngas to ethanol'. Journal of Catalysis 261, 9-16.

Hayashi H., Kishida, M., and Wakabayashi, K., (2002a). 'Metal-support and catalysis of the catalyst prepared using microemulsion'. *Catalysis Surveys from Japan* 6, 9-17.

Hayashi, H., Chen, L.Z., Tago, T., Kishida, M., and Wakabayashi, K., (2002b). 'Catalytic properties of Fe/SiO_2 catalysts prepared using microemulsion for CO hydrogenation'. *Applied Catalysis A: General*, 231, 81–89.

Hindermann, J., Hutchings, G., and Kiennemann A., (1993). 'Mechanistic aspects of the formation of hydrocarbons and alcohols from CO hydrogenation'. *Catalysis Reviews: Science & Engineering* 35, 1–127.

Huang, Y., and Schwarz, J., (1987). 'The effect of catalyst preparation on catalytic activity: II. the design of Ni/Al_2O_3 catalysts prepared by wet impregnation'. *Applied Catalysis* 30, 255–263.

Ichikawa, M., Fukushima, T., Yokoyama, T., Kosugi, N., and Kuroda, H., (1986). 'EXAFS evidence for direct Rh-Fe bonding in SiO_2-supported Rh-Fe bimetallic catalysts'. *The Journal of Physical Chemistry* 90, 1222-1224.

Iglesia, E., Reyes, S.C., Madon, R.J., and Soled, S.L., (1993). 'Selectivity control and catalyst design in the Fischer-Tropsch synthesis: sites, pellets, and reactors'. *Advances in Catalysis* 39, 221-302.

Ioannides, T., Verykios, X., (1993). 'Influence of the carrier on the interaction of H_2 and CO with supported Rh'. *Journal of Catalysis* 140, 353-369.

Johnston, P., and Joyner, R.W., (1993). 'Structure-function relationships in heterogeneous catalysis: the embedded surface molecule approach and its applications'. *Studies in Surface Science and Catalysis* 75, 165-180.

Kim, T., Kobayashi, K., and Nagai, M., (2007). 'Preparation and characterization of platinum-ruthenium bimetallic nanoparticles using reverse microemulsions for fuel cell catalyst'. *Journal of Oleo Science* 56, 553-562.

Kishida, M., Umakoshi, K., Ishiyama, J., Nagata, H., and Wakabayashi, K., (1996). 'Hydrogenation of carbon dioxide over metal catalysts prepared using microemulsion'. *Catalysis Today* 29, 355–359.

Lin, P.-Z., Liang, D.-B., Luo, H.-Y, Xu, C.-H., Zhou, H.-W., Huang, S.-Y. and Lin, L.-W., 1995. 'Synthesis of C_{2+} -oxygenated compounds directly from syngas'. *Applied Catalysis A: General* 131, 207-214.

Lin, H-Y., Chen, Y-W., and Li, C., (2003). 'The mechanism of reduction of iron oxide by hydrogen'. *Thermochimica Acta* 400, 61-67.

Liu, Z., Lee, J.Y., Han, M., Chen, W., and Gan, L.M., (2002). 'Synthesis and characterization of PtRu/C catalysts from microemulsions and emulsions'. *Journal of Materials Chemistry* 12, 2453-2458.

Mabaso, E., (2005). 'Nanosized iron crystallites for Fischer-Tropsch synthesis'. *Ph.D. thesis, University of Cape Town, Cape Town.*

Maitlis, P. M., Quyoum, R., Long, H. C., and Turner, M. L., (1999). 'Towards a chemical understanding of the Fischer-Tropsch reaction: alkene formation'. *Applied Catalyis A: General* 186, 363-374.

Minai, Y., Fukushima, T., Ichikawa, M., and Tominaga, T., (1984). 'Characterization of silica supported rhodium-iron catalysts by Mössbauer technique'. *Journal of Radioanalytical and Nuclear Chemistry* 87, 189-201.

Mo, X., Gao, J., Umnajikaseam, N., and Goodwin Jr, J.G., (2009a). 'La, V, and Fe promotion of Rh/SiO_2 for CO hydrogenation: Effect on adsorption and reaction'. *Journal of Catalysis* 267, 167-176.

Mo, X., Gao, J., and Goodwin Jr, J.G., (2009b). 'Role of promoters on Rh/SiO_2 in CO hydrogenation: A comparison using DRIFTS'. *Catalysis Today* 147, 139-149.

Moulijn, J.A., van Diepen, A.E., and Kapteijn, F., (2001). 'Catalyst deactivation: is it predictable? What to do?'. *Applied Catalysis A: General* 212, 3-16.

Nakamula, I., Yamanoi, Y., Imaoka, T., Yamamoto, K., and Nishihara, H., (2011). 'A uniform bimetallic rhodium/iron nanoparticle catalyst for the hydrogenation of olefins and nitroarenes'. *Angewandte Chemie, International Edition* 50, 5830-5833.

Mungwe, N., (2013). 'CO hydrogenation based on rhodium crystallites and clusters of different sizes'. *Internal Report, University of Cape Town, Cape Town*

Ojeda, M., Rojas, S., Boutonnet, M., Perez-Alonso, F. J., Garcia-Garcia, F.J., and Fierro, J.L.G., (2004a). 'Synthesis of Rh nano particles by the microemulsion technology: Particle size effect on the CO and H_2 reaction'. *Applied Catalysis A: General* 274, 33-41.

Ojeda, M., Rojas, S., García-García, F.J., Granados, M.L., Terreros, P., and Fierro, J.L.G., (2004b). 'Inhibition of oxygenated compounds formation during CO hydrogenation over $Rh/\gamma\text{-}Al_2O_3$ catalysts calcined at high temperature'. *Catalysis Communications* 5, 703-707.

Pichler, H., and Schulz, H., (1970). 'Neue Erkenntnisse auf dem Gebiet der Synthese von Kohlenwasserstoffen aus CO und H_2'. *Chemie-Ingenieur-Technik* 42, 1162–1174.

Ponec, V., (2001). 'Alloy catalysts: the concepts'. *Applied Catalysis A: General* 222, 31-45.

Reuel, R., Bartholomew C., (1984). 'Effects of support and dispersion on the CO hydrogenation activity/selectivity properties of cobalt'. *Journal of Catalysis* 85, 78–88.

Riedel, T., Claeys, M., Schulz, H., Schaub, G., Nam, S-S., Jun, K-W., Choi, M-J., Kishan, G., and Lee, K-W., (1999). 'Comparative study of Fischer-Tropsch synthesis with H_2/CO and H_2/CO_2 syngas using Fe- and Co-based catalysts'. *Applied Catalysis A: General* 186, 201-213.

Schulz, H., van Steen, E., and Claeys, M., (1995). 'Specific inhibition as the kinetic principle of Fischer-Tropsch synthesis'. *Topics in Catalysis* 2, 223–234.

Schulz, H., and Claeys, M., (1999). 'Reactions of α-olefins of different chain length added during Fischer-Tropsch synthesis on a cobalt catalyst in a slurry reactor'. *Applied Catalysis A: General* 186, 71.

Schulz, H., Nie, Z., and Ousmanov, F., (2002). 'Construction of the Fischer-Tropsch regime with cobalt catalysts'. *Catalysis Today* 71, 351–360.

Schulz, H., (1999). 'Short history and present trends of Fischer-Tropsch synthesis'. *Applied Catalysis A: General* 186, 3-12.

Schulz, H., 2003. 'Major and minor reactions in Fischer-Tropsch synthesis on cobalt catalysts'. *Topics in Catalysis* 26, 73-85.

Schunemann, V., Trevino, H., Lei, G.D., Tomczak, D.C., Sachtler, W.M.H., Fogash, K., and Dumesic, J.A., (1995). 'Fe promoted Rh-clusters in zeolite NaY: characterization and catalytic performance in CO hydrogenation'. *Journal of Catalysis* 153, 144-157.

Stenius, P., Kizling, J., and Boutonnet, M., (1984). 'Liquid suspension of particles of a metal belonging to the platinum group and a method for the manufacture of such a suspension'. *US Patent*, 4,425,261.

Swartzendruber, L.J., (1984). 'The Fe-Rh (iron-rhodium) system'. *Bulletin of Alloy Phase Diagram* 5, 1099.

Storch, H.H., Golumbic, N., and Anderson, R.B., (1951). 'The Fischer-Tropsch and related synthesis'. New York: John Wiley and Sons.

Tago T., Hanaoka, T., Dhupatemiya, P., Hayashi, H., Kishida, M., and Wakabayashi, K., '2000', 'Effect of Rh content on catalytic behavior in CO hydrogenation with Rh-silica catalysts prepared using microemulsion'. *Catalysis Letters* 64, 27-31.

Tojo, C., de Dios, M., and Lopez-Quintela, M.A., (2009). 'On the structure of bimetallic nanoparticles synthesized in microemulsions'. *The Journal of Physical Chemistry* 113, 19145-19154.

Trevino, H., Lei, G-D., and Sachtler, W.M.H., (1995). 'CO hydrogenation to higher oxygenates over promoted rhodium: nature of the metal-promoter interaction in RhMn/NaY'. *Journal of Catalysis* 154, 245-252.

Vannice, M.A., (1975). 'The catalytic synthesis of hydrocarbons from H_2/CO mixtures over the group VIII metals: I. The specific activities and product distributions of supported metals'. *Journal of Catalysis* 37, 449-461.

van't Blik, H.F.J., and Niemantsverdriet, J.W., (1984). 'Characterization of bimetallic FeRh/SiO_2 catalysts by temperature programmed reduction, oxidation and mossbauer spectroscopy'. *Applied Catalysis* 10, 155-162.

van't Blik, H.F.J., and Prins, R., (1986). 'Characterization of supported cobalt and cobalt-rhodium catalysts I. temperature-programmed reduction (TPR) and oxidation (TPO) of Co-Rh/Al_2O_3'. *Journal of Catalysis* 97, 188-199.

van Steen, E., Claeys, M., Dry, M. E., van de Loosdrecht, J., Viljoen, E. L., and Visagie, J. L., (2005). 'Stability of Nanocrystals: Thermodynamic Analysis of Oxidation and Re-reduction of Cobalt in Water/Hydrogen Mixtures'. *Journal of Physical Chemistry B* 109, 3575–3577.

Wachs, I.E., Deo, G., Kim, D.S., Vuurman, M.A., and Hu, H., (1993). 'Molecular design of supported metal oxide catalysts'. In: Guczi, L., Solymosi, F., and Tetenyi, P.: Proceedings of the 10th International Congress on Catalysis, Budapest, 1992, *Studies in Surface Science and Catalysis* 75. Elsevier: Amsterdam, 543-557.

Weihua, W., Xuelin, T., Kai, C., and Gengyu, C., (2006). 'Synthesis and characterisation of Pt-Cu bimetallic alloy nanoparticles by reverse micelles method'. *Colloids and Surfaces A: Physicochemical and Engineering Aspects* 273, 35-42.

Welker, C.A., (2007). 'Ruthenium based Fischer-Tropsch synthesis on crystallites and clusters of different size'. *Ph.D. thesis, University of Cape Town, Cape Town.*

Xu B-Q., Sun, K-Q., Zhu, Q-M., and Sachtler, W. M. H., (2000), 'Unusual selectivity of oxygenates synthesis: Formation of acetic acid from syngas over unpromoted Rh in NaY zeolite'. *Catalysis Today* 63, 453-460.

Yin, H., Ding, Y., Luo, H., Zhu, H., He, D., Xiong, J., and Lin, L., (2003). 'Influence of iron promoter on catalytic properties of Rh-Mn-Li/SiO_2 for CO Hydrogenation'. *Applied Catalysis A: General* 243, 155-164.

Yuan, Y., Yan, N. and Dyson, P.J., (2012). 'Advances in the rational design of the rhodium nanoparticle catalysts: control via manipulation of the nanoparticle core and stabilizer'. *ACS Catalysis* 2, 1057-1069.

Appendix

A. Calculation of Total and Exposed Surface Atoms

In order to determine the number of exposed surface atoms, a statistical method published by van Hardeveld and Hartog (1969) was used. The surface atoms ($N_{exp,cryst}$) of a metal crystallite can be differentiated by the number and arrangement of nearest neighbours. Surface atoms differ from bulk atoms of the crystal in that they have an incomplete set of nearest neighbours and vary with the place where that atom is situated. The total number of atoms ($N_{total,cryst}$) equals the number of bulk atoms (N_{bulk}) and the number of surface atoms ($N_{exp,cryst}$). The number of surface and bulk atoms depends on the geometry of the crystal structure.

Rhodium and Rh/Fe catalysts

It was found in the study that rhodium crystallite has face-centred cubic cubo-octahedron structure. The total number of atoms ($N_{total,cryst}$) for f.c.c. structured phases can be determined as first estimation by:

$$N_{total,cryst} = \left[\frac{d_{cryst}}{d_{Rh}.1.105}\right]^3 \quad \text{(A1)}$$

where $N_{total,cryst}$ is the number total number in a crystallite, d_{cryst} is the crystallite diameter and d_{Rh} is the atomic radius of rhodium (0.134 nm).

The total number of atoms is also given by equation A2, with m the number of atoms lying on an equivalent edge including corner atoms. Number of exposed atoms ($N_{exp,cryst}$) can be calculated using equation A3.

$$N_{total,cryst} = 16.m^3 - 33.m^2 + 24.m - 6 \quad \text{(A2)}$$

$$N_{exp,cryst} = 30.m^3 - 60.m + 32 \quad \text{(A3)}$$

Iron catalyst

For a body centred cubic structure found for iron the following set of equations was used to calculate the different atoms. The total number of atoms ($N_{total,cryst}$) for b.c.c. structured phases can be determined as first estimation by:

$$N_{total,cryst} = \left[\frac{d_{cryst}}{d_{Fe}.1.137}\right]^3 \quad \text{(A4)}$$

where $N_{total,cryst}$ is the number total number in a crystallite, d_{cryst} is the crystallite diameter and d_{Fe} is the atomic radius of iron (0.126nm).

The total number of atoms is also given by equation A5 and number of exposed atoms ($N_{exp,cryst}$) can be calculated using equation A6.

$$N_{total,cryst} = m^3 + (m-1)^3 \quad \text{(A5)}$$

$$N_{exp,cryst} = 6.m^2 - 12.m + 8 \quad \text{(A6)}$$

B. CO Hydrogenation Performance of Model Catalysts

TCD Chromatography

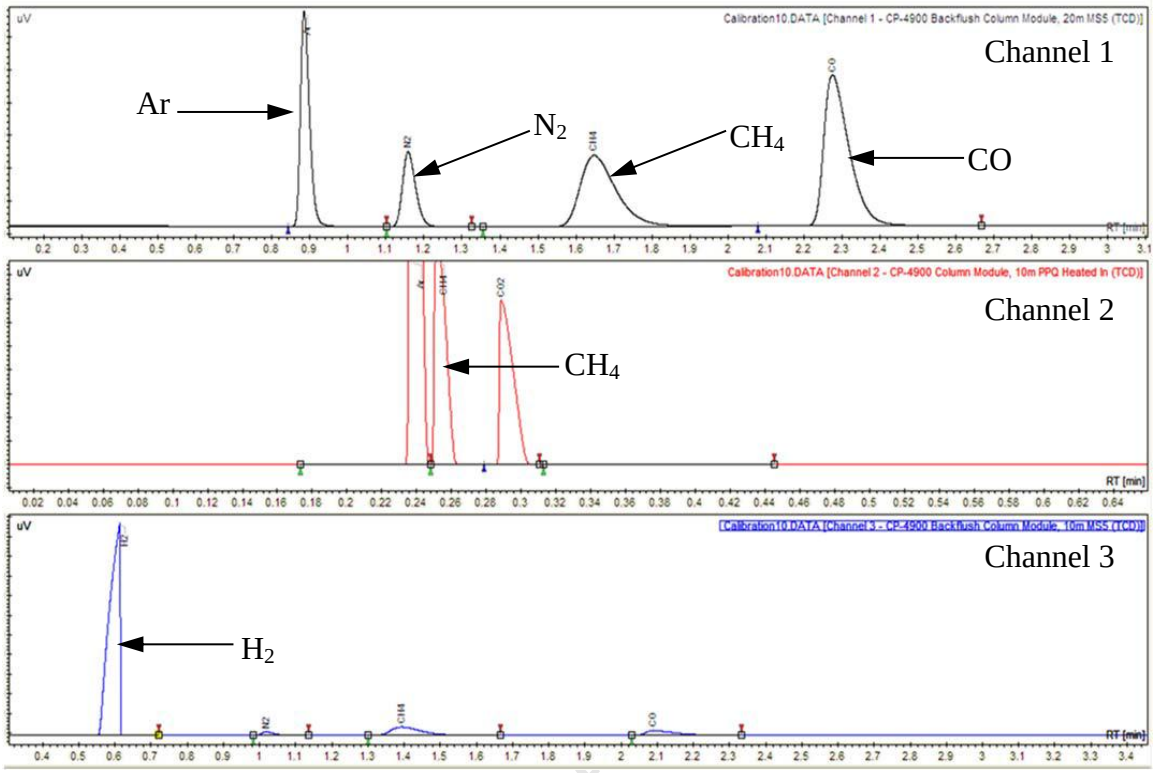

Figure B. 1: A typical chromatograph obtained from GC-TCD analysis in FT synthesis

Table B. 1: Typical calibration factors used in this study

Gas	Calibration Factor
f_{TCD,H_2}	0.05
$f_{TCD,CO}$	0.99
f_{TCD,CH_4}	0.27

FID Chromatography

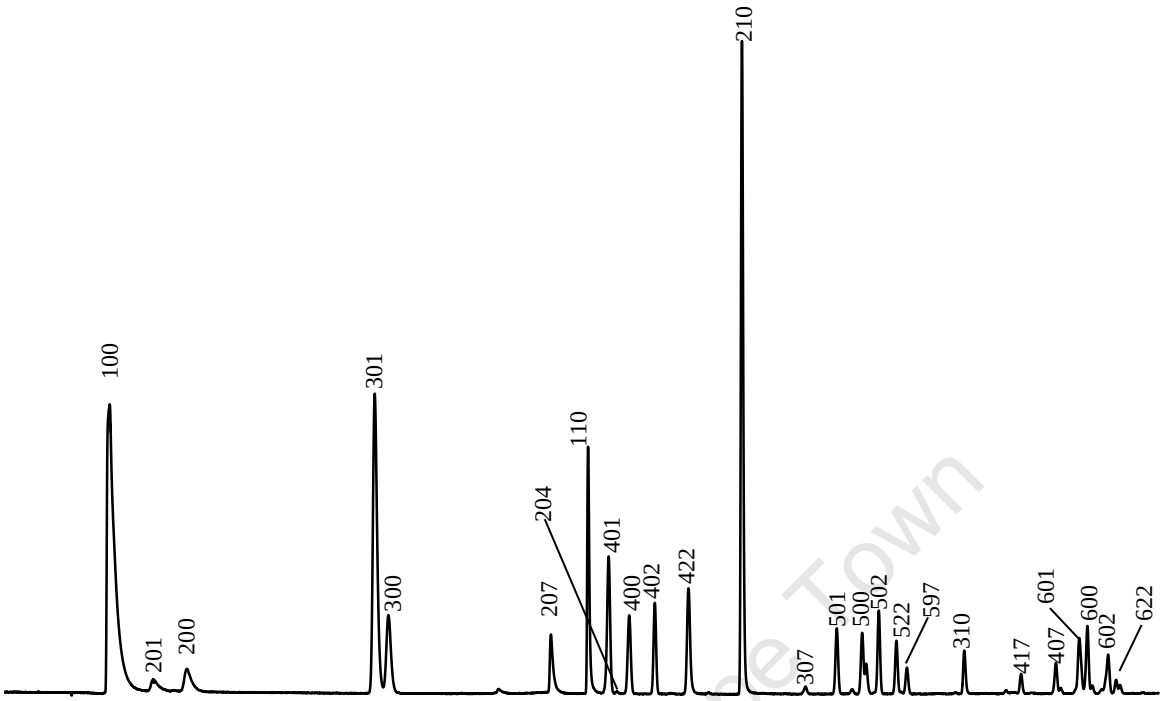

Figure B. 2: A typical chromatogram obtained from GC-FID analysis at 180 °C and 10 bar for the pure rhodium sample after 7 hours runtime

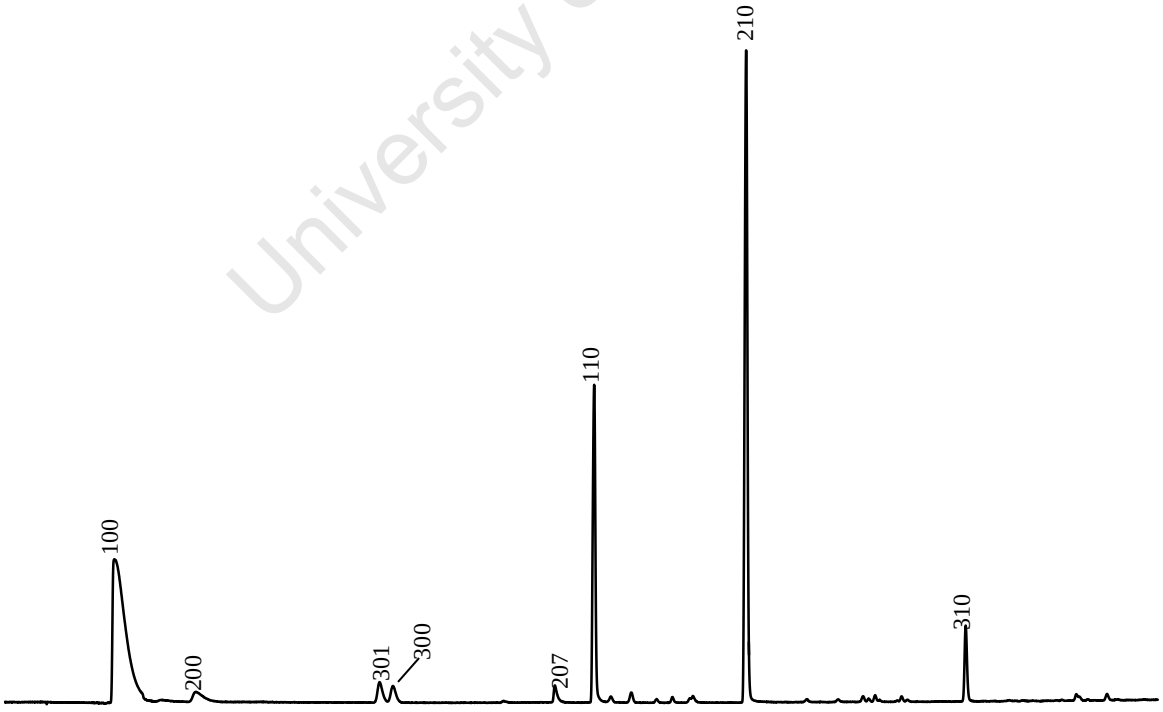

Figure B. 3: A typical chromatogram obtained from GC-FID analysis at 180 °C and 10 bar for the Rh1Fe0.5 sample after 7 hours runtime

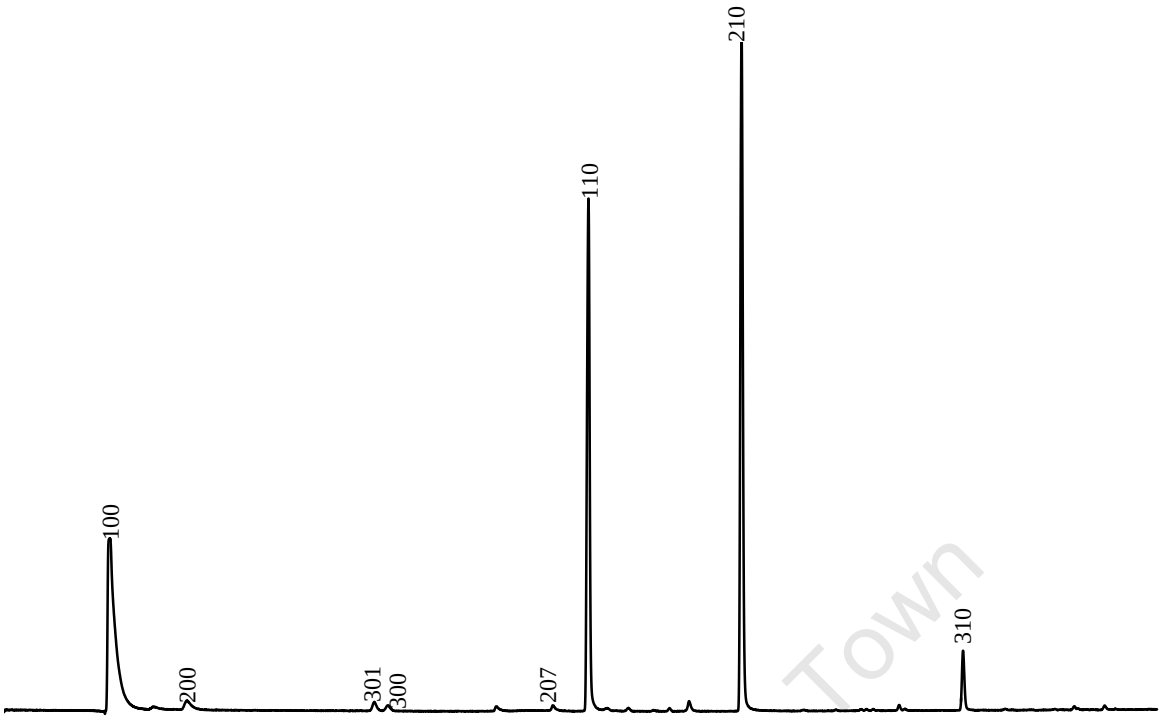

Figure B. 4: A typical chromatogram obtained from GC-FID analysis at 180 °C and 10 bar for the Rh1Fe1 sample after 7 hours runtime

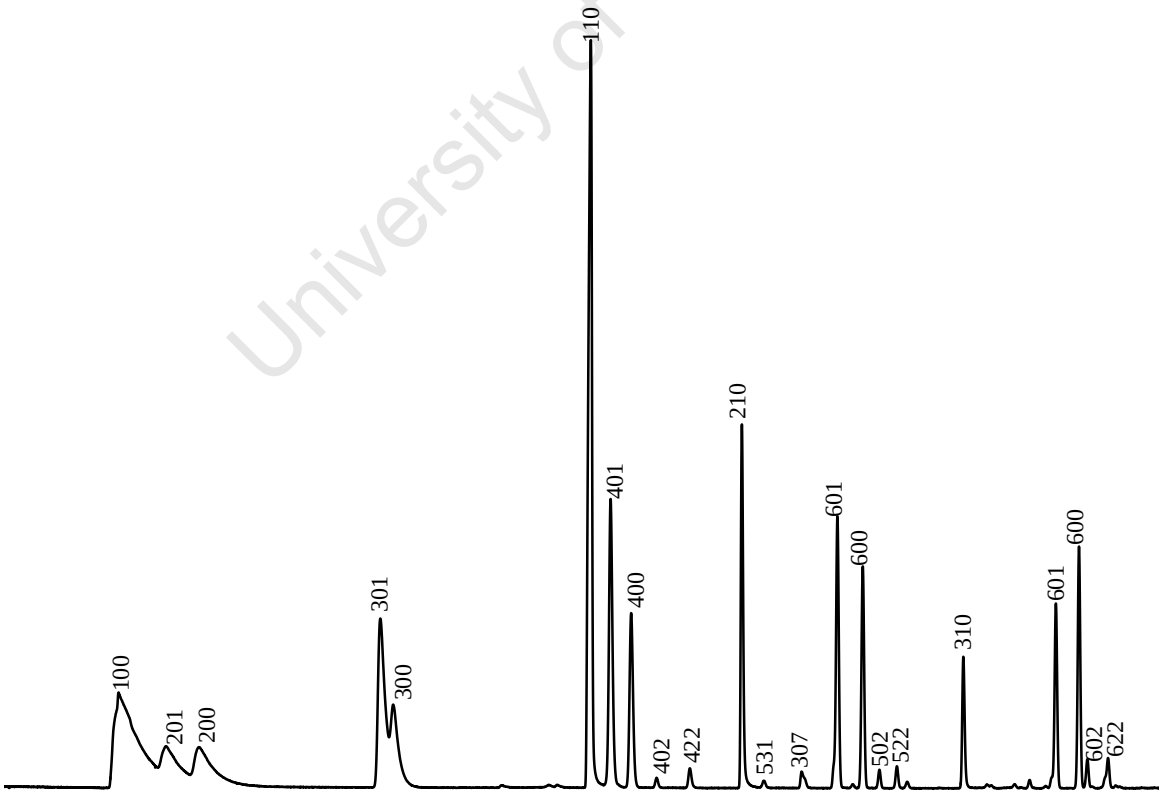

Figure B. 5: A typical chromatogram obtained from GC-FID analysis at 180 °C and 10 bar for the pure iron sample after 7 hours runtime

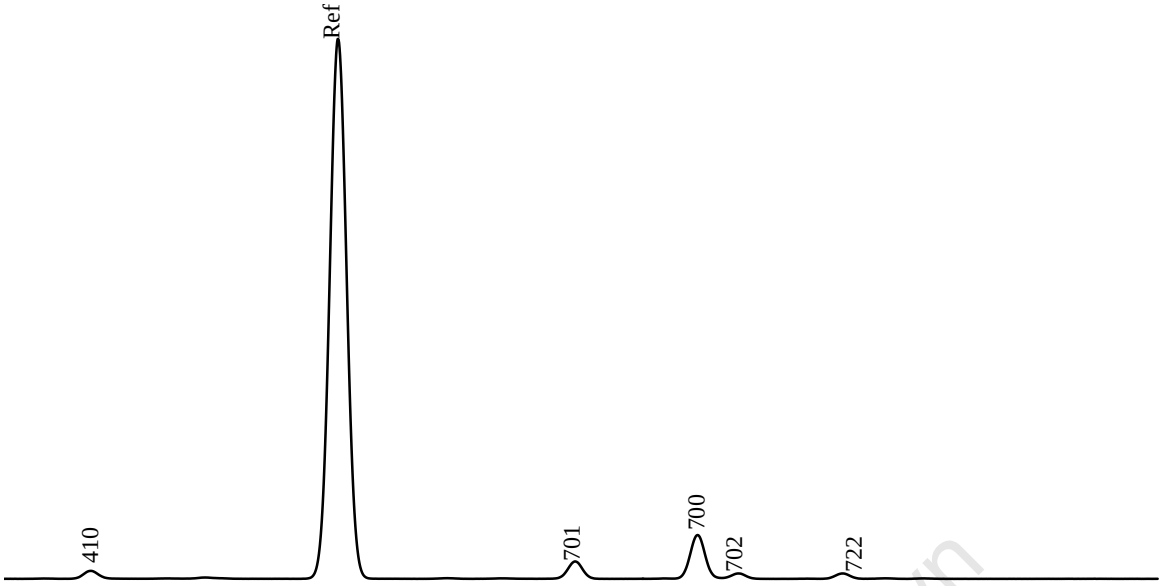

Figure B. 6: A typical chromatogram obtained from GC-FID analysis at 180 C and 10 bar for the pure iron sample including the reference gas cyclohexane after 7 hours runtime

Table B. 2: Compounds analysed using offline FID method

Compound	Code	Factor Response
Methane	**100**	**1.00**
Methanol	110	1.82
Ethane	**200**	**1.00**
Ethene	201	1.00
Ethanol	210	1.29
Ethanal	207	1.29
Acetic acid	204	1.81
Propane	**300**	**1.00**
Propene	301	1.00
Propanol-1	310	1.18

Propanal	307	1.50
n-Butane	**400**	**1.00**
Butene-1	401	1.00
trans-Butene-2	402	1.00
cis-Butene-2	422	1.00
Butanol-1	410	1.13
Butanal	407	1.33
Butanone-2	417	1.33
n-Pentane	**500**	**1.00**
Pentene-1	501	1.00
trans-Pentene-2	502	1.00
cis-Pentene-2	522	1.00
3-Methyl butane-1	531	1.00
n-Hexane	**600**	**1.00**
Hexene-1	601	1.00
trans-Hexene-2	602	1.00
cis-Hexene-2	622	1.00
n-Heptane	**700**	**1.00**
Heptene-1	701	1.00
trans-Heptene-2	702	1.00
cis-Heptene-2	722	1.00